Aus der

Medizinischen Universitätsklinik und Poliklinik Tübingen

Abteilung VIII, Medizinische Onkologie und Pneumologie

Application of Skepinone-L, a p38α MAP (mitogen-activated-protein) kinase inhibitor, to overcome antiviral resistances to immunovirotherapy of colon, hepatocellular and renal carcinomas

Inaugural-Dissertation
zur Erlangung des Doktorgrades
der Medizin

der Medizinischen Fakultät
der Eberhard Karls Universität
zu Tübingen

vorgelegt von
Gottesleben, Joschka

2024

Dekan: Professor Dr. B. Pichler

1. Berichterstatter: Professor Dr. U. Lauer

2. Berichterstatter: Professor Dr. A. D. Hartkopf

Tag der Disputation: 18.04.2024

Table of content

Abbreviations

5-FC	flucytosine
5-FU	fluorouracil
ANOVA	analysis of variance
BSA	bovine serum albumin
CAR	chimeric antigen receptor
CEA	carcinoembryonic antigen
CD	cluster of differentiation
CDC	Centers for Disease Control and Prevention
CFDA	China Food and Drug Administration
CTCL	cutaneous T-cell lymphoma
DAMP	damage associated molecular pattern
DMEM	Dulbecco's Modified Eagle's Medium - high glucose
DMSO	dimethylsulfoxide
DNA	deoxyribonucleic acid
EDTA	ethylendiamintetraacetat
ELISA	Enzyme-linked Immunosorbent Assay
EMA	European Medicines Agency
FBS	fetal bovine serum
FDA	U.S. Food and Drug Administration
GFP	green fluorescent protein
HER2	human Epidermal Growth Factor Receptor 2
hpi	hours post infection
hpt	hours post treatment
HSP27	heat shock protein 27
HSV	herpes simplex Virus
HVEM	herpes virus entry mediator
ICD	immunogenic cell death
IFN	interferon
IRF	interferon regulatory factor
kb	kilobase

MAPK	mitogen-activated protein kinase
MeV	measles virus
MeV-Edm	Edmonston vaccine strain measles virus
MeV-GFP	measles vaccine virus expressing green fluorescent protein
MeV-SCD	suicide gene armed measles virus
MeV-CEA	measles vaccine virus expressing carcinoembryonic antigen
MeV-NIS	measles vaccine virus expressing sodium iodide symporter
MOI	multiplicity of infection
NCI	National Cancer Institute
NF-κB	nuclear factor 'kappa-light-chain-enhancer' of activated B-cells
NIS	sodium iodide symporter
OV	oncolytic virus
PAGE	polyacrylamide gel electrophoresis
PBS	phosphate buffered saline
PFU	plaque forming unit
RIG	retinoic acid-inducible gene-I-like receptors
RIR	RIG-I like receptors
RKI	Robert Koch-Institute
RNA	ribonucleic acid
rpm	revolutions per minute
RPMI	Roswell Park Memorial Institute
SCD	super-cytosine deaminase
SDS	sodium dodecyl sulfate
SLAM	signaling lymphocytic activation molecule
SRB	sulforhodamine B
TBS-T	tris-buffered saline with Tween20
TEMED	tetramethylethylendiamin
TCA	trichloroacetic acid
TLR	toll-like receptor
TRIS	tris(hydroxymethyl)aminomethane
T-VEC	Talimogene laherparepvec

VSV	Vesicular stomatitis virus
WHO	World Health Organization

Introduction

1.1 Oncolytic Virotherapy

1.1.1 *Principles of oncolytic virotherapy*

Oncolytic virotherapy is the attempt to infect and lyse tumor cells specifically without having a negative effect on healthy human cells (Russell and Peng 2007). This concept is based on the natural preference of most viruses to tumor tissue, which varies between different viral strains but can be attributed to the special microenvironment that tumor cells can create to survive. Healthy human body cells are reacting to viral infection with the release of interferon-β (IFN-β) to activate the immune system and subsequently go into apoptosis to prevent the virus from spreading. Viral particles are being recognized via pattern recognition receptors (PRRs) leading to activation of proinflammatory signaling cascades. Release of IFN-β and other proinflammatory enzymes of the infected cell are the result. The IFN-β release is stimulating surrounding uninfected cells to downregulate their own translational machinery, protecting themselves against viral infection by activating their own viral defenses (Russell and Peng 2007). In tumor cells, anti-viral cell responses and immune defenses in general are depleted as the tumor tries to avoid detection of the human immune system by stopping the IFN-β release. Tumor cells are also able to resist apoptosis and translational suppression in order to survive, which benefits viral replication within the tumor cell with the virus keeping the host cell alive until the virus exploited the cells resources for its own replication. The viral load of the cell is increasing drastically and at a certain point the tumor cell can no longer cope with the viral load and bursts. This subsequently leads to the infection of surrounding tumor cells. The specific mechanisms of oncolytic viruses to induce cell death are complex varying from virus mediated cytotoxicity to different cytotoxic immune effector mechanisms, which ultimately lead to immunogenic cell death (ICD) and to viral tumor cell lysis. Furthermore, it causes the change of the tumor microenvironment by releasing specific tumor antigens, e.g. damage associated molecular patterns (DAMPs) (Guo et al. 2017), which can

induce the recruitment and activation of T-cells and dendritic cells leading to a specific anti-tumor immune response (Marelli et al. 2018).

Besides, oncolytic viruses can modify the tumors blood supply by destroying blood vessels to further harm uninfected tumor cells (Russell, Peng, and Bell 2012).

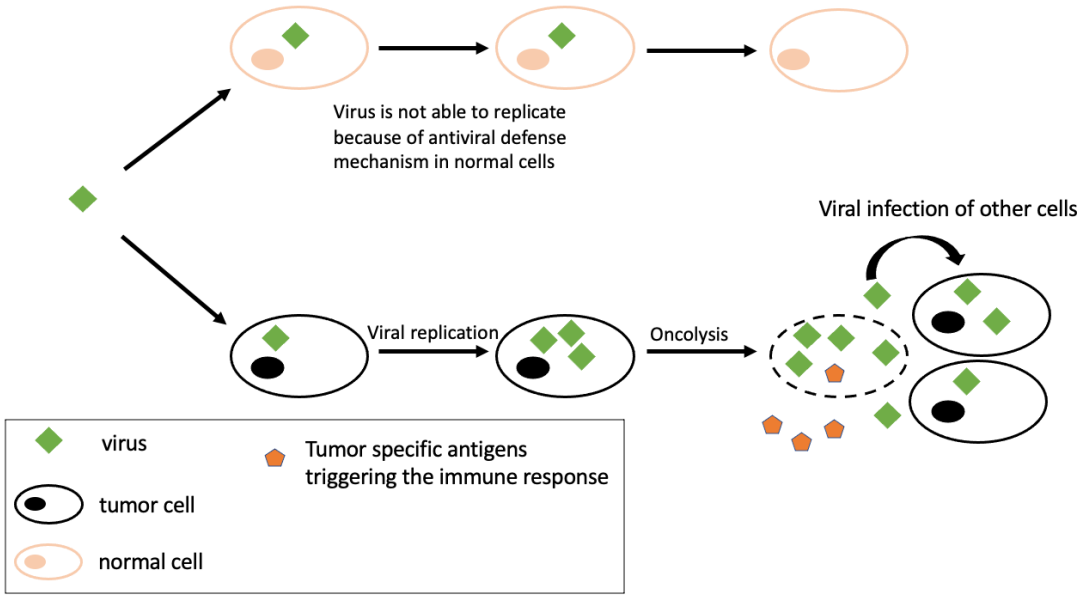

Figure 1: Principles of oncolytic virotherapy

Viral infection of normal body cells usually leads to an antiviral response of cells against the virus preventing viral replication in target cells. In most tumor cells this mechanism is not properly functioning, and the virus is able to replicate and cause tumor lysis. Tumor lysis leads to virus release and hence to viral infection of surrounding tumor cells. Besides, tumor specific antigens are released triggering the immune system which was deceived by the tumor.

Viral engineering is an important research field in oncolytic virotherapy as the goal is to make virotherapeutics as safe, selective and highly effective as possible to ensure translation into clinical practice. There are different approaches which can lead to higher selectivity e.g. depletion of genes or functional regions, which are necessary for viral replication in normal cells but not involved in the viral replication in tumor cells (Kirn, Martuza, and Zwiebel 2001). Some viruses are tumor selective by nature e.g. measles vaccine viruses

that enter tumor cells via CD46 receptor (Dörig et al. 1993), which is overexpressed in a variety of tumor cells (Elvington, Liszewski, and Atkinson 2020). HSV-1 viruses, such as T-VEC, enter tumor cells via the HSV entry receptors HVEM, Nectin-1 or Nectin-2 (Kohlhapp, Zloza, and Kaufman 2015). Other viruses require further engineering to also ensure specific replication only in cancer cells (Rehman et al. 2016).

Safety is a big issue, most importantly the prevention of replication in healthy tissue and the possibility to inactivate the virus if needed (Kirn, Martuza, and Zwiebel 2001; Nettelbeck et al. 2021). Also, the genomic stability of current oncolytic viruses is undergoing preclinical investigation and is an important factor in the development of new viruses (Leber, Hoyler, et al. 2020; Kelly and Russell 2007). Non-invasive monitoring of viral infection is a method commonly used in oncolytic virotherapy to ensure correct viral targeting, monitoring of viral spread, viral release by tumor cells and viral clearance from the body. It describes the insertion of gene sequences into the viral genome to assure monitoring of the virus in both *in vitro* and *in vivo* experiments. In oncolytic virotherapy there have been multiple approaches to adapt virus genomes for monitoring purposes or a higher viral toxicity for example MeV-CEA (Peng et al. 2002), MeV-NIS (Dingli et al. 2004), MeV-GFP (1.2.3, (Scheubeck et al. 2019)),

The efficacy of the virus must be improved, as intravenously injected viruses can be cleared by the immune system on their way to the target regions by antibody neutralization or elimination by phagocytes (Parato et al. 2005). Currently examined options to evade the immune system include shielding the virus with engineered capsids (Kratzer et al. 2017; Wu et al. 2019). Another possibility is the intratumoral application of the viral dose, which minimizes the effect of the immune system and limit the spread of virus in other areas and decrease potential viral infection of normal cells.

1.1.2 *History and current state of virotherapy*

The beginnings of oncolytic virotherapy date back in the 20th century, when influenza viruses caused beneficial effects on patients with leukemia (Dock 1904). In the following years the positive effect of viral infections against malignant diseases was demonstrated and one of the first viruses used for their oncolytic effect were hepatitis viruses. In 1949 Hoster et al. discovered the remission of two patients with Hodgkin disease, which were infected with hepatitis viruses and clinical trials followed, showing tumor regression (Hoster, Zanes, and von Haam 1949).

Experimental research using *ex vivo* human cell models has been possible since 1948. This was followed by the first experiments on rodents to study the response to viral infection *in vivo* (Sanford, Earle, and Likely 1948). Moore et al. showed in rodent models that infection with Russian Far East encephalitis virus resulted in almost complete elimination of sarcoma tumor cells (Moore 1951). In the 1980s, Hodgkin disease reduction was seen in patients vaccinated against measles (Schattner 1984).

Although many approaches in the 20th century were very promising and the oncolytic effect of numerous virus types could be demonstrated, the effect of viruses on normal body cells remained a problem for a potential transfer into clinical application (Kelly and Russell 2007). For oncolytic viruses to be an effective alternative therapy for cancer, these side effects had to be eliminated. To do so, researchers used recombinant DNA technology, developed in 1990s, to alternate the viral genome. Martuza et al. were able to genetically modify an HSV-1 virus to replicate only in rapidly proliferating tissue in a mouse model by creating a thymidine kinase-negative mutant of the HSV-1 virus (Martuza et al. 1991). This initiated a boost to oncolytic virotherapy and viruses were now genetical engineered to ensure safety, specificity and enhancement of oncolytic effects using a variety of different strategies.

A good overview of preclinical activities in Germany and the transfer of oncolytic virotherapy into clinical practice is given by Nettelbeck et al. (Nettelbeck et al. 2021).

Besides the ongoing development of new virus strains (e.g. adenoviruses (Zhang et al. 2017; Zhang et al. 2020; Mach et al. 2020), or coxsackieviruses (Hazini et al. 2018)), enhancing the immunostimulatory potency is a promising strategy, for example increasing $CD8^+$ T cell activation with a designed measles vaccine virus (Busch et al. 2020) or measles virus-induced tumor antigen presentation leading to activation of an anti-tumor immune response (Hutzler et al. 2017).

The success of virotherapy in preclinical experiments has led to an increase of clinical studies, with one of the main challenges being to translate the effects demonstrated *in vitro* and in mouse experiments into clinical trials in order to approve therapeutics for clinical use.

Only a few oncolytic viruses have been approved by the drug authorities of the respective countries, with the first accepted in China. The State Food and Drug administration of China (CFDA) approved the adenovirus rAd-p53 for the treatment of head and neck squamosa cell carcinoma in 2003 (Peng 2005) and the adenovirus H101 shortly after for the same indication (Xia et al. 2004).

A breakthrough in Europe and the US was reached with the approval of *Talimogene laherparepvec* (T-VEC) by the European Medical Agency (EMA) and the U.S. Food and Drug Administration (FDA) in 2015 for treatment of melanoma (Greig 2016; Rehman et al. 2016). T-VEC, a herpes simplex virus, that expresses GM-CSF, proved to be a good therapeutic option for unresectable stage III or IV melanoma. Studies have shown that the life of melanoma patients could be prolonged by up to 3.5 month (18.9 month (only GM-CSF) to 23.3 month (T-VEC) (Andtbacka et al. 2015).

Teserpaturev or G47Δ (DELYTACT), a third generation oncolytic HSV-1, received a conditional and time-limited approval in Japan in 2021 for treatment of malignant gliomas or any type of primay brain cancer (Sugawara et al. 2021). The phase II trial leading to approval of G47Δ in Japan proved an efficacy and safety of G47Δ for glioblastoma (Todo et al. 2022).

While T-VEC is the only approved oncolytic virotherapeutic in the European Union, many others are under development.

Combining oncolytic virotherapeutics with other treatment strategies is another important research field, with adenoviruses being the most explored virus platform. Many OVs (measles, VSV and HSV among others) have been genetically modified to express the sodium iodide symporter (NIS), which can enhance the uptake of radionuclides like ^{131}I in targeted tumor cells (Zhang and Cheng 2020). Studies to the genetically modification of measles vaccine virus with NIS are included later in chapter 1.2.4. Many studies have been conducted combining OVs and chemotherapy, with the combination resulting in increased apoptosis induction. For example, the oncolytic adenovirus (YDC002), which expresses relaxin could increase the therapeutic impact of gemcitabine in pancreatic cancer (Jung et al. 2017).

The combination of immune checkpoint inhibitors and OVs is an important and promising research field in recent years (Hwang, Hong, and Yun 2020). Immune checkpoint inhibitor making a big impact in immuno-oncology but despite the success in clinical settings, there have been limitations in the clinical application, e.g. the lack of effectiveness against tumors with a low tumor infiltrating count (immunologically “cold” tumors”) (Bonaventura et al. 2019). OVs on the other hand are known for inducing a tumor microenvironment with increased lymphocyte and immune cell infiltration (Bonaventura et al. 2019). Preclinical success led to a drastic increase of clinical studies combining OVs and immune checkpoint inhibitors. There are many OVs (adenovirus, HSV-1, vaccinia virus, coxsackievirus, reovirus, vesicular stomatitis virus, maraba virus and newcastle disease virus) currently being investigated in combination with PD-1- inhibitors (Pembrolizumab and Nivolumab) which are the most commonly used, but CTLA-4 inhibitors (Ipilimumab) and PD-L1 inhibitors (Atezolizumab, Avelumab, and Durvalumab) are also being used (Hwang, Hong, and Yun 2020). Unfortunately, the first global phase III study of T-VEC in combination with Pembrolizumab, which enrolled 692 patients with advanced melanoma, did not result in a significant improvement of overall survival or progression-free survival in patients (Chesney et al. 2022), although a previously conducted

phase Ib study showed an acceptable safety profile and a promising complete response rate (Long et al. 2020).

Another interesting approach is the combination of oncolytic virotherapy and CAR-T cell therapy. CAR-T cells need certain antigens e.g. CD19t expressed by the targeted cell for their development but many solid tumors lack these antigens and limit the applicability of CAR-T cells. Genetically modified OVs are used to deliver the gene sequence of CD19t into tumor cells. Tumor cells expressing CD19t in this way can be recognized by CAR-T cells, making CAR-T cell therapy more effective in solid tumors. Park et al. used oncolytic chimeric orthopoxviruses carrying CD19t for this purpose and could prove a successful delivery of CD19t in solid tumors (Park et al. 2020). Besides, CAR-T cells need a certain microenvironment with functioning dendritic cells and an inflammatory stimulus such as type I IFNs and interleukin-12 to be an effective therapeutic option. It remains unclear if these signals can be provided *in vivo* by the microenvironment of solid tumors (Ajina and Maher 2017). OVs are known for providing this inflammatory stimulus, e.g. cytokines like type I IFNs, and have therefore the potential to complement CAR-T cell treatment (Zarezadeh Mehrabadi et al. 2022), while additionally having their oncolytic effects. Currently, there is one approved clinical phase I study in patients with HER2 positive cancer evaluating the combination of HER2-specific-CAR-T cells and the oncolytic adenovirus CAdVEC (both investigational products and not FDA approved), which is specifically designed to help the immune system fight the tumor (NCT03740256).

1.2 Measles virus

1.2.1 *Measles virus - an overview*

Measles virus is highly contagious and caused an estimated 2-3 million deaths worldwide in the 1960s before a vaccine against measles virus was developed. Transmission routes are droplets or contact to infectious fluids and incubation times vary up to 21 days. The contagion index of measles is close to 100 % and with manifestation rates of 95 - 98 % measles is one of the most infectious viral

diseases that can lead to severe complications (rki.de, 2020). Due to the vaccine available today, measles prevalence and mortality have declined dramatically. However, major outbreaks have occurred worldwide, most notably in the spring of 2019 (cdc.gov, 2022), with peaks in New York and Madagascar, demonstrating the importance of measles vaccination in the society to prevent outbreaks. Especially in regions with low vaccination rates, outbreaks can still pose a serious threat because there is no specific treatment for measles. Diseases caused by measles infection include otitis media, bronchitis, pneumoniae and bacterial superinfection as well as more severe complications such as postinfectious encephalitis. Measles infections are mandatory to report in Germany (rki.de, 2020).

1.2.2 *Morphology of measles virus*

Measles virus (MeV) is a single-stranded negative sense RNA virus of the family of paramyxoviruses (morbillivirus). The genome is 16 kb long and contains six genes encoding for eight viral proteins. The proteins can be categorized in six viral proteins located in the virion and two surface proteins (hemagglutinin (H) and fusion protein (F)). While F is in contact with H and the cell matrix and therefore also important for cell entry, H can interact and attach to the viral receptor of susceptible cells. The six viral proteins are nucleoprotein (N), phosphoprotein (P), large protein (L), matrix protein (M), C- and V-Protein. N, P and L are important for wrapping the helical nucleocapsid, which is built by the RNA of the virus. M forms the matrix in which the RNA is embedded and is attached to the surface proteins H and F. C and V are encoded in the P gene and are nonstructural but important for modulating the IFN-β signaling and interfering with the immune defense mechanism of affected cells to avoid recognition by the cells` immune system (Griffin 2018; Aref, Bailey, and Fielding 2016).

The WHO classifies measles into eight clades (A-H) with 24 genotypes. The classification is based on a genome section on the N gene (rki.de, 2020).

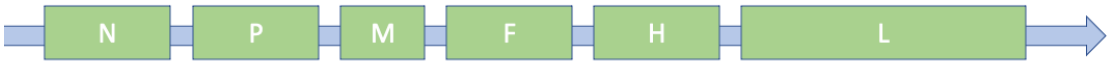

Figure 2: Schematic illustration of the measles genome.

Measles wildtype virus is able to enter various types of cells including B- and T-lymphocytes, monocytes, epithelial and endothelial cells. It uses predominantly the CD150 (SLAM) or nectin-4 receptor for cell entry (Tatsuo et al. 2000). CD150 is mostly expressed on lymphocytes, monocytes and dendritic cells (Aref, Bailey, and Fielding 2016), whereas nectin-4 is mostly located on epithelial cells of the respiratory tract (Noyce et al. 2011). Measles wild type virus first enters dendritic cells via CD150 and then replicates in dendritic tissues. CD150+ lymphocytes then mediate viremia leading to a systemic viral infestation (de Vries et al. 2012).

1.2.3 *Measles vaccine virus*

First isolated in 1954 the measles virus strain Edmonston has since then be adapted into many attenuated strains with Edmonston A being the first and Edmonston B being the second generation strain. The measles vaccine virus was firstly licensed by John Enders in 1963 and derived from the Edmonston B-strain of measles virus (cdc.gov 2020). In 1968, Hillemann developed an improved vaccine also derived from the Edmonston B-strain (Hilleman et al. 1968). Baldo et al. is providing a good overview of the differences between wild type measles viruses and attenuated measles vaccine derived from the Edmonston strain (Baldo et al. 2016).

All attenuated measles vaccine viruses derived from the Edmonston strain are able to enter cells via CD46 as well as CD150 (SLAM) and nectin-4 (Dörig et al. 1993; Naniche et al. 1993). CD46 is expressed on every human body cell except erythrocytes (Johnstone, Loveland, and McKenzie 1993). In 1997, it was discovered that this only applies to attenuated measles vaccine viruses and CD46 cannot be used by wild type measles viruses to enter cells (Buckland and Wild 1997). CD46 is a membrane-bound complement-regulatory protein which among other proteins like CD55 and CD5 can inhibit parts of the complement

system (Buettner et al. 2007). There are four isoforms of CD46 that can bind on the binding sites of C3b and C4b of the complement system. A lack of CD46 would cause an uncontrolled activation of the complement system (Yamamoto et al. 2013). As tumor cells often have a dysregulated complement system, in an attempt to escape the human immune system, an overexpression of CD46 in multiple human tumor cells could be detected (Geller and Yan 2019). Measles vaccine viruses enter cells via CD46 (Dörig et al. 1993) and are therefore a potentially selective oncolytic virotherapeutic as they would enter most tumor cells preferably.

While CD150 is overexpressed in hematological malignancies including the Burkitt`s Lymphoma (Leber, Neault, et al. 2020; Gordiienko et al. 2016), CD46 is overexpressed in most tumor cells, which gives the measles vaccine virus a natural ability to enter and replicate in tumor cells, while being a safer option when applied to humans (Anderson et al. 2004).

Although measles is a potentially dangerous and highly contagious disease, the attenuated measles vaccine virus has a good safety record (Cutts and Dabis 1994) and, therefore, with overexpression of CD46 on most tumor cells as another key factor, is a promising approach to target tumor cells. Other factors that make measles vaccine virus a very attractive candidate for virotherapy include the cytoplasmic replication of the virus and therefore the lack of genomic integration into the host cell genome with high genetic stability for an RNA virus (Baldo et al. 2016). The high insertion capacity (>kb) is also relevant for potential virus modifications, which was exploited in this thesis for insertion of GFP or SCD (Lampe et al. 2013).

1.2.4 *Measles vaccine virus as oncolytic agent in immunovirotherapy*

With the observation of spontaneous regression of Burkitt lymphoma in children caused by a measles wild type infection (Bluming and Ziegler 1971), the potential of measles virus in the treatment of tumors has been known for a long time. Since then, multiple *in vitro* and *in vivo* studies have been conducted. Although there are no measles vaccine viruses authorized for clinical use as cancer therapeutics to date, promising phase I and phase II trials have been

completed or are currently ongoing (current measles vaccine virus trials are summarized below). In 2005, five measles immune patients with ≥ stage IIb refractory or recurrent cutaneous T-cell lymphoma (CTCL) were treated intratumoral with measles vaccine virus (Zagreb strain). In total six tumor lesions were treated with MV (one of the patient had two lesions) with complete regression of one, partially regression of four and no response of one infected lesion (Heinzerling et al. 2005). Some CTLCs show an interferon signaling deficiency and express CD150 and CD46 and therefore are potential promising targets to MV-Edm (Heinzerling et al. 2005). A leading role in translating preclinical tests into clinical application is taken by researchers of the Mayo Clinic, Rochester, Minnesota. Multiple phase I and phase II studies with the engineered MV-Edm strains MV-CEA and MV-NIS are being conducted there. Galanis et al. engineered a measles vaccine virus to express the carcinoembryonic antigen (CEA), which normally functions as a marker for infectious or malignant diseases, to monitor viral expression of measles virus in tumor cells. 21 patients with recurrent ovarian cancer were treated, with the genetically engineered virus proving to be well tolerated and the median survival time of the patients was higher (12 month) than the expected survival time in this group of patients (6 month) (Galanis et al. 2010). In another promising phase I study, patients with glioblastoma multiforme were treated with MV-CEA (NCT00390299). Another example of successful measles vaccine virus engineering is the insertion of the sodium iodide symporter (NIS) into the viral genome. NIS is naturally expressed in the follicular cells of the thyroid gland and leads to iodide trapping. The insertion of NIS into the viral genome leads to a NIS expression only in infected cells. As a second step iodine 123 (I^{123}) treatment leads to tumor ablation via ionizing radiation and enables the monitoring of I^{123} uptake with gamma-camera imaging (Dingli et al. 2004). One of the first clinical studies using MV-NIS were conducted treating resistant ovarian cancer (Galanis et al. 2015; Hasegawa et al. 2006). Promising results with MV-NIS led to several ongoing phase I and phase II studies treating patients with ovarian cancer, multiple myeloma (NCT02192775), mesothelioma (NCT01503177), squamous cell head and neck cancer or breast cancer

(NCT01846091) and recurrent or irremovable malignant peripheral nerve sheath tumor (NCT02700230).

An important step in understanding the effects of measles vaccine virus on tumor cells and possible resistance phenomena was the screening of 54 tumor cells lines (only solid tumors were examined) of the NCI-60 panel by Noll et al. (Noll et al. 2013a). As the NCI-60 panel contains tumor cells from nine different originating organs (Shoemaker 2006) the experiments could give an insight of how tumor cells could be tackled by a modulated measles vaccine virus (MeV-SCD). Tumor cells were infected with MeV-SCD with a multiplicity of infection 1 (MOI 1) and the remaining cell mass was determined 96 hpi. 27 of 54 tumor cell lines were classified as susceptible (remaining cell mass < 50 % in comparison to MOCK). 21 were defined as partially resistant (remaining cell mas between 50 - 75 % in comparison to MOCK) and six cell lines were graded as highly resistant (remaining cell mass > 75 % in comparison to MOCK). The super-cytosine deaminase (SCD) inserted in the MeV genome is able to convert the prodrug 5-fluorocytosine (5-FC) into the chemotherapeutic 5-fluorouracil (5-FU). Adding 5-FC to MeV-SCD infected tumor cell lines lead to a cell mass of < 50 % in all tested 54 tumor cell lines of the NCI-60 panel (Noll et al. 2013a).

1.2.5 *Measles vaccine virus construct MeV-GFP*

The measles vaccine virus MeV-GFP used in this thesis is 100 % derived from the Schwarz vaccine strain which is also derived from the Edmonston A and B strains (Lampe et al. 2013). MeV-SCD used by Noll et al. (Noll et al. 2013a) and Lampe et al. (Lampe et al. 2013) and MeV-GFP have an additional insertion of SCD or GFP respectively at genome position one (**Figure 3**). The function of green-fluorescent-protein (GFP) being the visibility of infected tumor cells under the microscope and not interfering with the entry or replication mechanisms of the virus. The oncolytic effects of MeV on tumor cells are mostly initiated by viral fusogenic proteins expressed in tumor cells. These proteins are causing fusion of uninfected tumor cells into multinuclear cell aggregates that undergo apoptosis (Galanis et al. 2010).

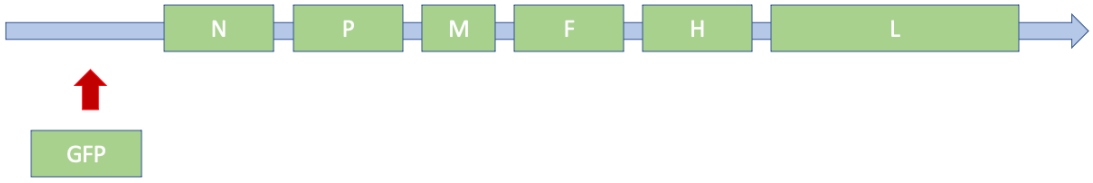

Figure 3: Schematic illustration of the measles genome showing the location of the GFP insertion.

1.3 p38α MAP kinase signaling

1.3.1 *Function and role of the p38α MAP kinase*

The p38-mitogen-actived-protein kinase (p38 MAPK) is part of the large MAPK family and grouped in four isoforms (α, β,γ,δ) of which the p38α MAPK is the most examined (Ono and Han 2000). p38α MAPK functions by phosphorylating transcription factors or enzymes and can therefore affect many different signaling pathways in a cell (Ono and Han 2000). Main regulation purposes of the p38α MAPK are the stress response, inflammation apoptosis, but also different affected cell processes including differentiation, survival and proliferation.

1.3.2 *p38α MAP kinase as part of the anti-viral response of cells*

p38α MAPK is involved in the regulation of type I IFN antiviral responses, as inhibition of kinases leads to a negative effect on type I IFN expression (Platanias 2003; Li et al. 2004; Jiang et al. 2015). p38α MAPK is involved in regulating the IFN-γ and IFN-β gene expression by activation of transcription factors such as IRF7 and NF-κB. However, also other mechanisms, as shown in **Figure 4**, play an important role in activating these transcription factors (Jiang et al. 2015).

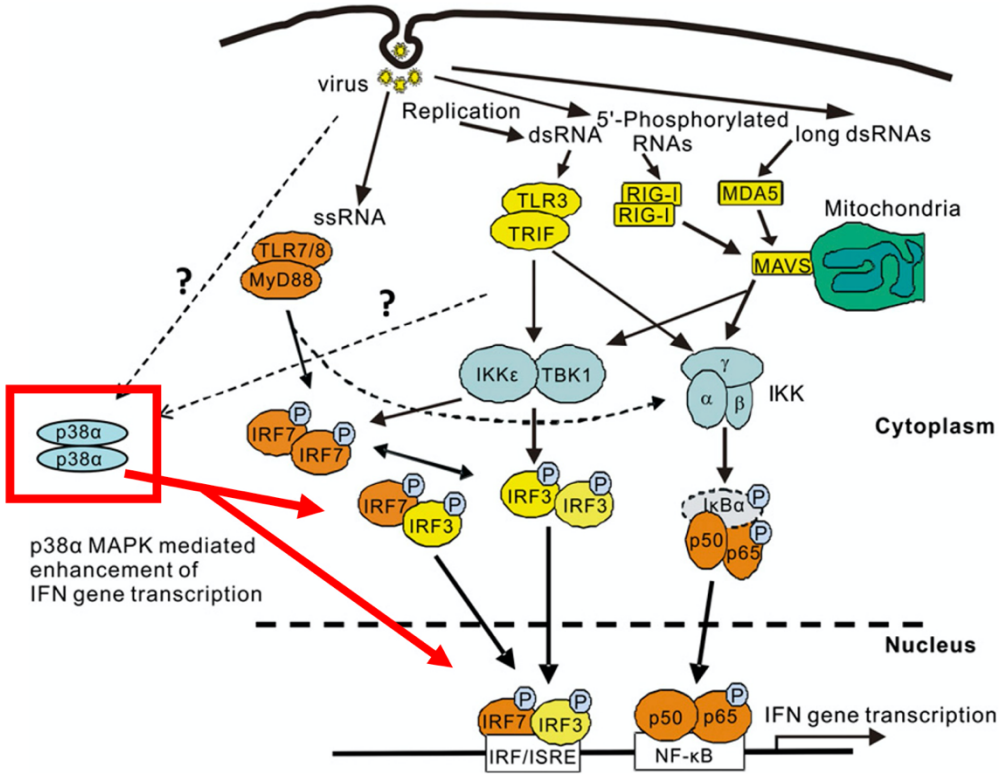

Figure 4: Possible role of p38-α MAPK in IFN immune response of host cells after viral infection (Jiang et al. 2015).

IFN type I is able to bind the type I IFN receptor with its two subunits IFNAR1 and IFNAR2. The type I IFN receptor is then able to interact with a kinase of the Janus-activated-kinases (JAK) family and activates the JAK-STAT signaling pathway (Darnell, Kerr, and Stark 1994). While the JAK-STAT pathway is the most studied type I IFN-induced pathway with STAT being phosphorylated by JAKs and leading to the initiation of gene transcription, also non-STAT pathways can be activated by type I IFN (Platanias 2005; Silvennoinen et al. 1993). This leads to the expression of IFN-stimulated genes, which are causing a stable antiviral state of the cell (Noll et al. 2013a).

Jiang et al. could prove that the inhibition of the p38α MAPK resulted in a low IFN-β and IFN-γ-1 mRNA expression (Jiang et al. 2015).

1.4 Skepinone-L

1.4.1 *Functionality of Skepinone-L*

Skepinone-L is a selective p38α MAPK inhibitor developed by Laufer et al. in Tübingen, Germany (Koeberle et al. 2011). At time of development, Skepinone-L was the first ATP-competitive p38α MAPK inhibitor on the market. Advantages of the inhibitor of the dibenzosuberone-type proved to be highly selective and potent *in vivo* (Koeberle et al. 2011). Rudalska et al. exploited two major differences of p38α MAPK in comparison to other kinases. Addressing these differences was the key to selectivity of Skepinone-L. The first difference involves a gatekeeper residue (Thr106) and the second relates to the ability of p38α MAPK to perform a glycine flip (Koeberle et al. 2011). p-HSP27 and HSP27 are downstream enzymes of the p38α MAPK and were used to examine the potency of Skepinone-L. The Ambit screen and the ProQinase screen were used for selectivity testing: In the Ambit screen, out of 402 kinases, Skepinone-L could only bind to p38α MAPK and p38β MAPK at a concentration of 1000 nM (K_d value of 1.5 nM); comparable results were obtained in the ProQinase screen (Koeberle et al. 2011).

Skepinone-L has already been tested in different approaches in oncology. Rudalska et al. described in 2014 ways to overcome resistance to sorafenib in liver cancer via RNAi screening (Rudalska et al. 2014). In their experiments p38α MAPK knockdown led to a longer survival of mice. They used different specific MAP kinase inhibitors (Skepinone-L among others) which showed effects in *in vivo* mouse models and in other human HCC cell lines like Hep3B, Huh7 and PLC/PRF/5 in combination with sorafenib (Rudalska et al. 2014). The high specificity has made Skepinone-L interesting for other medical fields e.g. the precise role of p38α MAPK signaling in the activation and regulation of platelet function (Borst et al. 2013) and the effect of p38α MAPK inhibition in enzymatically modified LDL-stimulated monocytes in the development of atherosclerosis (Cheng et al. 2017). A promising effect in experimental K/BXN serum arthritis showed the potential importance of Skepinone-L for the

development of an effective drug to treat inflammatory diseases like rheumatoid arthritis (Guenthoer et al. 2019).

1.5 Objective

This doctoral thesis is an attempt to create a further understanding of resistance mechanisms of tumor cells to measles vaccine viruses, which is important for potential clinical treatment options with measles vaccine viruses.

The idea was to target the p38α MAPK signaling of MeV-GFP infected tumor cells with Skepinone-L to reduce the type I IFN expression of tumor cells *in vitro* in order to suppress the antiviral response of tumor cells. The tumor cell lines chosen were two of the high-grade resistance (HCT-15 and ACHN) and two of the susceptible tumor cell lines (HT-29 and HCT-116) of the NCI-60 panel which were screened with MeV-SCD by Noll et al. Additionally, a hepatocellular carcinoma cell line (Hep3B) was used to explore another tumor entity, which had not been tested before in this setup.

At first, the oncolytic effect of MeV-GFP in these selected tumor cell lines of the NCI-60 panel was examined.

Further experiments were performed, looking into to the mechanism behind the observed oncolytic effects. Therefore, IFN-β modulation of the p38α MAPK pathway caused by Skepinone-L treatment as well as viral replication was investigated.

2 Materials and Methods

2.1 Materials

2.1.1 *Tumor Cell lines*

The US National Cancer Institute's NCI-60 tumor cell panel was purchased from Charles River Laboratories (Charles River Laboratories Inc., New York, NY, USA). African green monkey kidney (Vero) cells were obtained from the German Collection of Microorganisms and Cell Cultures (DSMZ, Braunschweig, Germany).

Table 1: Tumor cell lines used in this thesis

Name	Cell culture medium	Growth	Tumor type
HCT-15	RPMI + 10 % FCS	adherent	colorectal
HCT-116	RPMI + 10 % FCS	adherent	colorectal
HT-29	RPMI + 10 % FCS	adherent	colorectal
Hep3B	DMEM + 10 % FCS	adherent	hepatocellular
ACHN	RPMI + 10 % FCS	adherent	renal

2.1.2 *Viruses*

Table 2: Oncolytic viruses used in this thesis

Name	Gene disruptions	Gen insertions	Source
MeV-GFP	none	GFP	(Scheubeck et al. 2019)

2.1.3 *Media, Sera and buffer*

Table 3: Media, Sera and buffer used in this thesis

Dulbecco’s Modified Eagle’s Medium (DMEM)	Sigma-Aldrich

RPMI-1640 Medium	Gibco
Opti-MEM	Gibco
Fetal Calf Serum (FCS)	Sigma-Aldrich
Phosphate buffered saline (PBS)	Sigma-Aldrich
0.05 % Trypsin-EDTA	Sigma-Aldrich
0.1 % Ponceau Solution S in 5 % acetic acid	Sigma-Aldrich
TEMED 99 %	Roth (Carl Roth GmbH & Co. KG)

2.1.4 *Chemicals*

Table 4: Chemicals used in this thesis

Sulforhodamine B (SRB)	Sigma-Aldrich
Trichloracetic acid (TCA)	Carl Roth
Dimethylsulfoxid (DMSO)	AppliChem
Trizma Base (TRIS)	Sigma-Aldrich
Isopropanol (70 %)	SAV Liquid Production
NaCl	Merck
Tryptan Blue	Sigma-Aldrich

2.1.5 *Self-made solutions*

Table 5: Self-made solutions used in this thesis

Separating gel	see 2.2.4.4	
Stacking gel	see 2.2.4.4	
Transfer buffer	TRIS	48 mM
	Glycine	39 mM
	Methanol	20 %
	H_2O_{dd}	filled up to 1 l
Running buffer	TRIS	15.1 g
	Glycine	72 g
	SDS	5 g

	H_2O_{dd} filled up to 1 l
Loading Buffer	5ml: 0.4 % Bromphenolblau 20 mg 0.4 % Xylen-Cyanol FF 20 mg 0.4 % Orange-J 20 mg 50 % Glycerol in Water
TRIS-buffered saline including 0.02 % Tween 20 (TBS-T)	NaCl 150 nm TRIS 13 mM Tween 20 0.02 %
TCA 10 % Solution	TCA 100 g H_2O_{dd} filled up to 1 l
SRB-Staining solution (0.4 % in 1 % acetic acid)	SRB 4 g Acetic Acid 10 ml H_2O_{dd} filled up to 1 l
Tris base (10 mM)	TRIS 1.21 g H_2O_{dd} filled up to 1 l pH 10.5
Freezing Medium	DMEM containing FBS 20 % DMSO 10 %

2.1.6 *Laboratory equipment*

Table 6: Laboratory equipment used in this thesis

HERAsafe laminar flow laboratory hood	Heraeus
Mini Spin	Eppendorf
Biofuge fresco	Heraeus
Megafuge 2.0 R	Unity
Autoclave 3850 EL	Systec
Freezing container Mr. Frosty	Nalgene

Light Microscope CK40	Olympus
Fluorescence microscope	Olympus
Hemocytometer	Hecht Assistant
Incubator (37 °C, 5 % CO_2, > 95 % Humidity)	Memmert/Sanyo/Hereaus
Laminar flow work bench	Heraeus
Shaker	Heidolph
Water Bath 3042 (37 °C)	Köttermann
Refrigerator (-18 °C, -80 °C, -120 °C)	Liebherr
Multistepper pipette (100 µl, 1200 µl)	Eppendorf
Pipettes (10 µl, 100 µl, 200 µl, 1000 µl)	Eppendorf
Pipette Boy	Integra
Multi-Detection Microplate Reader Synergy HT with GEN 5 1.11 Software	BioTech
Amersham Hybond P membrane	GE Healthcare
Mini Trans-Blot® Cell and Criterion™ Blotter	BIO-RAD
Culture flask, 750 ml, 175 cm^2 growth area	Greiner Bio-One Gmbh
Culture flask, 300 ml, 75 cm^2 growth area	TPP
1.5 ml safe-lock tubes	Eppendorf
2.0 ml safe-lock tubes	Eppendorf
Amersham ECL Western blotting detection reagents and analysis system	GE Healthcare

2.2 Methods

2.2.1 *Cell Culture*

2.2.1.1 General growing conditions

Tumor cells were grown in cell culture flasks which were placed in an incubator at 37 °C, 5 % CO_2 and at least 95 % humidity. HCT-15, HT-29, HCT-116 and ACHN were cultured in Roswell Park Memorial Institute 1640 cell culture medium (RPMI 1640) including 10 % heat-inactivated fetal bovine serum (FBS). Hep3B cells were cultured in Dulbecco's modified eagle medium (DMEM) including 10 % heat inactivated FBS.

Components essential for cell culture (media, PBS and EDTA-Trypsin) were stored at -20 °C prior to the experiments, while FBS had to be heat-inactivated at 56 °C for 30 minutes. Before usage, media, PBS and EDTA-Trypsin had to be warmed up in the water bath at 37 °C for 10 minutes. FBS, EDTA-Trypsin, media and PBS were stored at 4 °C in the fridge when opened. Cell culture was performed in a laminar flow work bench to ensure sterile conditions.

Tumor cells were examined on daily basis with a light microscope (4-10x objective) and were passaged if cell growth was confluent and the bottom of the tissue cell culture flask was covered.

2.2.1.2 Thawing of cells

Tumor cells were stored with cell freezing medium in liquid nitrogen at -140 °C in cryovials (1 - 1.8 ml). Cryovials were thawed in a shaking water bath at 37 °C. The content was transferred to a 15 ml falcon and mixed with 8 ml of cell culture medium. The cell pellet was isolated via centrifugation (1000 rpm for 4 min at 22 °C). Supernatant was removed and cells were resuspended in 10 ml cell culture medium.

Cell culture medium containing cells was transferred to labelled tissue culture flasks and 5 ml of DMEM or RPMI + 10 % FCS was added.

2.2.1.3 Passaging of cells

For detachment, growth medium was removed and cells were washed with 8 ml phosphate buffered saline (PBS). PBS was removed and cells detached from tissue cell culture flask by using 2 ml Trypsin (incubation time 2 - 3 min at 37 °C, 5 % CO_2). Cell culture medium was added, and cells were transferred in 15 ml reaction tubes. After centrifugation (Megafuge 2.0 R) and removal of cell culture medium including Trypsin, fresh medium was added. Only a certain percentage of cell culture medium including cells was transferred back to a tissue cell culture flask and cell culture medium was added up to 15 ml.

2.2.1.4 Freezing cells

After detachment (see 2.2.1.3), cells were centrifuged in a 15 ml falcon and medium was removed and freezing medium was added. After thorough resuspension, cells were transferred into cryovials (1 ml per cryovial) which were stored in liquid nitrogen storage containers. Cryovials in storage containers were stored in -80 °C freezer and transferred into -150°C freezer after one day.

2.2.1.5 Counting cells via hemocytometer (improved Neubauer-chamber)

After detachment of cells (see above: 2.2.1.3), 10 µl of cell suspension was added to 90 µl Trypan blue to generate a 1:10 dilution. Trypan blue stains only dead cells and therefore vital cells could be separated while counting in the hemocytometer. The hemocytometer was prepared by attaching a cover glass on the cell chamber. 10 µl of cell suspension was transferred close to the edge of the covering glass and was sucked in by the capillary force of the chamber. Tumor cells were counted using a light microscope. Tumor cells located in four large (blue marked, see **Figure 5** below) 1 mm^2 squares were counted. For calculation of the total cell concentration, the counted cell number was multiplied by 10.000 and by the dilution factor (always 10 in our experiments) and divided by 4 (number of counted squares) (**Figure 6**).

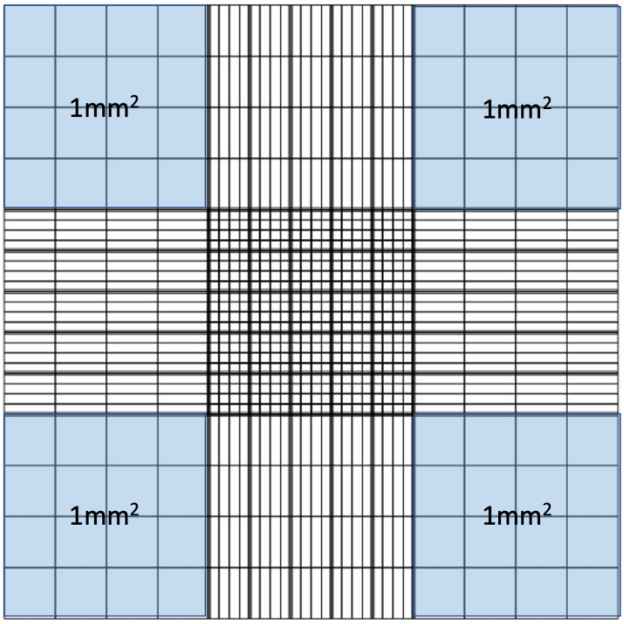

Figure 5: Grid of improved Neubauer hemocytometer.

Concentration of $\frac{cells}{ml} = \frac{counted\ cells \times 10.000 \times 10\ (Dilution\ factor)}{4\ (number\ of\ large\ squares\ counted)}$

Figure 6: Formula for calculating the concentration of cells in cell culture medium per ml.

The total volume needed per well was calculated using the formula in **Figure 7** below.

$$\frac{Required\ amount\ of\ cells\ per\ well}{Counted\ concentration\ of\ \frac{cells}{ml}} \times Number\ of\ required\ wells = Volume\ of\ cell\ suspension\ in\ ml$$

Figure 7: Formula for calculation of needed cell suspension volume.

For each performed assay, different cell culture plates were used and cell line specific cell numbers, which were seeded per well, are shown in **Table 7.**

Table 7: Number of seeded cells/wells used per tumor cell line in each experiment

Assay type	Used late	Amount of cell culture medium per well	Cell lines	Number of seeded cells per well
SRB-Assay	24-well-plate	500 µl	HCT-15 HT-29 ACHN Heb3B HCT-119	2×10^4 2.5×10^4 2.5×10^4 3×10^4 2×10^4
INF-β-ELISA	96-well-plate	-	HCT-15 HT-29	2×10^4 2.5×10^4
Immunoblot Assay	6-well plate	2 ml	HCT-15 Heb3B HT-29	2×10^5 3×10^5 2.5×10^5
Virus Growth Curves	6-well plate/ 96-well plate	2 ml/ 200 µl	HCT-15 HT-29	2×10^5 2.5×10^5
xCELLigence® Assay	E-96-well-plate	200 µl	HCT-15 HT-29	2×10^3 2.5×10^3

2.2.2 *Virological methods*

2.2.2.1 Infection of cells with MeV-GFP and treatment with Skepinone-L

Tumor cells were passaged, counted, and seeded two days before treatment with MeV-GFP.

Tumor cells were treated with Skepinone-L and/or infected with MeV-GFP. Each Assay was performed in triplicates or quadruplicates to ensure reproductivity.

The treatment scheme below was used for every assay performed in this thesis and proven most effective in previous tests (**Figure 8**).

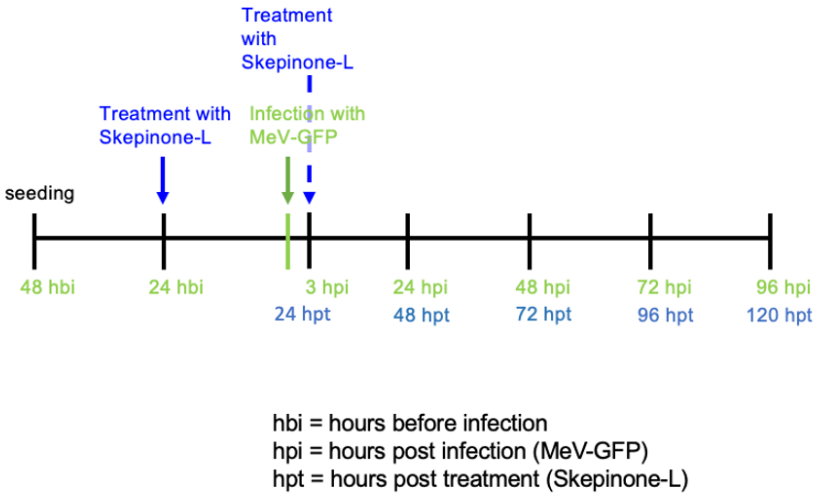

Figure 8: Scheme of Skepinone –L treatment and MeV-GFP infection.

Tumor cells were grown for 24 hours, then cell culture medium was removed and medium containing Skepinone-L or only medium as negative control was added into the wells. 48 hours post seeding cell culture medium was removed and Opti-MEM containing MeV-GFP in an assay-dependent multiplicity of infection (MOI) was added for three hours. The unit MOI is used to determine the applied virus concentration. MOI of 1, for example, indicates that one virus particle per cell was added at the time of infection. After three hours, the inoculum (Opti-MEM containing virus particles) was removed and cell culture medium with the same amount of Skepinone-L used at the beginning of the experiment was added. Tumor cells were fixed or used (dependent on the experiment) to defined time points after treatment (24, 48, 72, and 96 hours post infection (hpi)). Depending on the tumor cell lines, MeV-GFP and/or Skepinone-L concentrations varied based on different responsiveness of tumor cell lines in prior results (3.2 and 3.3). HCT-15 cells were treated either with 2.5 μM or 5 μM Skepinone-L and/or infected with MeV-GFP at MOI 10 or left untreated. ACHN cells were treated with 10 μM Skepinone-L and/or MeV-GFP

at MOI 1 or MOI 2.5 or left untreated. Hep3B cells were treated with 10 μM Skepinone-L and MeV-GFP at MOI 0.01 and 0.025 or left untreated. HT-29 cells were treated with 1 μM or 2.5 μM Skepinone-L and/or MeV-GFP at MOI 0.25 or left untreated. HCT-116 cells were treated with 10 μM Skepinone-L and/or MeV-GFP at MOI 0.25 or MOI 0.5 or left untreated.

2.2.2.2 Viral growth curves

2.2.2.2.1 Obtaining virus samples

Tumor cells (HCT-15 and HT-29) were seeded and treated as described in 2.2.2.1 (**Figure 8**).

After 3, 24, 48, 72 and 96 hpi, medium was removed and 1 ml OPTI-MEM was added. Cells were scraped of the well and 1 ml cell suspension was transferred to a 1.5 ml reaction tube and frozen at -80 °C.

2.2.2.2.2 Virus titration on Vero cells

To identify the titer of measles vaccine virus in the samples, a $TCID_{50}$ (tissue culture infective dose 50) endpoint dilution assay on Vero cells was performed. Therefore, Vero cells were seeded at 5 x 10^5 cells per well in 200 μl DMEM plus 5 % FCS in 96 well-plates. After 24 hours, the samples were thawed and dilution series were prepared. For this, a 96-well plate was prepared leaving the first row of wells empty as shown below (**Figure 9**) and adding 270 µl of DMEM plus 5 % FCS into the remaining wells. 300 μl of each sample was added in quadruplicates to the wells in the first row. Then, 30 µl of the original sample was transferred in the second row and mixed with the already added 270 µl DMEM plus 5 % FCS. 30 µl of cell suspension of the second well was then transferred to the next well, proceeding until the 8^{th} well, while creating a 1:10 dilution series (**Figure 9**).

Vero cells were infected in quadruplicates using 50 µM of the diluted virus suspension for each well and 96 hpi the titration could be examined via fluorescence microscopy.

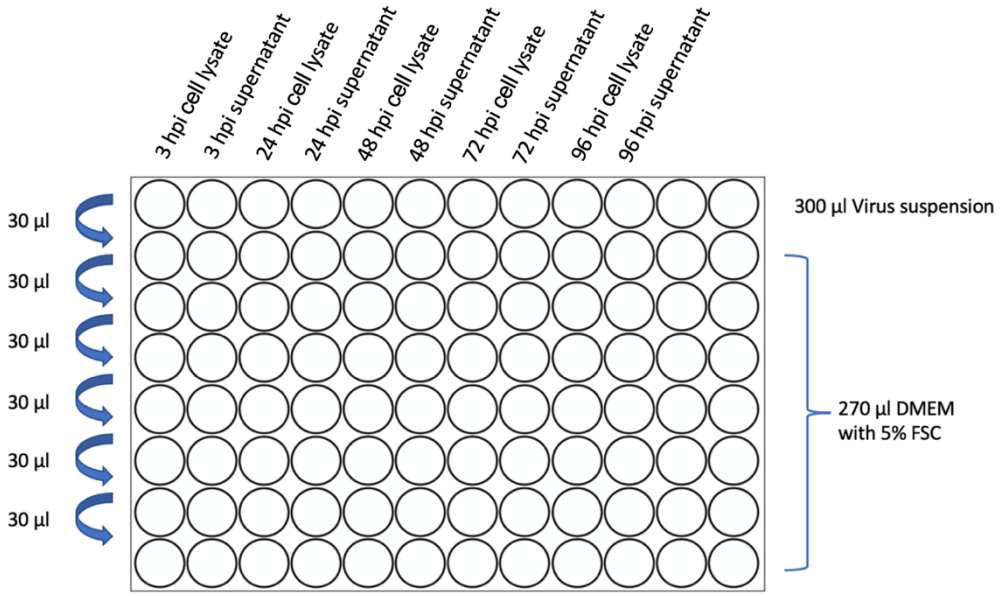

Figure 9: Dilution series of samples in 96-well plate.

2.2.2.2.3 Analysis of viral growth curves

At 96 hpi, the infected Vero cells were observed using a fluorescence microscope. A well was claimed positive if a single dot of green light confirmed the infection of the virus. The analysis is based on a formula used by Spearman and Kärber (SPEARMAN 1908; Kärber 1931) calculating the tissue culture infective dose ($TCID_{50}$) as a value of the amount of virus needed to cause cytopathic effects in 50 % of the infected cells. First, the number of infected wells of the quadruplicates was counted and the viral titer was calculated using the formula below in PFU/ml. Viral growth curve was created using Graph Pad Prism 8.

$$\frac{10^{1+\Sigma \text{infected wells}-0{,}5\text{x}\log 10}}{0{,}03ml\ inserted\ viral\ solution} = \frac{viral\ particles}{ml} = \frac{TCID_{50}}{ml}$$

Figure 10: Spearman and Kärber algorithm for calculation of the $TCID_{50}$.

2.2.2.3 Fluorescence microscopy of MeV-GFP infected cells

Since MeV-GFP expresses the marker protein green fluorescent protein (GFP), successful virus infection, replication as well as oncolysis of cells could be detected using fluorescence microscopy. Cell death could be tracked over time by taking photos of the same region at 24, 48, 72, and 96 hpi.

2.2.3 *Cell mass and viability assays*

2.2.3.1 Sulforhodamine B (SRB) cell viability assay

The SRB-assay was first developed by Skehan et al. (Skehan et al. 1990). SRB dissolved in 1 % acetic acid is able to bind on basic amino acid of cells and the amount of binding SRB proved to be linear to the cell mass. Hence, it was possible to dissolve SRB with Tris pH 10.5 and the density of dye could be detected giving information's about the cell mass of examined cells. Cells were seeded in 24-well-plates with 0.5 ml cell culture medium per well. The number of cells per well varied between cell lines (**Table 1**). Tumor cells were treated and infected according to the experiment scheme in 2.2.2.1 (**Figure 8**). At 24, 48, 72 and 96 hpi cell culture medium was removed and tumor cells were washed with ice cold PBS and fixed with trichloroacetic acid (TCA 10 %). After 30 min incubation at 4 °C, plates were washed four times in VE-water and dried overnight in a 40 °C incubator.

In a next step, 250 µl sulforhodamine B was added to each well and plates were incubated for 10 min. Then, plates were washed in 10 % acetic acid solution four times and dried in 40 °C incubator overnight. For direct measurement, 1 ml of 10 mM Tris pH 10.5 (depended on color intensity) was added in each well and plates were agitating on shaker for 10 min. 80 µl of SRB-cell-solution was transferred in duplicates to 96 well plates and optical density was measured with ELISA-Reader at 550 nm and 620 nm as control.

Extracted data was calculated in Microsoft Excel 16.45 and values were displayed comparing them to the MOCK value which was set at 100 %. Graph Pad Prism 8 was used for statistical analysis of the results using an ordinary

one-way ANOVA with multiple comparisons and a Bonferroni test for the correction of the p-value.

2.2.3.2 xCELLigence® assay

With the xCELLigence® Real-Time Cell Analyzer, it was possible to determine the cell proliferation rate over a period of up to 150 hours. Since the xCELLigence® reader measures the electric impedance change, meaning the differences in cells adhering to the E-plate, this assay can be used to measure cell growth in real time. In our experiment the electric impedance was measured every 30 minutes for 150 hours. Three duplicates were used for each treatment, blank and control.

Tumor cells were seeded as shown in **Table 1** to assure the cells were in the growth phase throughout the whole experiment. Therefore, the interaction between Skepinone-L and MeV-GFP and their effect on growing tumor cells could be monitored in real time.

First, 50 µl of cell culture medium was added into each well of an E 96-well plate and 150 µl of PBS was pipetted in the interspaces between the wells in order to prevent the cells from drying out. The medium-filled wells were used for a one-time background measurement using the xCELLigence® reader.

Then, tumor cells were added into the medium-prepared wells (**Table 1**). The E-96-well plate was immediately placed in the xCELLigence® reader and the impedance was measured every 30 minutes. After 24 hours tumor cells were treated with Skepinone-L and infection with MeV-GFP was performed after 48 hours using the scheme in 2.2.2.1 (**Figure 8**). Tumor cells were treated with Skepinone-L in 50 µl cell culture medium. To assure the right concentration of Skepinone-L, the concentration was calculated for 100 µl of cell culture medium as 50 µl was already in each well. After 140 hours the experiment was stopped and the single measurements were analyzed.

2.2.4 Immunoblotting

2.2.4.1 Preparation of cell lysates

Tumor cells in 6-well plates were treated with Skepinone-L (24 hbi) and infected with MeV-GFP as displayed in 2.2.2.1 (**Figure 8**). 24, 48, 72, and 96 hpi tumor cells were harvested with the use of a cell scraper in PBS. Tumor cells were centrifuged at 1000 rpm. The cell pellet was resuspended in lysate buffer and stored at -20 °C.

2.2.4.2 Freeze-thaw lysis

Tumor cell lysates were obtained by performing three freeze-thaw-lysis cycles. First, cells were thawed in a thermomixer (Eppendorf AG). Cell components were mixed through vortexing and the cell lysate was frozen immediately in liquid nitrogen and thawed again for the next round of freeze-thaw-lysis cycle.

Tumor cell lysates were centrifuged at 10000 rpm at 4 °C for 10 min. Supernatants containing the cell protein were transferred to new reaction tubes.

2.2.4.3 Bradford protein assay

To identify the amount of protein per milliliter solution and to be able to use the same amount of protein in the following SDS-Page for each sample the Bradford protein assay was performed.

The prepared cell lysates were diluted at 1:40. BSA (Bovine serum albumin) was used as control covering protein concentrations of 0.5 to 0.05 mg/dl. The controls were pipetted in the first two rows of a 96-well plate and ddH_2O was added into two wells as blank control (**Figure 11**). Then, Bradford-reagent was diluted 1:5 with ddH_2O and 200 µl were added to each well. The extinction was measured with an ELISA Reader at 595 nm as the Coomassie Brilliant Blue G-250 dye, contained in the Bradford reagent, forms complexes with the proteins to shift the absorption spectrum from 465 nm to 595 nm.

The amount of protein in the cell lysates was calculated using the BSA standard control curve.

BSA 0,5	BSA 0,25	BSA 0,1	BSA 0,05	ddH_2O							
BSA 0,5	BSA 0,25	BSA 0,1	BSA 0,05	ddH_2O							
Lysat 1	Lysat 2	Lysat 3	Lysat 4	…							
Lysat 1	Lysat 2	Lysat 3	Lysat 4	…							
Lysat 13	…										
Lysat 13	…										
…	…										

Figure 11: Layout plan of a 96-well plate with a BSA standard control curve and samples (lysates).

2.2.4.4 SDS-Page

A sodium dodecyl sulfate polyacrylamide gel electrophoresis (SDS-Page) was performed to separate the proteins according to their size. A method first implemented by Laemmli (Laemmli 1970). The SDS unfolds proteins by disrupting non-covalent bonds. This results in the proteins being negatively charged and can be separated according to their size, as the charge is no longer considered.

The amount of each cell lysate was calculated to ensure that each sample contains 50 μg of protein. The calculated amount of each cell lysate was pipetted into Eppendorf cups and filled up with the respective amount of ddH_2O to level the volume. Loading buffer (6-fold) was added (for example 15μl/5 = amount of added loading buffer). These samples were denaturized in a thermomixer at 95° for 5 minutes and stored on ice before usage. Gels were prepared using the Mini Trans-Blot-Cell and Criterion Blotter. TEMED was used as polymerizing agent and was only added right before casting the gels as the time frame of polymerization especially for the stacking gel (**Table 8)** was rather short. Two glass plates (1.5 mm apart) were used to shape the gels. First the separating gel was filled in between the plates and was topped with isopropanol to flatten the surface when the gel polymerized after 10-15 min. After removing the isopropanol, stacking gel was added on top of the separating gel (**Table 8**).

Before the gel hardened, a small comb was inserted to create pockets for the samples. Polymerization of the stacking gel was reached after 5-10 min.

Table 8: Composition of 10 % separating gel and 5 % stacking gel.

Solution components in ml	**10 % separating gel**	**5 % stacking gel**
H_2O	7.9	4.1
30 % acrylamide mix	6.7	1.0
1.5 M Tris (pH 8.8) Separating gel 1.0 M Tris (pH 6.8) Stacking gel	5.0	0.75
10 % SDS	0.2	0.06
10 % ammonium persulfate	0.2	0.06
TEMED	0.012	0.006

The electrophoresis chamber was filled with running buffer. After polymerization, the comb was removed and the pockets were washed with ddH_2O.

Pocket number one was filled with transfer page ruler plus (5 µl) followed by the samples adding the positive control at the end. The electrophoresis chamber was closed and connected to the power supply for 2 gels at 70 V until the samples passed the stacking gel and all bonds had formed a thin line. Then the power unit was reduced to 40 mV.

2.2.4.5 Western blot

After the SDS-Page was performed the gels were blotted. The now separated proteins were transferred to a polyvinylidene difluoride- (PVDF) membrane.

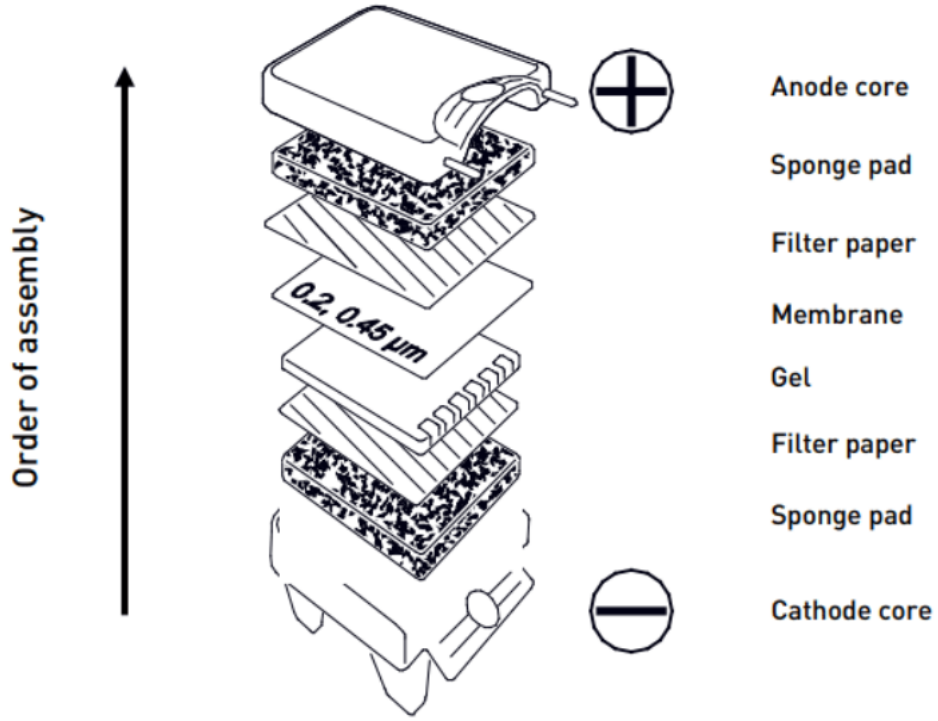

Figure 12: Blot sandwich (Illustration from thermo fisher)

The western blot sandwich consists of an anode and cathode core layered by a sponge pad and filter paper. In between the gel and the membrane was placed with the aim of transferring the protein bonds from gel to membrane (**Figure 12**). The components were fixed within two clamps and put in transfer buffer for an hour at 200 mA, transferring the proteins to the membrane. The membrane was washed in methanol and treated with Ponceau S red dye solution to make the proteins visible and to control if they were properly transferred to the membrane. TBS-T and 5 % milk powder solution was used for blocking the membrane for one hour to make sure antibodies didn't accidently attach to the membrane instead of the proteins of interest.

The primary antibodies were applied to the membrane in TBS-T/milk powder solution in certain concentrations. Vinculin (1:8000 dilution) or β-actin (1:5000 dilution) were used as controls. P-HSP27-MAP-Kinase/HSP27-MAP-Kinase antibodies (1:1000 dilution) were used to determine the activity (phosphorylated

form = active form) of the IFN-β pathway of treated tumor cells. The antibodies were incubated on a shaker at 4 °C overnight.

The next day, the respective secondary antibody was added to the membrane after washing with TBS-T 3 x for 10 min. The secondary antibody was diluted 1:8000 (2.5 µl of antibody with 20 ml TBS with 5 % milk). The controls vinculin and β-actin were treated with an anti-mice secondary antibody, while the p-HSP27 and HSP27 were treated with an anti-rabbit secondary antibody.

After one hour incubation time, the secondary antibody was discarded and the membrane was washed again 3x for 10 min.

The Amersham ECL Western blotting detection reagents and analysis system was used and two detecting reagents (1.5 ml) were mixed in accordance to the kit description and applied to the membranes using plastic bags to keep the solution on the membrane and incubated for 1 min. Afterwards the solution was removed and the membranes inside their plastic bags were put into a film cassette together with a photosensitive film.
The membranes were developed in a dark room with adequate exposure times. The membrane treated with the p-HSP27 antibodies was stripped to remove the antibodies and then treated again with HSP27-MAP-Kinase antibodies. For membrane stripping NaOH was used for 10 min.

2.2.5 *Interferon (IFN)-β-ELISA*

Interferon (IFN)-β released by infected cells functioned as a marker for the intact viral response of tumor cells. Therefore, IFN-β output of cells was used to examine the blockage of the antiviral response pathway with Skepinone-L. Cells were treated and fixed as shown in 2.2.3.1. Before fixation, medium of treated cells was transferred into reaction tubes and stored at -80°C. An I was used and experiments were performed using the standard protocol of the manufacturer.

3 Results

3.1 Project focus and cell line selection

Based on prior experiments by Noll *et al.*, the resistances of cells out of the NCI-60 panel against MeV-SCD were tested and results below were obtained (**Figure 13**) (Noll et al. 2013a). Since MeV-SCD and MeV-GFP have a similar genomic structure, it could be expected that infecting tumor cells of the NCI-60 panel with MeV-GFP would show similar oncolytic effects of the vaccine virus. Therefore, in this study two high grade resistant tumor cell lines (HCT-15 and ACHN) and two susceptible cell lines (HCT-116 and HT-29) against MeV-SCD (**Figure 13**) were tested together with a hepatocellular carcinoma line (Hep3B) which was not pretested with measles vaccine virus.

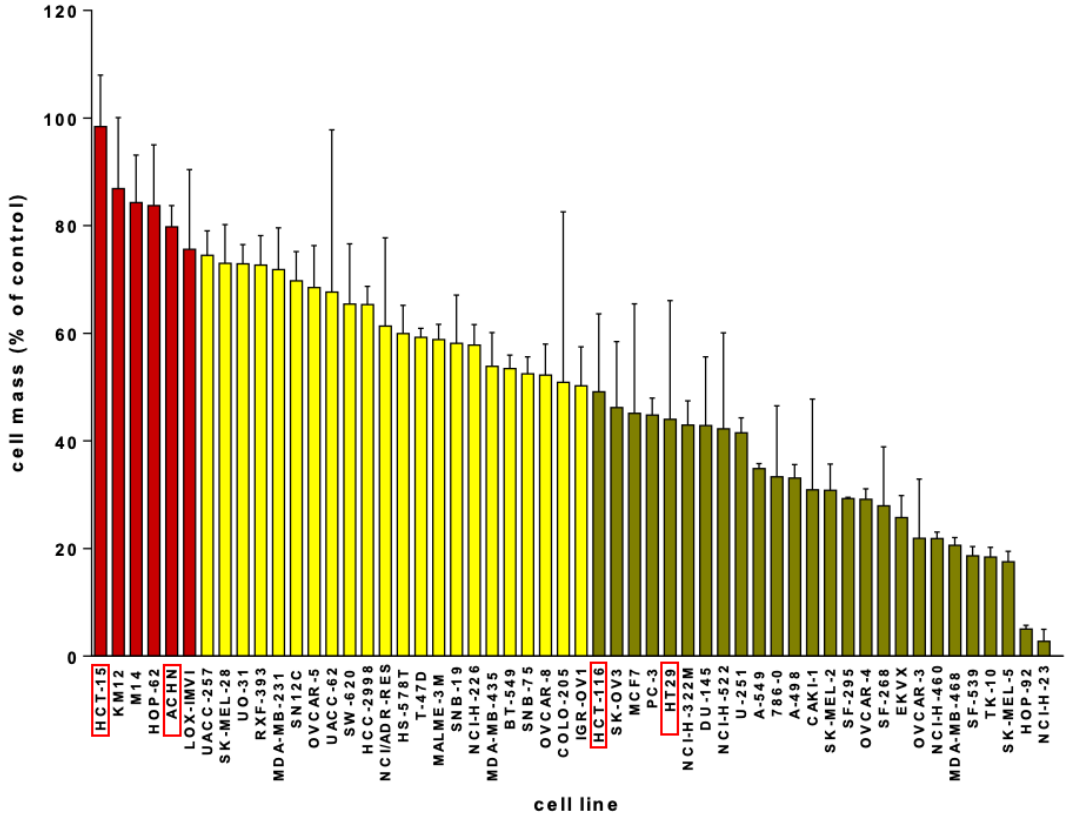

Figure 13: Oncolytic effect of MeV-SCD infecting tumor cell lines of the US-National Cancer Institute NCI-60 tumor cell panel (Noll et al. 2013a).

Initially, cell toxicity of MeV-GFP, Skepinone-L and co-treatment (in the following always refers to a combined treatment of tumor cells with MeV-GFP and Skepinone-L) was examined using SRB assays to explore a potential effect on tumor cell lines in view of future cancer treatment options. Besides, images of infected tumor cells were taken using fluorescence microscopy to examine the differences in viral replication of co-treated or single treated/infected cells. Subsequently, the mechanism of action of Skepinone-L was investigated to verify, whether the hypothesis that Skepinone-L leads to a reduced release of immune modulating IFN-β of tumor cell lines by inhibiting the p38α MAPK signaling is valid. The inhibition of the p38α MAPK signaling pathway in co-treated tumor cell lines was examined by immunoblotting using the downstream enzyme of the p38α MAPK: HSP27. In addition, the change in IFN-β release of infected and co-treated tumor cell lines was detected in an IFN-β ELISA. Decreased IFN-β output from co-treated tumor cells suggests inhibition of IFN-β expression by blocking the p38α MAPK signaling by Skepinone-L. Finally, the viral replication and release of MeV-GFP in tumor cells was tested using viral growth curves to examine the effect of co-treatment. Furthermore, the cell proliferation was monitored over time via xCELLigence® assay.

3.2 Cytotoxic effect of MeV-GFP monotherapy on tumor cell lines

The cytotoxic effect of MeV-GFP on tumor cell lines of the NCI 60 panel could be assumed based on the promising results of MeV-SCD as similar structured oncolytic virotherapeutics as shown above (**Figure 13**) (Noll et al. 2013a). However, experiments must be carried out to determine the appropriate virus concentrations for the following experiments.

Since HCT-15 and ACHN are well established cell lines, no further experiments were necessary to determine suitable virus concentrations. HCT-15 cells were infected with MOI 10 (multiplicity of infection; MOI 1 is defined as one virus particle per cell). The reason for the relatively high MOI used in HCT-15 is due to the high resistance of this tumor cell line to MeV-SCD in previous experiments by Noll et al. (Noll et al. 2013a). The cell line ACHN was infected with MOI 1 and 2.5.

In Hep3B, HT-29 and HCT-116 different MeV-GFP concentrations were analyzed using SRB assays to examine the respective cytotoxic effects (**Figure 14)**

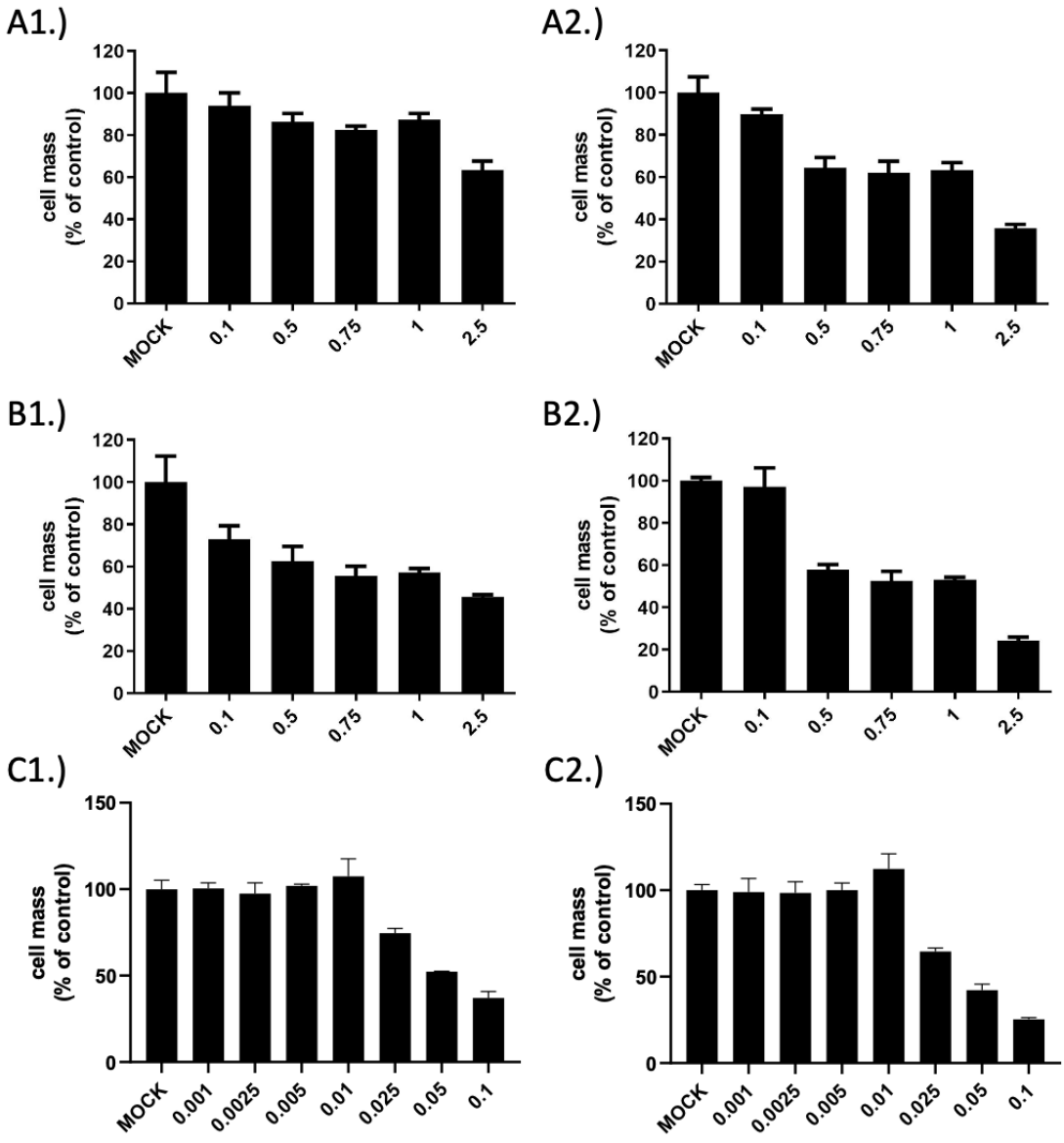

Figure 14: SRB assay of the tumor cell lines HCT-116, HT-29 and Hep3B treated with MeV-GFP

The tumor cell lines HCT-116 (**A**), HT-29 (**B**), and Hep3B (**C**) were seeded in 24-well plates and treated with MeV-GFP ranging from 0.1-2.5 MOI (HCT-116 and HT-29) and 0.001-0.1 MOI (Hep3B). SRB assays were performed 72 (**A1, B1, C1**) and 96 (**A2, B2, C2**) hpi (hours post infection). MOCK; untreated control. Experiments were conducted in quadruplicates.

HCT-116 showed cell reduction from 94 % to 87 % (all values compared to MOCK value in %) at MOI 0.1 and MOI 1 and an oncolytic effect down to a cell

mass of 63 % after infection with MOI 2.5 (72 hpi) (**Figure 14A**). 96 hpi the cell mass was reduced to around 63 % at MOIs ranging from 0.5 to 1 with a maximum cell mass reduction to 36 % at MOI 2.5 (**Figure 14A**).

HT-29 proved to be susceptible. At MOI 0.1 and MOI 0.5, cell mass was reduced to 73 % and 63 %, respectively, whereas infection at MOI 2.5 (72 hpi) resulted in cell mass reduction to 45 % (**Figure 14B**). 96 hpi, cells infected with MOI 0.1 showed only slight reduction (97 %), whereas cell mass was highly reduced at higher MeV-GFP concentrations (e.g., MOI 2.5 = 24 %) (**Figure 14B**).

Hep3B didn't show any signs of cell mass reduction in the SRB assay compared to the MOCK value when infected with MeV-GFP MOI 0.001, MOI 0.0025, MOI 0.005 and MOI 0.01 (**Figure 14C**). However, when cells were infected with MOI 0.025 cell mass was reduced to 75 % of the MOCK value at 72 hpi and 65 % at 96 hpi. Infection of Hep3B with MOI 0.05 MeV-GFP reduced cell mass to 52 % at 72 hpi and to 42 % at 96 hpi. Infection with MeV-GFP MOI 0.1 reduced the cell mass to 37 % (72 hpi) and 25 % (96 hpi), respectively (**Figure 14C**).

The concentrations chosen for the following experiments were selected based on the MOI which resulted in a remaining cell mass of 60-90 %. This would ensure that a combinational effect could still be assessed without depleting the cell lines completely by the monotherapy of MeV-GFP. Hence, for HCT-116 MOI 0.25 and 0.5, for HT-29 MOI 0.25 MeV-GFP and for Hep3B MOI 0.01 and 0.025 were used in further experiments.

3.3 Effect of Skepinone-L on tumor cell lines

To examine the effect of Skepinone-L on the selected tumor cell lines, cells were treated with different concentrations of Skepinone-L (0.1 - 10 μM) and cytotoxicity was measured using SRB assay.

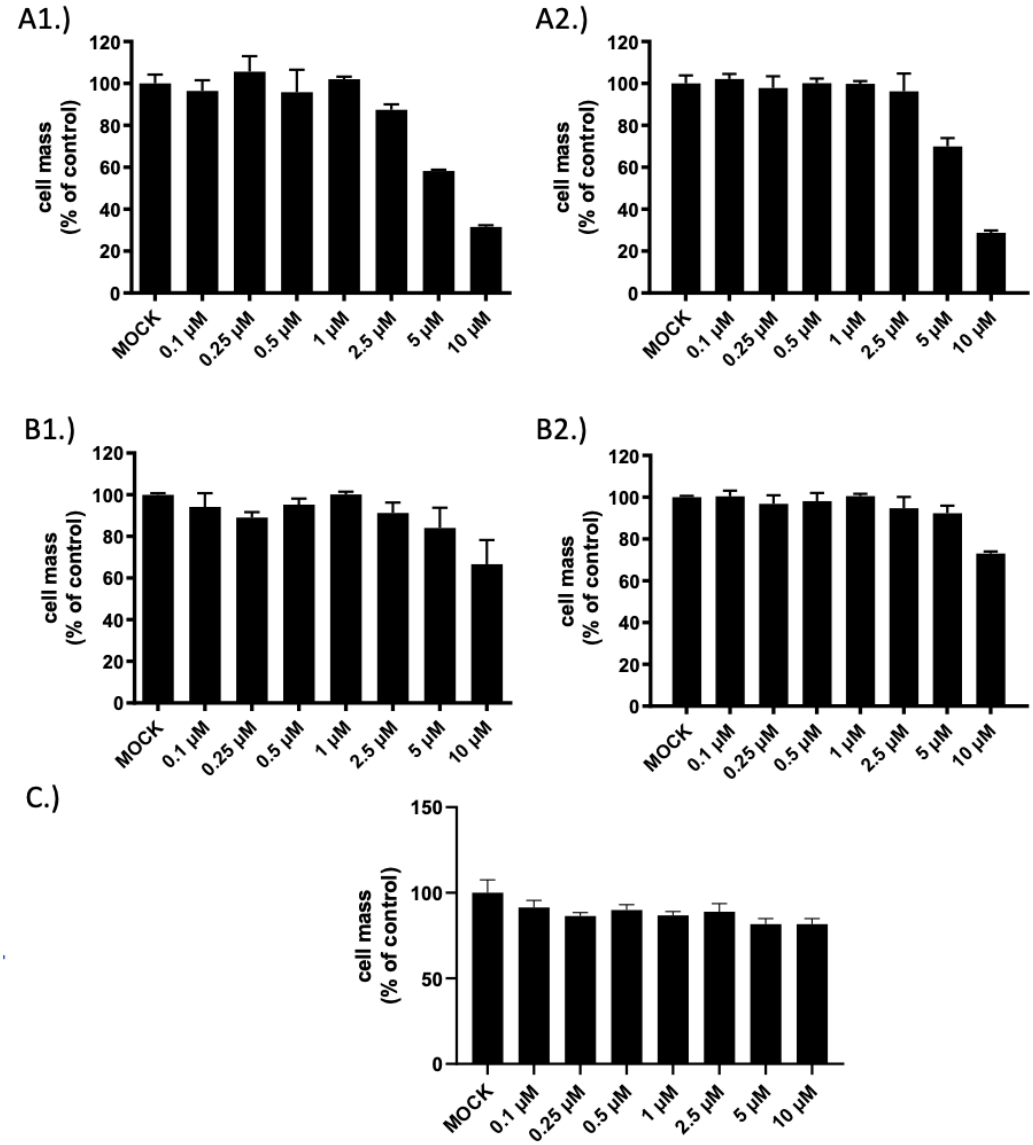

Figure 15: SRB assay of tumor cell lines HCT-15, ACHN and Hep3B treated with Skepinone-L

HCT-15 (**A**), ACHN (**B**) and Hep3B (**C**) were seeded in 24-well plates and treated with Skepinone-L 24 hours post seeding with increasing concentrations (0.1 - 10 μM). SRB assays were performed at 72 (**B1 und A1**) and 96 (**B2, A2 und C**) hpt (hours post treatment). Experiments were conducted in triplicates. MOCK; untreated control.

HCT-15 cells showed only slight effects at Skepinone-L concentrations of 0.1 - 2.5 μM 72 and 96 hpt (hours post treatment). After treatment with 5 μM Skepinone-L, cell mass was reduced to 58 % (72 hpt) and 70 % (96 hpt). The use of 10 μM Skepinone-L resulted in cell mass reductions to 32 % at 72 hpt and 29 % at 96 hpt (**Figure 15A**).

ACHN cells showed only slight effects at Skepinone-L concentrations ranging from 0.1 - 5 μM at 72 and 96 hpt with concentration of 5 μM Skepinone-L reduced cell mass to 84 % (72 hpt) and 92 % (96 hpt). The use of 10 μM Skepinone-L resulted in ACHN cell mass reductions to 67 % (72 hpt) and 73 % (96 hpt) (**Figure 15B**).

The cell mass of Hep3B was only reduced by higher concentrations (5 μM and 10 μM) Skepinone-L at 96 hpt to around 80 % in comparison to the MOCK value, while at concentrations ranging from 0.1 - 2.5 μM cell mass was reduced to around 90 % (**Figure 15C**).

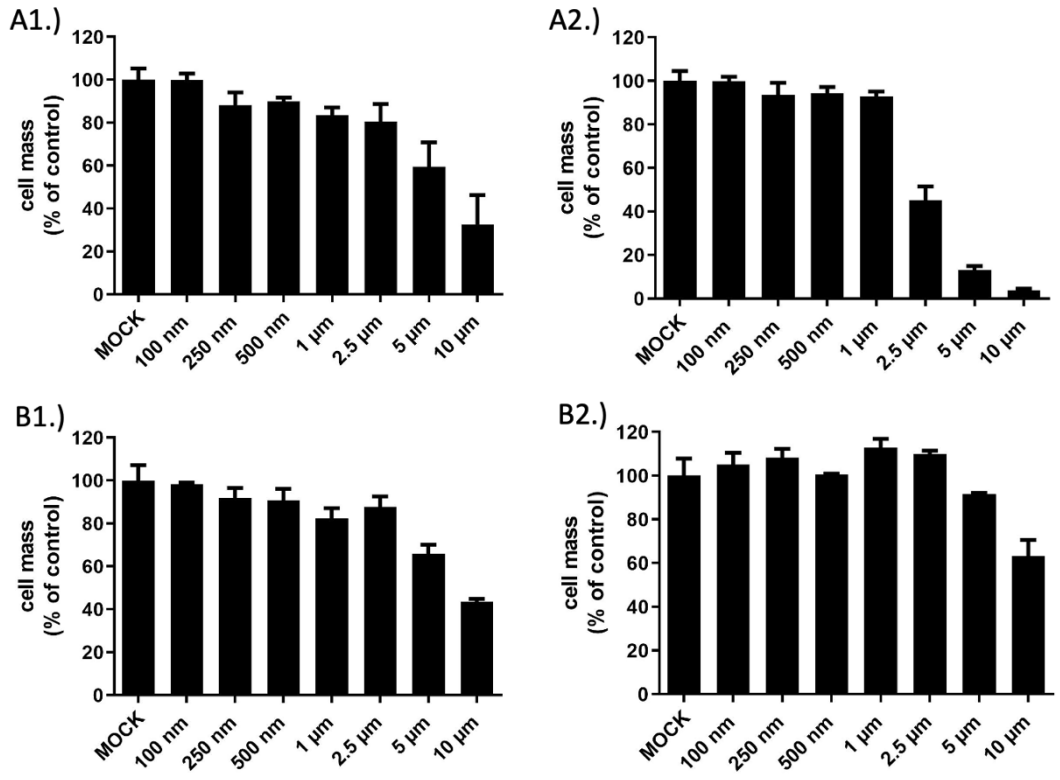

Figure 16: SRB assay of tumor cell lines HT-29 and HCT-116 treated with Skepinone-L.

HT-29 (**A**) and HCT-116 (**B**) were seeded in 24-well plates and treated with Skepinone-L 24 hours post seeding with increasing concentrations (0.1 - 10 µM). SRB assays were performed at 72 (**A1 und B1**) and 96 hpt (**B2 und A2**) (hours post treatment). Experiments were conducted in triplicates. MOCK; untreated control.

HT-29 cells showed cell reduction at Skepinone-L concentrations of 0.1 µM to 1 µM at both 72 and 96 hpt to 80 - 90 %. At 72 hpt cell mass was reduced drastically at 5 µM Skepinone-L to 60 % and at 10 µM to 33 %, while at 96 hpt reduction started at a concentration of 2.5 µM (45 %) with tumor cells almost completely depleted at higher concentrations (5 µM = 13 % and 10 µM = 4 %) (**Figure 16A**).

In HCT-116 cells, cell reduction was observed only at higher Skepinone-L concentrations both at 72 and 96 hpt. Treatment with 5 µM Skepinone-L reduced cell mass to 66 % (72 hpt) and 91 % (96 hpt) and at a concentration of 10 µM Skepinone-L cell mass was reduced to 43 % (72 hpt) and 63 % (96 hpt) (**Figure 16B**).

Based on the same principles applied to determine suitable MeV-GFP concentrations, we used 1 µM and 2.5 µM Skepinone-L in HT-29 cells, 2.5 µM

and 5 μM Skepinone-L in HCT-15 cells and 10 μM Skepinone-L in Hep3B, ACHN and HCT-116 cells in all further combinatorial experiments.

3.4 Cytotoxic effect of MeV-GFP as monotherapy in comparison to combinational treatment with Skepinone-L

To examine the oncolytic effects of MeV-GFP infection in tumor cell lines and possible differences of combinational therapy of MeV-GFP and Skepinone-L SRB assays were performed. Tumor cell lines tested were HCT-15, ACHN, Hep3B, HT-29 and HCT-116. All cell lines were treated with the appropriate MeV-GFP and Skepinone-L concentrations determined previously.

3.4.1 *Cytotoxic effect of combinational treatment of HCT-15 cells with MeV-GFP and Skepinone-L*

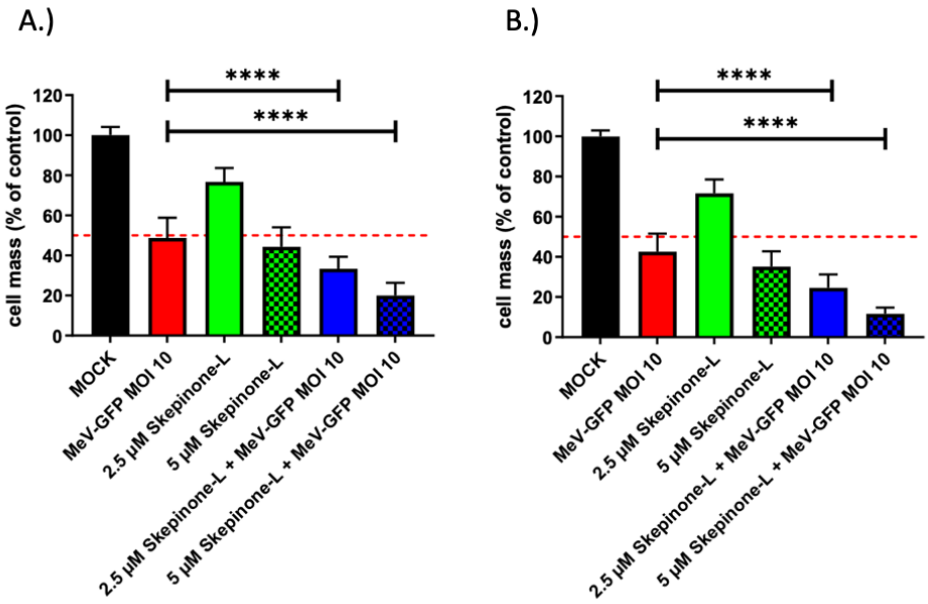

Figure 17: HCT-15 cells infected with MeV-GFP and treated with Skepinone-L.

HCT-15 cells were seeded in 24-well plates and treated 24 hours post seeding with 2.5 μM or 5 μM Skepinone-L or left untreated. 48 hpt (hours post treatment) tumor cells were infected with MeV-GFP at MOI 10 for three hours and afterwards again treated with 2.5 or 5 μM Skepinone-L or left untreated until the time of fixation. SRB assays were performed at 72 (**A**) and 96 hpi (**B**) (hours post infection). Displayed are mean values of three independent experiments performed in quadruplicates. MOCK; untreated control. Statistical significance: ✱✱✱✱: $p \leq 0.0001$

Infection of HCT-15 cells with MeV-GFP at MOI 10 as monotherapy reduced cell mass to 49 % (72 hpi) and 43 % (96 hpi). While the lower concentration of Skepinone-L (2.5 μM) monotherapy resulted in a cell mass of more than 60 % after both time points, the cell mass decreased to 44 % (72 hpi) and 35 % (96 hpi) when HCT-15 cells were treated with Skepinone-L (5 μM) monotherapy. All three different therapy options led to a significant cell mass reduction in HCT-15 cells. When comparing MeV-GFP monotherapy to combinational therapy with MeV-GFP and Skepinone-L, a significant reduction of cell mass was observed (**Figure 17)**. 72 hpi cell mass was reduced to 33 % (2.5 μM Skepinone-L + MeV-GFP MOI 10) and to 20 % (5 μM Skepinone-L + MeV-GFP MOI 10), while 96 hpi cell mass could be reduced even further (25 % after treatment with 2.5 μM Skepinone-L and 12 % after 5 μM Skepinone-L).

3.4.2 Cytotoxic effect of combinational treatment of ACHN cells with MeV-GFP and Skepinone-L

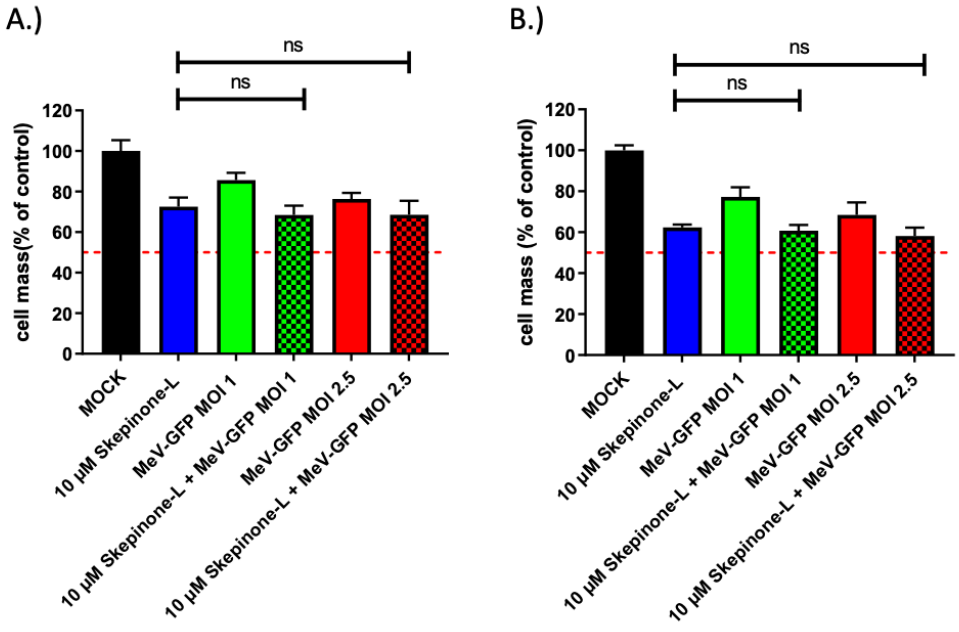

Figure 18: ACHN cells infected with MeV-GFP and treated with Skepinone-L.

ACHN cells were seeded in 24-well plates and treated with Skepinone-L 24 hours post seeding with a concentration of 10 μM or left untreated. 48 hours post treatment, tumor cells were infected with MeV-GFP MOI 1 or MOI 2.5 in Opti-MEM for three hours and afterwards treated with 10 μM Skepinone-L or left untreated until the time of fixation. SRB assays were performed at 72 (**A**) and 96 hpi (**B**) (hours post

infection). Displayed are mean values and SD of two independent experiments 72 hpi and three independent experiments 96 hpi performed in quadruplicates. MOCK; untreated control. Statistical significance: ns: not significant.

ACHN cells were treated with 10 μM Skepinone-L in combination with either MeV-GFP MOI 1 or MOI 2.5 or left untreated. As displayed in **Figure 18,** ACHN cells were reduced to 73 % (72 hpi) and 62 % (96 hpi) when treated with 10 μM Skepinone-L alone. ACHN cells infected with MeV-GFP showed an oncolytic effect which was lower than the Skepinone-L monotherapy. 72 hpi 86 % (MOI 1) respectively 76 % (MOI 2.5) of the infected ACHN cells were still alive, while 96 hpi cell mass of ACHN cells was reduced to 77 % respectively 68 %. However, compared to the Skepinone-L monotherapy the combinational therapy with Skepinone-L and MeV-GFP only reduced the cell mass of ACHN cells slightly to 68 % (10 μM Skepinone-L + MeV-GFP MOI 1) and 67 % (10 μM Skepinone-L + MeV-GFP MOI 2.5) 72 hpi and 61 % (10 μM Skepinone-L + MeV-GFP MOI 1) and 58 % (10 μM Skepinone-L + MeV-GFP MOI 2.5) 96 hpi. The effect of the combinational therapy in comparison to the Skepinone-L monotherapy was not significant (**Figure 18**). Hence, ACHN cells were not tested in any further experiments.

3.4.3 *Cytotoxic effect of combinational treatment of Hep3B cells with MeV-GFP and Skepinone-L*

The following experiments were performed using MeV-GFP MOI 0.01 and 0.025 and 10 μM Skepinone-L as displayed in **Figure 19.**

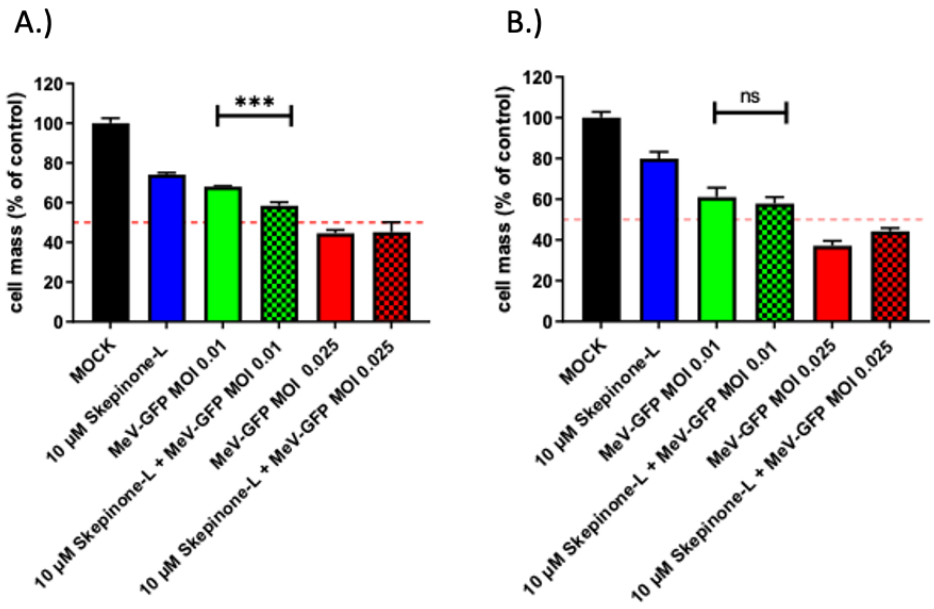

Figure 19: Hep3B cells infected with MeV-GFP and treated with Skepinone-L.

Hep3B cells were seeded in 24-well plates and treated with Skepinone-L 24 hours post seeding with a concentration of 10 µM or left untreated. 48 hours post treatment tumor cells were infected with MeV-GFP MOI 0.01 or MOI 0.025 in Opti-MEM for three hours and afterwards treated with 10 µM Skepinone-L or left untreated until the time of fixation. SRB assays were performed at 72 (**A**) and 96 (**B**) hpi (hours post infection). Displayed are mean values and SD of one experiment performed in quadruplicates. MOCK; untreated control. Statistical significance: ✱✱✱: $p \leq 0.001$; ns: not significant.

Infection of Hep3B cells with MeV-GFP MOI 0.01 reduced the cell mass to 68 % (72 hpi) and 61 % (96 hpi). The combinational treatment with 10 µM Skepinone-L showed a slight cell mass reduction in comparison to the MeV-GFP mono-therapy to 58 % (72 hpi) and 58 % (96 hpi) (**Figure 19).** However, only 72 hpi the combinational treatment proved to have a significant advantage over MeV-GFP monotherapy on Hep3B cells while no significant cell mass reduction could be shown at 96 hpi. The co-treatment of MeV-GFP MOI 0.025 and Skepinone-L did not show a significant cell mass reduction in comparison to single MeV-GFP infection.

3.4.4 *Cytotoxic effect of combinational treatment of HT-29 cells with MeV-GFP and Skepinone-L*

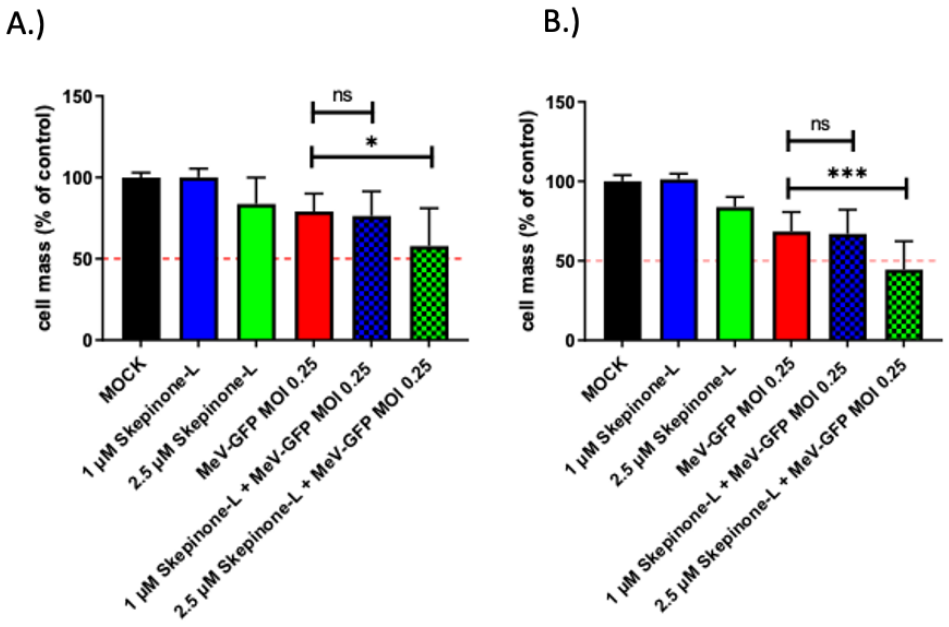

Figure 20: HT-29 cells infected with MeV-GFP and treated with Skepinone-L.

HT-29 cells were seeded in 24-well plates and treated with Skepinone-L 24 hours post seeding with a concentration of 1 µM, 2.5 µM or left untreated. 48 hours post treatment tumor cells were infected with MeV-GFP MOI 0.25 in Opti-MEM for three hours and afterwards treated with 1 µM, 2.5 µM Skepinone-L or left untreated until the time of fixation. SRB assays were performed at 72 (**A**) and 96 hpi (**B**) (hours post infection). Displayed are mean values and SD of two independent experiments performed in quadruplicates. MOCK; untreated control. Statistical significance: ✱: $p \leq 0.05$; ✱✱✱: $p \leq 0.001$; ns: not significant.

Infection with MeV-GFP alone reduced the tumor cell mass to 79 % (72 hpi) and 68 % (96 hpi). Monotherapy with 1 µM Skepinone-L did not reduce the tumor cell mass at either 72 hpi or 96 hpi (**Figure 20**). However, treatment with a concentration of 2.5 µM Skepinone-L resulted in a reduction of tumor cell mass to 84 % (72 hpi and 96 hpi). The combinational treatment showed a significant reduction of cell mass when using 2.5 µM Skepinone-L and MeV-GFP MOI 0.25 in comparison to each monotherapy; at 72 hpi only 58 % of cells were detectable and 44 % at 96 hpi. The combinational treatment of MeV-GFP MOI

0.25 and 1 μM Skepinone-L only showed slight cell mass decrease at 72 hpi (76 %) and 96 hpi (67 %).

3.4.5 *Cytotoxic effect of combinational treatment of HCT-116 cells with MeV-GFP and Skepinone-L*

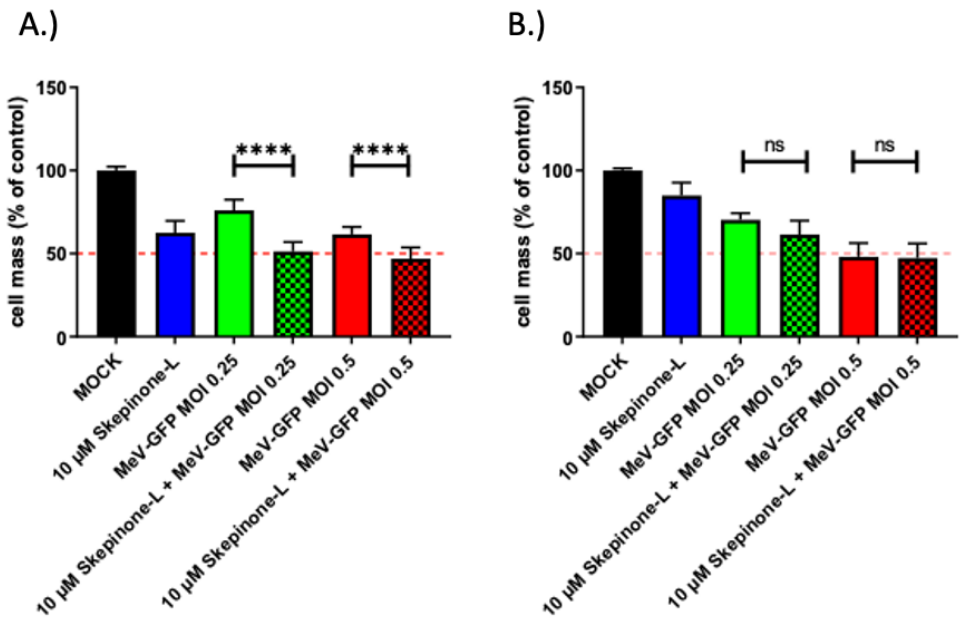

Figure 21: HCT-116 cells infected with MeV-GFP and treated with Skepinone-L.

HCT-116 cells were seeded in 24-well plates and treated with Skepinone-L 24 hours post seeding with a concentration of 10 μM or left untreated. 48 hours post treatment tumor cells were infected with MeV-GFP MOI 0.25 or 0.5 in Opti-MEM for three hours and afterwards treated with 10 μM Skepinone-L until the time of fixation. SRB assays were performed at 72 (**A**) and 96 hpi (**B**) (hours post infection). Displayed are mean values and SD of two independent experiments performed in quadruplicates. MOCK; untreated control. Statistical significance: ✱✱✱✱: $p \leq 0.0001$; ns: not significant.

HCT-116 cells were treated with 10 μM Skepinone-L or left untreated and were then infected with MeV-GFP MOI 0.25, MOI 0.5 or left untreated (**Figure 21)**.

Treatment with 10 μM Skepinone-L reduced the cell mass of HCT-116 cells to 63 % (72 hpi) and 84 % (96 hpi). HCT-116 cell viability (72 hpi) of the combination therapy with the lower viral dose (MOI 0.25) decreased significantly

(51 %) in comparison to HCT-116 cells infected with MeV-GFP as monotherapy (71 %). A similar oncolytic advantage (72 hpi) could be shown in HCT-116 cells infected with the higher viral doses (MOI 0.5) and Skepinone-L (10 µM) with a cell viability of 47 %, while MeV-GFP monotherapy (MOI 0.5) led to a cell viability of 62 %. Unfortunately, though the combinational approach showed slight advantages at 96 hpi, no significant cell mass reduction could be detected in comparison to MeV-GFP monotherapy in both tested MOI.

3.5 Monitoring of real time dynamic cell proliferation of tumor cell lines treated with MeV-GFP and/or Skepinone-L via xCELLigence®

To examine the real time cell proliferation of untreated or single treated cells in comparison to the impact of co-treatment of Skepinone-L and MeV-GFP over time and not only after certain fixed time points the xCELLigence® RTCA system was used. As colon cell lines proved to be the more susceptible to combinational therapy with MeV-GFP and Skepinone-L, only HT-29, HCT-116 and HCT-15 cell lines were monitored via xCELLigence assay. The aim was to examine the cell proliferation over time and to analyse the effect of MeV-GFP and Skepinone-L on tumor cells.

A.)

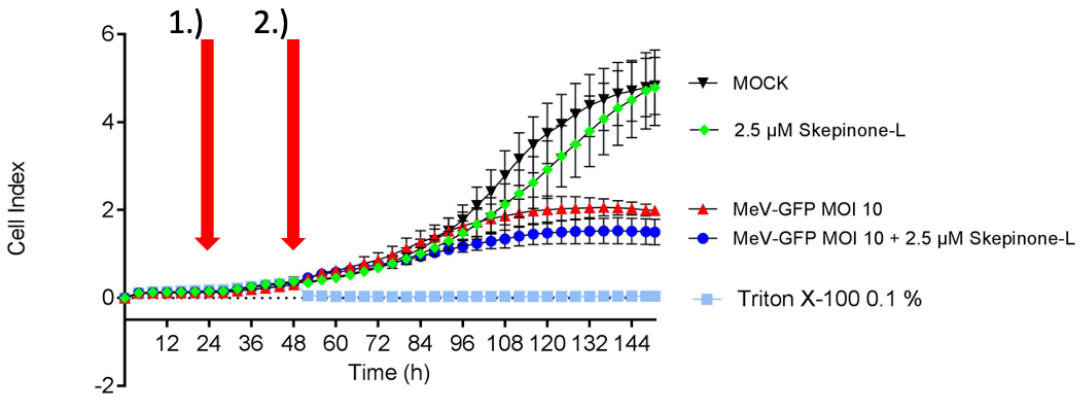

B.)

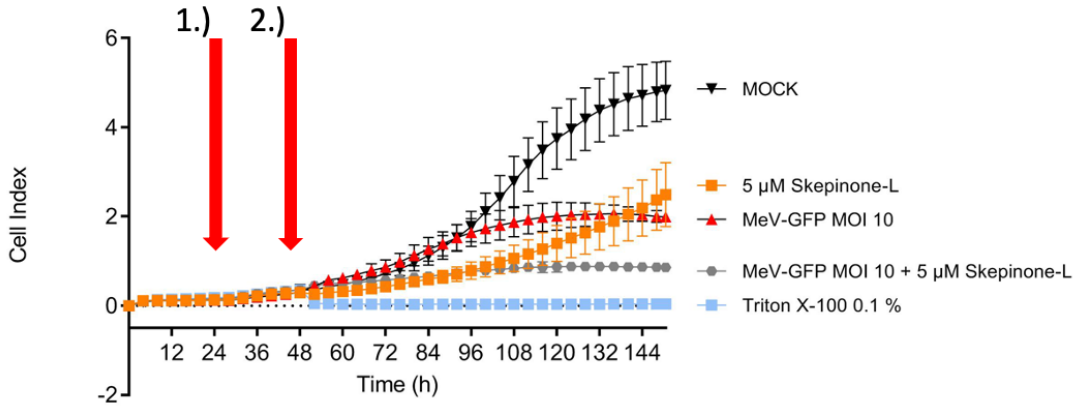

Figure 22: Real-time dynamic cell proliferation of HCT-15 cells using xCELLigence® RTCA system.

HCT-15 cell proliferation was monitored for 150 hours after treatment with 2.5 µM (**A**) or 5 µM (**B**) Skepinone-L and/or infection with MeV-GFP (MOI 10). Measurements were taken every 30 min during the experiment. Arrows are indicating the time of treatment with Skepinone-L (**1**) (24 hours) and the infection with MeV-GFP (**2**) (48 hours). Controls were left untreated (MOCK) or only treated by either Skepinone-L or MeV-GFP. The cell treatment with Triton X-100 was performed 48 hours after starting the experiment and used as control. Displayed are mean values and SD of two independent experiments performed in quadruplicates.

HCT-15 cells that were treated with 2.5 µM Skepinone-L as well as cells which left untreated (MOCK) showed a continuous growth up to a cell index of 4.8

after 150 hours (**Figure 22A**). HCT-15 cells treated with 5 μM Skepinone-L showed a continuous slower growth (cell index = 2.5 after 150 hours). Infection with MeV-GFP (MOI 10) further reduced cell growth with a measurable impedance of cell index = 2.0 (**Figure 22B**). Consistent with the SRB data, combinational therapy of Skepinone-L and MeV-GFP infection resulted in the most severe attenuation of cell growth with impedance values of cell index = 1.5 (2.5 μM Skepinone-L plus MeV-GFP MOI 10) and cell index = 0.86 (5 μM Skepinone-L plus MeV-GFP MOI 10).

Furthermore, the xCELLigence assay was conducted with HT-29 cells treated with 1 μM Skepinone-L and/or infected with MeV-GFP, Triton X-100 or left untreated (MOCK) (**Figure 23**).

(A)

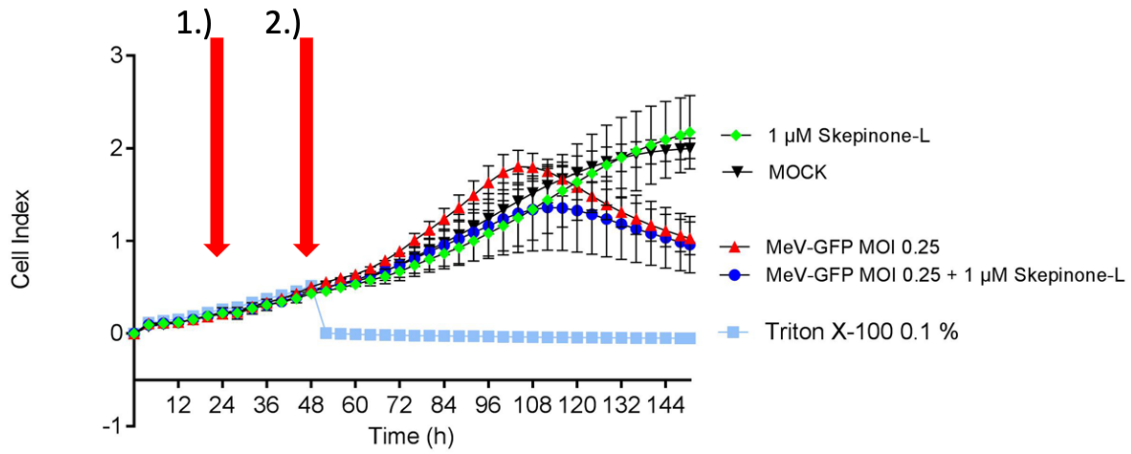

(B)

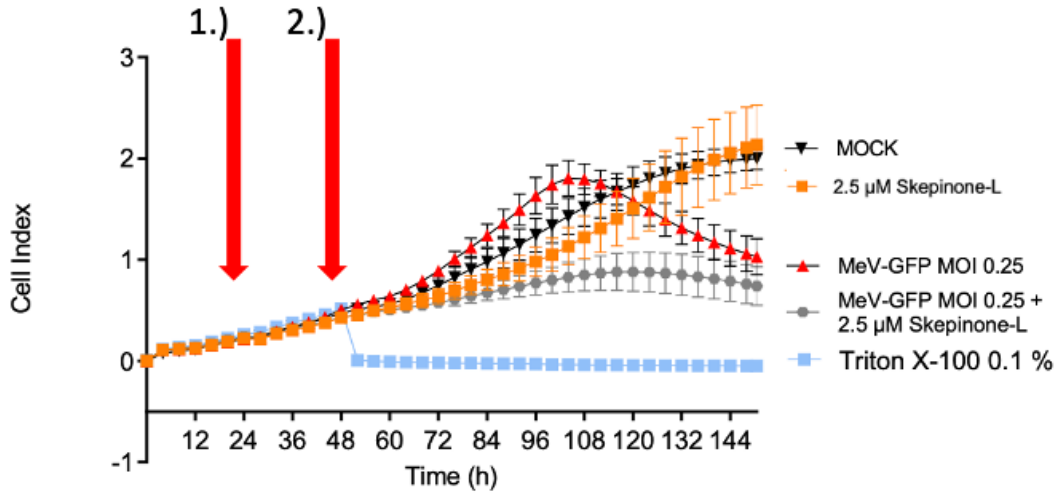

Figure 23: Real-time dynamic cell proliferation of HT-29 cells using xCELLigence® RTCA system.

HT-29 cell proliferation was monitored for 150 hours after treatment with 1 µM (**A**) or 2.5 µM (**B**) Skepinone-L and/or infection with MeV-GFP (MOI 0.25). Measurements were taken every 30 min during the experiment. Arrows are indicating the time of treatment with Skepinone-L (**1**) (24 hours) and the infection with MeV-GFP (**2**) (48 hours). Controls were left untreated (MOCK) or only treated by either Skepinone-L or MeV-GFP. Cell treatment with Triton X-100 was performed 48 hours after starting the experiment. Displayed are mean values and SD of two independent experiments performed in quadruplicates.

When comparing SRB data and xCELLigence® results, HT-29 cells showed similar effects in terms of cell growth under infection (MeV-GFP) and Skepinone-L treatment. Untreated HT-29 cells and cells treated only with 1 µM

Skepinone-L were growing constantly over the time period up to a cell index of 2.2 (Skepinone-L) and 2 (MOCK) **(Figure 23A).** MeV-GFP infected HT-29 cells showed an increase in cell mass up to a cell index of 1.8 at 104 hours post seeding before the virus showed its effect and the cell mass was reduced to a cell index of 1.03 (144 hours). HT-29 cells treated with Skepinone-L and MeV-GFP had their peak later after 112 hours (cell index = 1.36) but decreased to a cell index = 0.96 after 150 hours revealing only a slight difference of cell mass 96 hpi in the corresponding SRB assay.

The same experiment was performed with 2.5 μM Skepinone-L treatment and MeV-GFP MOI 0.25 infection of HT-29 cells **(Figure 23B).** The graphs of untreated HT-29 cells (MOCK) and cells treated with 2.5 μM Skepinone-L showed continuous cell growth. The co-treated HT-29 showed a higher cell reduction when treated with 2.5 μM Skepinone-L (cell index = 0.74) than with 1 μM Skepinone-L after 150 hours (cell index = 0.96) in comparison to HT-29 cells infected only with MeV-GFP MOI 0.25 (cell index = 1.03).

In addition, the xCELLigence assay was conducted with HCT-116 cells treated with 10 μM Skepinone-L and/or infected with MeV-GFP (MOI 0.25), Triton X-100 or left untreated (MOCK) (**Figure 24**).

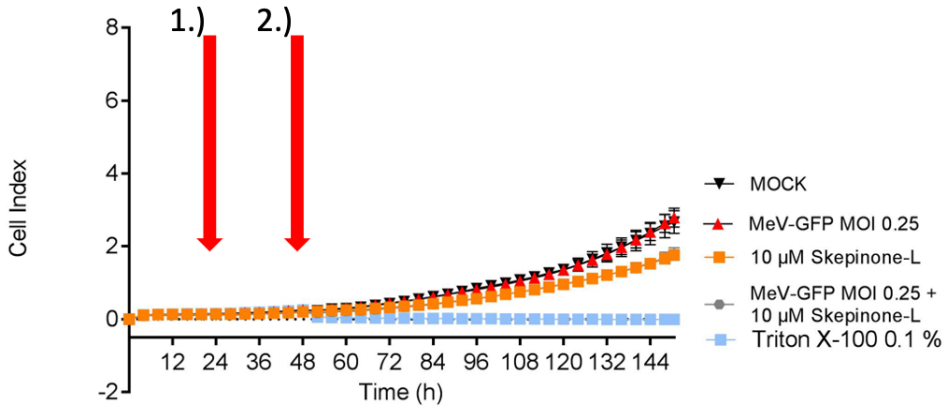

Figure 24: Real-time dynamic cell proliferation of HCT-116 cells using xCELLigence® RTCA system.

HCT-116 cell proliferation was monitored for 150 hours after treatment with 10 µM Skepinone-L and/or infection with MeV-GFP (MOI 0.25). Measurements were taken every 30 min during the experiment. Arrows are indicating the time of treatment with Skepinone-L (**1**) (24 hours) and the infection with MeV-GFP (**2**) (48 hours). Controls were left untreated (MOCK) or only treated by either Skepinone-L or MeV-GFP. The cell treatment with Triton X-100 was performed 48 hours after starting the experiment. The experiment was performed in triplicates.

HCT-116 cells were examined performing a xCELLigence® assay but only one concentration of Skepinone-L and MeV-GFP was tested (**Figure 24)**. Both MOCK (cell index = 2.67) and MeV-GFP MOI 0.25 infected HCT-116 cells (cell index = 2.79) showed continuous growth until 150 hours. Interestingly, this did not match the results found in the SRB assay, which showed significant reduction of cell mass of HCT-116 cells after viral infection even with monotherapy. The xCELLigence® assay did show a decrease in cell mass when HCT-116 cells were co-treated (cell index = 1.79) in comparison to monotherapy with MeV-GFP after 150 hours, however, the Skepinone-L monotherapy proved to be just as effective (cell index = 1.76), which is not consistent with previous results.

3.6 Fluorescence imaging of tumor cell lines treated with MeV-GFP and/or Skepinone-L

Since the measles vaccine virus construct used here carries the green fluorescent protein (GFP) as a marker gene, successful infection can be detected by fluorescence imaging. A stronger fluorescence signal corresponds to a higher amount of virus particles in examined wells. Fluorescence images of the cell lines HCT-15 (**Figure 25**), ACHN (**Figure 26**), Hep3B (**Figure 27**), HT-29 (**Figure 28**) and HCT-116 (**Figure 29**) 96 hpi with MeV-GFP were obtained (3.5.1-3.5.5).

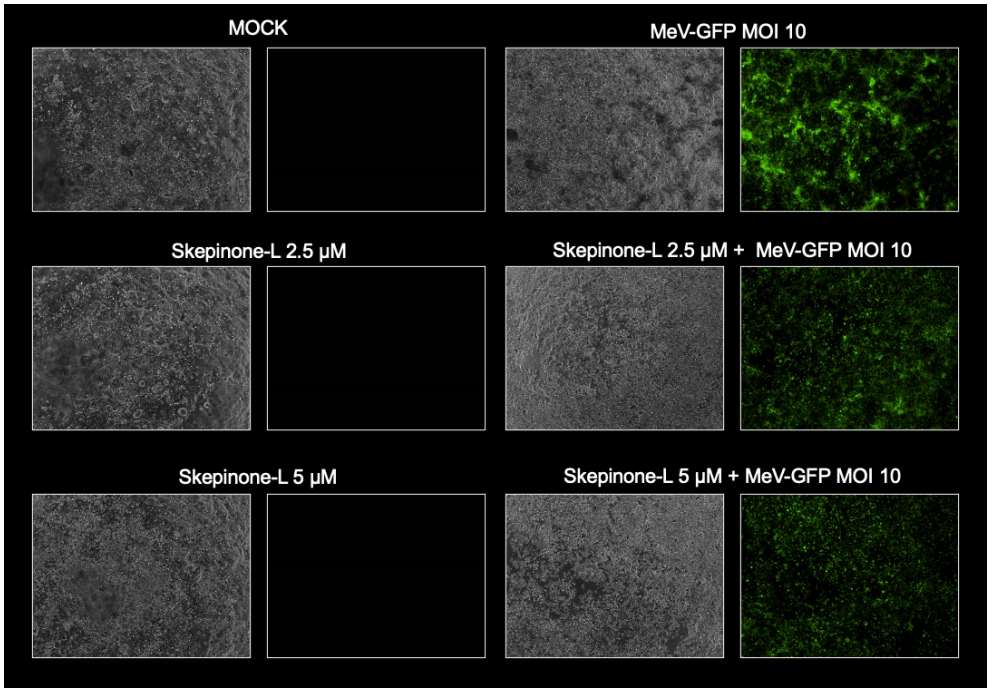

Figure 25: Fluorescence imaging of HCT-15 cells.

HCT-15 cells were seeded in 24-well plates and 24 hours post seeding treated with Skepinone-L 2.5 µM, 5 µM, or left untreated. 48 hours post treatment, HCT-15 cells were infected with MeV-GFP MOI 10 (or MOCK) in OPTI-Mem for three hours and afterwards treated with Skepinone-L 2.5 µM, 5 µM L or left untreated. Fluorescence imaging was performed 96 hpi.

Fluorescence imaging of HCT-15 cell showed viral infection in HCT-15 cells infected only with MeV-GFP MOI 10. In comparison to the combinational treatment of HCT-15 cells with 2.5 µM Skepinone-L and MeV-GFP MOI 10, the combinational approach with 5 µM Skepinone-L and MeV-GFP MOI 10 showed less GFP signal.

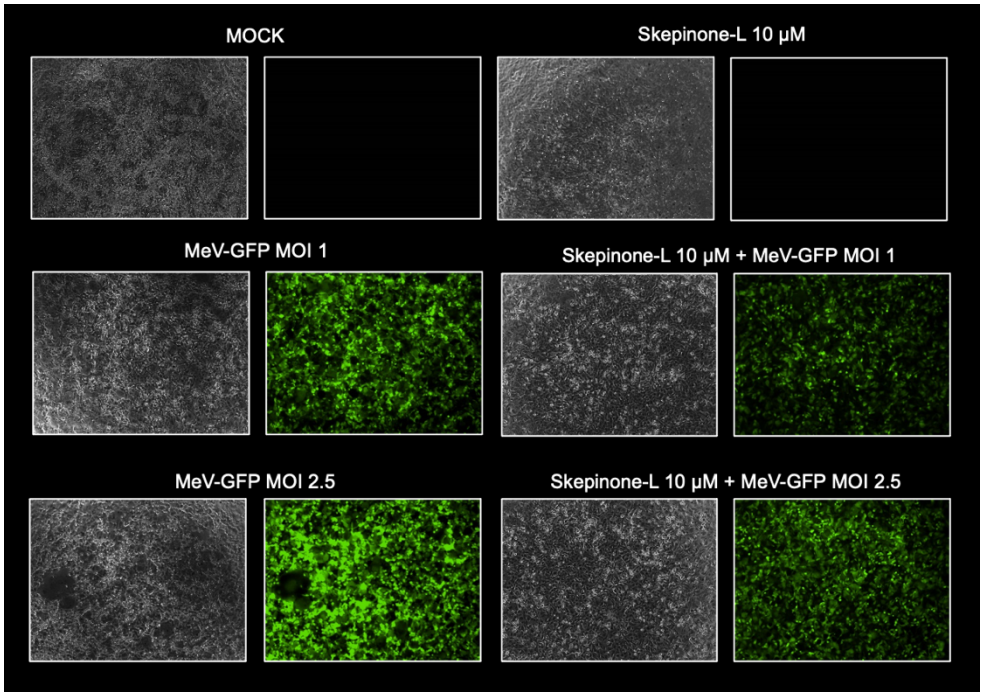

Figure 26: Fluorescence imaging of ACHN cells.

ACHN cells were seeded in 24-well plates and treated 24 hours post seeding with Skepinone-L 10 µM or left untreated. 48 hours post treatment, tumor cells were infected with MeV-GFP MOI 1 or MOI 2.5 in Opti-MEM for three hours and afterwards treated with 10 µM Skepinone-L or left untreated. Fluorescence imaging was performed after 96 hpi.

Fluorescence imaging of ACHN cells showed an increased viral infection in ACHN cells infected with a higher MOI (2.5) in comparison to MOI 1. In combination with Skepinone-L 10 µM the GFP signal decreased in both approaches with different viral concentrations.

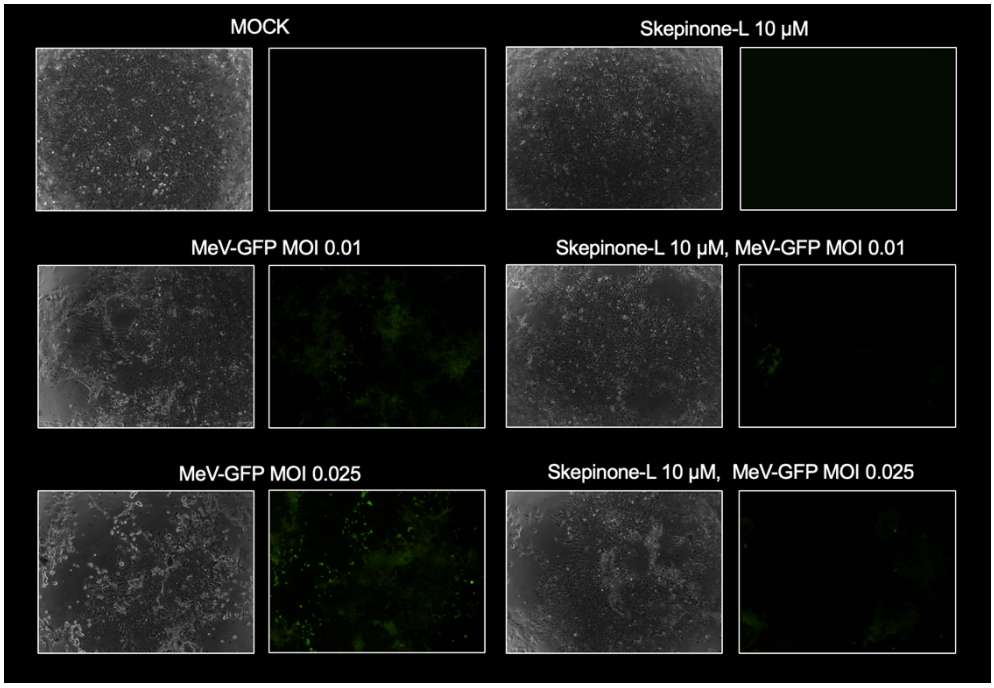

Figure 27: Fluorescence imaging of Hep3B cells.

Hep3B cells were seeded in 24-well plates and 24 hours post seeding treated with Skepinone-L 10 µM or left untreated. 48 hours post treatment, Hep3B cells were infected with MeV-GFP MOI 0.01 or MOI 0.025 (or MOCK) in OPTI-Mem for three hours and afterwards treated with Skepinone-L 10 µM or left untreated. Fluorescence imaging was performed 96 hpi.

Fluorescence imaging of Hep3B cells showed viral infection in both MeV-GFP concentrations (MOI 0.01 and MOI 0.025). In both combinational treatments the GFP signal decreased drastically.

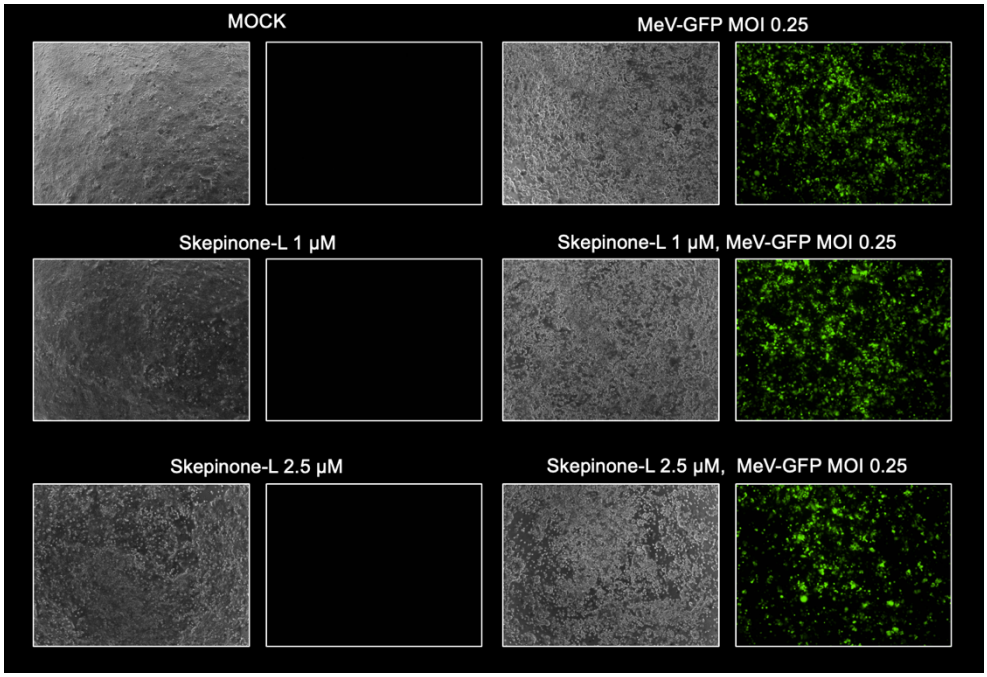

Figure 28: Fluorescence imaging of HT-29.

HT-29 cells were seeded in 24-well plates and 24 hours post seeding treated with Skepinone-L 1 µM, 2.5 µM or left untreated. 48 hours post treatment, HT-29 cells were infected with MeV-GFP MOI 0.25 (or MOCK) in OPTI-Mem for three hours and afterwards treated with Skepinone-L 1 µM, 2.5 µM or left untreated. Fluorescence imaging was performed 96 hpi.

Fluorescence imaging of HT-29 infected with MeV-GFP showed a viral infection comparable or slightly increased to the combinational treatment with Skepinone-L 1 µM and MeV-GFP MOI 0.25. While fluorescence imaging of HT-29 cells treated with Skepinone-L 2.5 µM and MeV-GFP MOI 0.25 showed less or comparable GFP signal.

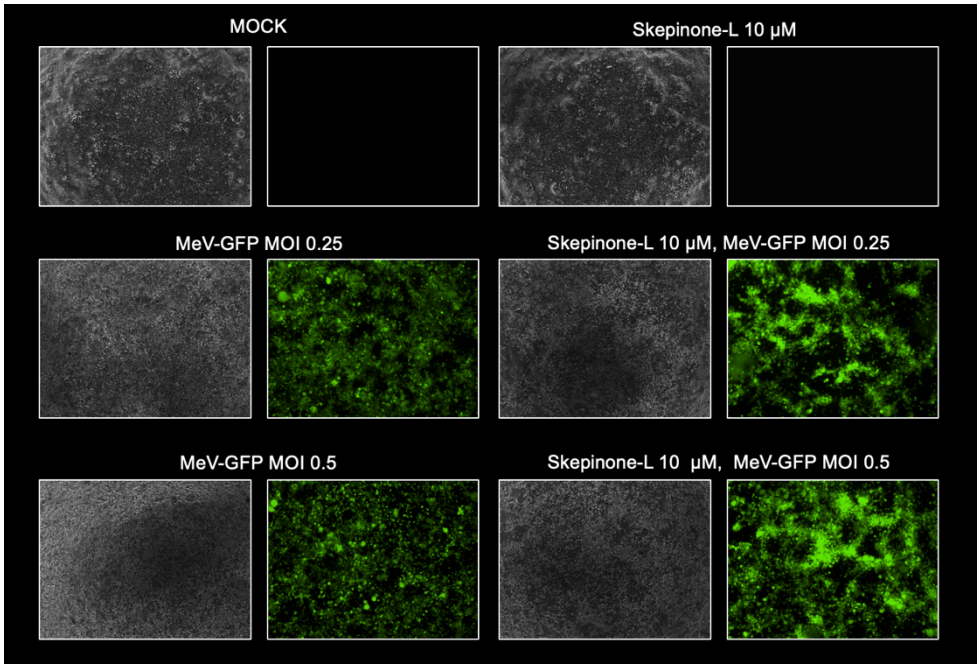

Figure 29: Fluorescence imaging of HCT-116.

HCT-116 cells were seeded in 24-well plates and 24 hours post seeding treated with Skepinone-L 10 µM or left untreated. 48 hours post treatment, HCT-116 cells were infected with MeV-GFP MOI 0.25 or MOI 0.5 (or MOCK) in OPTI-Mem for three hours and afterwards treated with 10 µM Skepinone-L or left untreated. Fluorescence imaging was performed 96 hpi.

Fluorescence imaging of HCT-116 showed an increased viral infection of the combinational treatment with MeV-GFP (MOI 0.25 and MOI 0.5) and Skepinone-L 10 µM in comparison to MeV-GFP monotherapy (MOI 0.25 and MOI 0.5). Interestingly the patterns of HCT-116 and HT-29 cells were in contradiction to the other tested cell lines.

Most cell lines showed a similar pattern of GFP signals during these experiments. HCT-15, ACHN and Hep3B showed a higher GFP signal when infected with MeV-GFP in comparison to cells infected with MeV-GFP and treated with Skepinone-L. A reason for this phenomenon could be the increased cell death of tumor cells treated with the combinational therapy, possibly caused by an increased oncolytic effect of MeV-GFP. This could lead to a detection of less GFP signal, because there would be less tumor cells to be infected. HCT-15 and HT-29 (HT-29 only when treated with 2.5 µM Skepinone-L) did show a decreased cell mass in SRB assays when treated with the combinational

approach, while ACHN, Hep3B and HCT-116 did not show a significant cell mass reduction at 96 hpi in comparison to the monotherapy of MeV-GFP or Skepinone-L (ACHN).

3.7 Immunoblot analysis of p38α MAPK signaling of tumor cells after co-treatment with MeV-GFP and Skepinone-L

p38α MAPK signaling is thought to be an important factor in the anti-viral response mechanisms of cells inducing IFN release (Jiang et al. 2015). The effect of Skepinone-L on the p38α MAPK was already proven by Koeberle et al. and Rudalska et al. (Koeberle et al. 2011; Rudalska et al. 2014) using the downstream enzyme p-HSP27 and HSP27 as marker for enzyme activation. The detection of p-HSP27 and HSP27 in the immunoblot can provide information about the activity of p38α MAPK. Detection of phosphorylated HSP27 indicated an active p38α MAPK. The treatment of tested tumor cells with Skepinone-L should therefore minimize the detection of p-HSP27 indicating a blocked p38α MAPK signaling pathway. To examine the inhibition of this pathway by Skepinone-L, a immunoblot was performed with cell extracts obtained from HCT-15, Hep3B and HCT-116 cells treated with MeV-GFP and/or Skepinone-L to detect p-HSP27 and HSP27.

Samples used for immunoblotting were collected from cell lines treated with the respective concentrations of Skepinone-L and MeV-GFP previously shown to be effective in the SRB assays at four different time points (24, 48, 72 and 96 hpi). A stronger band indicates a higher concentration of the detected enzyme in the examined cells under a certain treatment. A slim or non-existent band indicated the lack of p-HSP27/HSP27 protein expression in examined cells.

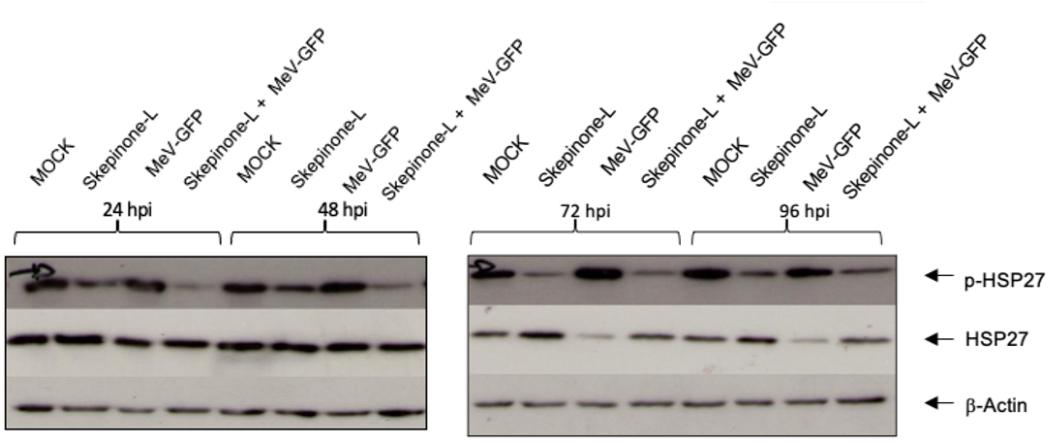

Figure 30: Detection of p-HSP27 and HSP27 in HCT-15 cells treated with Skepinone-L and/or infected with MeV-GFP.

HCT-15 cells were grown for 24 hours and then treated with 2.5 μM Skepinone-L or left untreated. After 48 hours post seeding Hep3B cells were infected with MeV-GFP MOI 10 or left untreated for three hours in Opti-MEM. After three hours HCT-15 cells were treated with 2.5 μM Skepinone-L or left untreated. Whole cellular protein extraction was performed at 24, 48, 72, and 96 hpi and immunoblots were conducted by using p-HSP27 or HSP27 antibodies. β-actin was used as a loading control. MOCK; untreated control.

HCT-15 cells showed a strong p-HSP27 band when MOCK treated at 24, 48, 72 and 96 hpi (**Figure 30**). The samples of HCT-15 cells infected with MeV-GFP also showed strong p-HSP27 bands at all tested time points. This indicates that in MOCK treated and MeV-GFP infected cells the p38α MAPK is functional because the downstream substrate (phosphorylated HSP-27) could be detected in all samples. In comparison, samples of HCT-15 cells treated with Skepinone-L showed thinner bands (24, 48, 72 and 96 hpi). The same effect could be observed comparing samples of HCT-15 cells infected with MeV-GFP and HCT-15 cells co-treated with MeV-GFP and Skepinone-L. The samples of the co-treated HCT-15 cells showed thinner bands than samples of HCT-15 cells infected with MeV-GFP. The thinner band of p-HSP27 in HCT-15 cells treated with Skepinone-L indicates a reduced activity of p38α MAPK in these cells (Skepinone-L monotherapy and co-treated HCT-15 cells). Therefore, the correct function of Skepinone-L as p38α MAPK inhibitor could be proven in HCT-15 cells.

HSP27 bands in HCT-15 cells did not show any differences (strong bands) regardless of the treatment (24 and 48 hpi). At 72 and 96 hpi the thinnest HSP27 band were seen in samples of HCT-15 cells infected only with MeV-GFP. β-Actin was used as loading control and proved that the amount of protein used in samples did not vary as displayed in **Figure 30**.

Although Hep3B cells showed only slight oncolytic effects in the SRB assay after co-treatment with Skepinone-L and MeV-GFP in comparison to MeV-GFP monotherapy, a immunoblot was performed to show the effect of Skepinone-L in combination with MeV-GFP on another tumor cell entity (Hep3B = hepato-cellular carcinoma) (**Figure 31**).

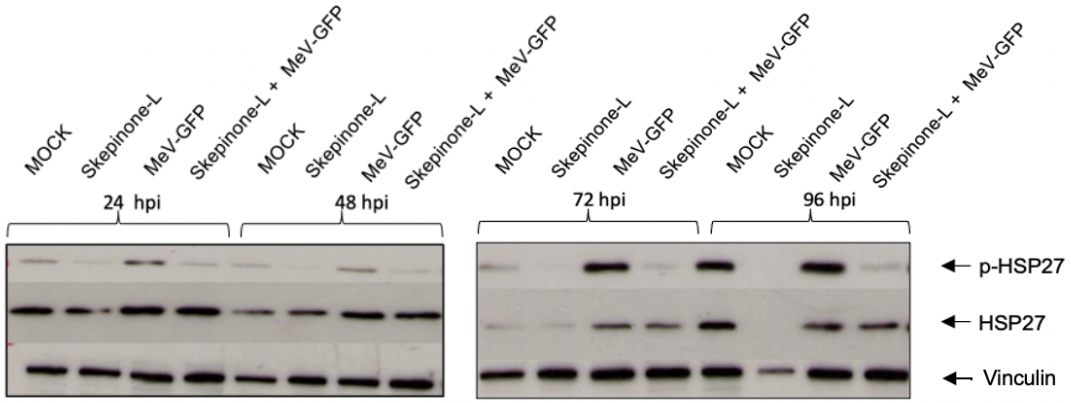

Figure 31: Detection of p-HSP27 and HSP27 in Hep3B cells treated with Skepinone-L and/or infected with MeV-GFP.

Hep3B cells were grown for 24 hours and then treated with 10 μM Skepinone-L or left untreated. After 48 hours post seeding Hep3B cells were infected with MeV-GFP MOI 0.01 or left untreated for three hours in Opti-MEM. After three hours, Hep3B cells were treated with 10 μM Skepinone-L or left untreated. Whole cellular protein extraction was performed at 24, 48, 72, and 96 hpi and immunoblots were conducted by using p-HSP27 or HSP27 antibodies. *Vinculin was used as a loading control. MOCK; untreated control.*

Hep3B cells responded weaker to MeV-GFP infection in comparison to HCT-15 cells in terms of p38α MAPK signaling, resulting in thinner bands of p-HSP27 in the immunoblots, particularly at 24 and 48 hpi. However, even at these time points, the differences between the treatments are clearly visible. Hep3B cells that were infected with MeV-GFP showed stronger bands in p-HSP27 expression indicating an increase of p38α MAPK signaling in Hep3B cells and

therefore its importance to the immune response of Hep3B cells. The observation that in co-treated tumor cells the p-HSP27 bands were weaker compared to MeV-GFP infected cells indicates that Skepinone-L does inhibit the p38α-MAPK signaling pathway when co treated. At 72 and 96 hpi this effect was even more pronounced as bands of p-HSP27 were a lot stronger compared to 24 and 48 hpi. At all time points, an effect of Skepinone-L in p38α MAPK signaling in terms of phosphorylation of HSP27 could be seen in comparison to the MOCK control. Regardless of the treatment the HSP27 bands 24 and 48 hpi were of comparable size. In comparison, the MOCK and Skepinone-L bands (HSP27) at 72 hpi were thinner. At 96 hpi the MOCK band of HSP27 was again comparable to 24 and 48 hpi MOCK bands but the 96 hpi Skepinone-L band was non-existent. Vinculin was used as positive control and showed that the amount of protein applied did not vary between samples, except for the 96 hpi band of Hep3B cells treated with Skepinone-L only.

In a further step, immunoblots were also performed with HCT-116 cells, as this tumor cell line responded quite well to the combinatorial treatment of Skepinone-L plus MeV-GFP in SRB-Assays (**Figure 32**).

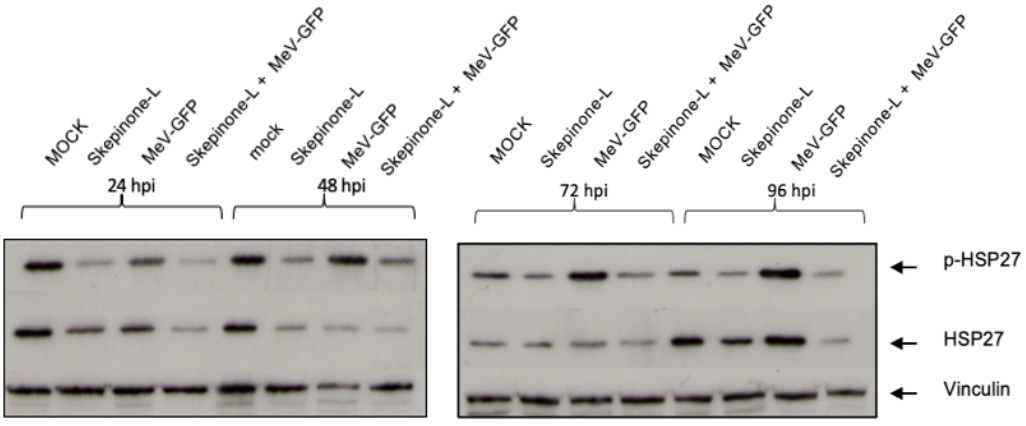

Figure 32: Detection of p-HSP27 and HSP27 in HCT-116 cells treated with Skepinone-L and/or infected with MeV-GFP.

HCT-116 cells were grown for 24 hours and then treated with 10 μM Skepinone-L or left untreated. After 48 hours post seeding Hep3B cells were infected with MeV-GFP MOI 0.025 or left untreated for three hours in Opti-MEM. After three hours HCT-116 cells were treated with 10 μM Skepinone-L or left untreated. Whole cellular protein extraction was performed at 24, 48, 72, and 96 hpi and immunoblots were conducted by using p-HSP27 or HSP27 antibodies. Vinculin was used as a loading control. *MOCK; untreated control.*

Immunoblots with HCT-116 cells showed similar effects compared to the two previously described tumor cell lines and demonstrated the effect of Skepinone-L both in monotherapy and in co-treatment with MeV-GFP on inhibition of the p38α MAPK signaling pathway. In **Figure 32** the strongest bands of p-HSP27 expression were produced in HCT-116 cells infected only with MeV-GFP especially at 48 to 96 hpi, while the band of the co-treated cells proved again to be thin and showed the inhibiting effect of Skepinone-L on p38α MAPK signaling. Vinculin showed as loading control that an equal amount of protein from each sample was used.

3.8 Quantification of virus replication in tumor cell lines to examine the effect of the p38α MAPK inhibitor Skepinone-L on MeV-GFP

Next, the effect of Skepinone-L on the viral replication of MeV-GFP was examined by quantification of virus particles in tumor cells by viral titration. This was important because it may show that the cytotoxic effect of Skepinone-L is caused by inhibition of the p38α MAPK signaling pathway, allowing MeV-GFP to replicate more efficiently, which subsequently leads to enhanced tumor cell lysis. Hence, cells were treated and infected as described previously (**Figure 8, 2.2.4.1**) and cell lysates and supernatants of tumor cell lines were harvested at 3, 24, 48, 72 and 96 hpi. Experiments were performed using the cell lines HCT-15 (**Figure 33**) and HT-29 (**Figure 34**). For each tumor cell line the single infection of MeV-GFP was compared to the co-treatment with Skepinone-L and MeV-GFP.

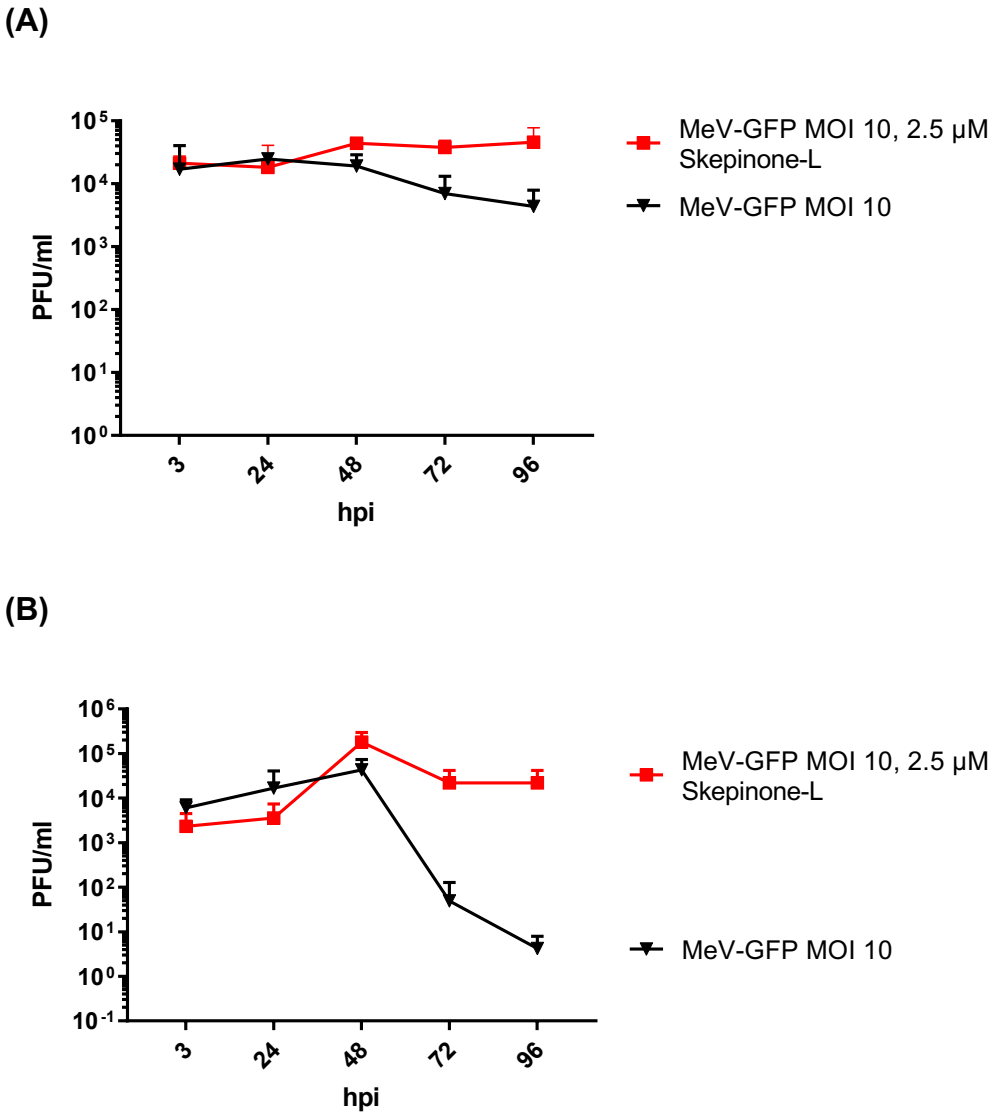

Figure 33: Viral growth curves of MeV-GFP infected and Skepinone-L plus MeV-GFP treated HCT-15 cells.

HCT-15 cells were treated with 2.5 µM Skepinone-L or left untreated and infected with MeV-GFP MOI 10. At 3, 24, 48, 72 and 96 hpi cell lysates (**A**) and supernatants (**B**) of the treated HCT-15 cells were taken. Samples were titrated on Vero cells to determine the number of viral particles (PFU/ml). Displayed are mean values of three independent experiments.

In HCT-15 cells co-treated with Skepinone-L and MeV-GFP a higher virus replication could be observed in cell lysates compared to MeV-GFP infected cells starting at 48 hpi. The calculated PFU/ml were 4.4 x 10^4 PFU/ml (48 hpi), 3.8 x 10^4 PFU/ml (72 hpi) and 4.6 x10^4 PFU/ml (96 hpi) after co-treatment in comparison to 1.9 x 10^4 PFU/ml (48 hpi), 7 x 10^3 PFU/ml (72 hpi) and 4.4 x 10^4 PFU/ml (96 hpi) after infecting cells only with MeV-GFP. While the viral

replication remains constant in co-treated HCT-15 cells, the viral replication decreases drastically in HCT-15 cells infected only with MeV-GFP (**Figure 33A**).

In the supernatants of HCT-15 cells this effect was also shown starting after 48 hpi (4.3 x 10^4 PFU/ml). Viral release decreased dramatically at 72 hpi (49 PFU/ml) and at 96 hpi (4 PFU/ml) when infected with MeV-GFP alone, while co-treated HCT-15 cells showed stable viral replication at 72 and 96 hpi (2.2 x 10^4 PFU/ml) after peaking at 48 hpi (1.8 x 10^5 PFU/ml) (**Figure 33B**).

(A)

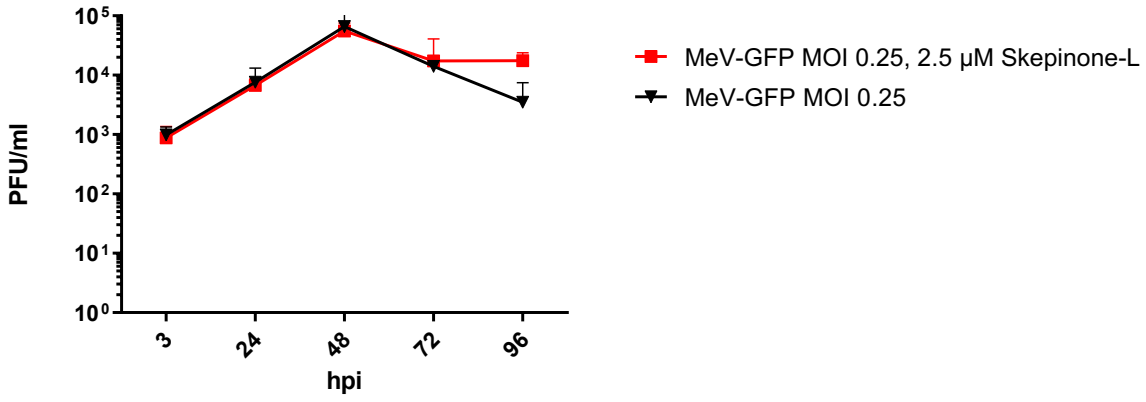

(B)

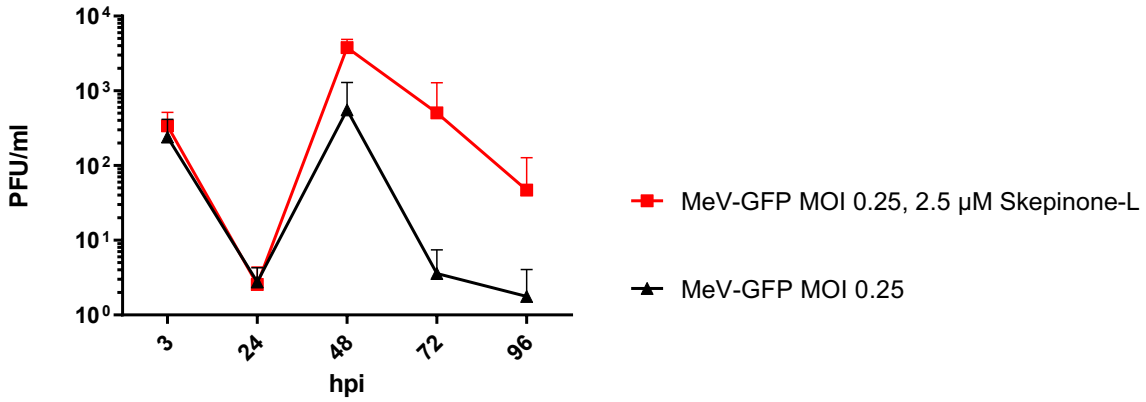

Figure 34: Viral growth curves of MeV-GFP infected and Skepinone-L plus MeV-GFP treated HT-29 cells.

HT-29 cells were treated with 2.5 µM Skepinone-L or left untreated and infected with MeV-GFP MOI 0.25. At 3, 24, 48, 72 and 96 hpi cell lysates (**A**) and supernatants (**B**) of the treated HT-29 cells were taken.

Samples were titrated on Vero cells to determine the number of viral particles (PFU/ml). Displayed are mean values of three independent experiments.

The viral titer in HT-29 cell lysate 3, 24, 48, 72 hpi were not significantly changed by the addition of Skepinone-L in comparison to MeV-GFP monotherapy. However, at 96 hpi, a considerable difference in viral replication could be seen in HT-29 cells (cell lysate) when co-treated with Skepinone-L and MeV-GFP (1.76 $x10^4$ PFU/ml) in comparison to HT-29 cells infected only with MeV-GFP (3.5 $x10^3$ PFU/ml) (**Figure 34A**). In supernatant of HT-29 the viral titer at 48 hpi differed in co-treated HT-29 cells (3.8 x 10^3 PFU/ml) compared to MeV-GFP infected HT-29 cells (558 PFU/ml). Viral titers were significantly reduced at 72 and 96 hpi, but the trend that the viral titer of co-treated HT-29 cells was higher than that of HT-29 cells treated with MeV-GFP monotherapy was confirmed (**Figure 34B**).

3.9 Analysis of IFN-β-response of tumor cell lines after co-treatment with MeV-GFP and Skepinone-L

The IFN-β release of co-treated tumor cells was important to one of the key statements of this thesis as it shows the effect of Skepinone-L by interfering with the p38α MAPK signaling pathway and therefore implicates a role of p38α MAPK signaling in IFN-β immune response of tumor cell lines examined. An IFN-β release would demonstrate that the enhancement of the cytotoxic effect of combinatorial treatment with MeV-GFP and Skepinone-L could be explained by the Skepinone-L mediated inhibition of the p38α MAPK signaling pathway and following inhibition of the antiviral immune response of tumor cells. Experiments were performed with tumor cell lines HCT-15 (**Figure 34**) and HT-29 (**Figure 35**). An IFN-β ELISA was performed to quantify the IFN-β release of tumor cells at four different time points after combinatorial treatment.

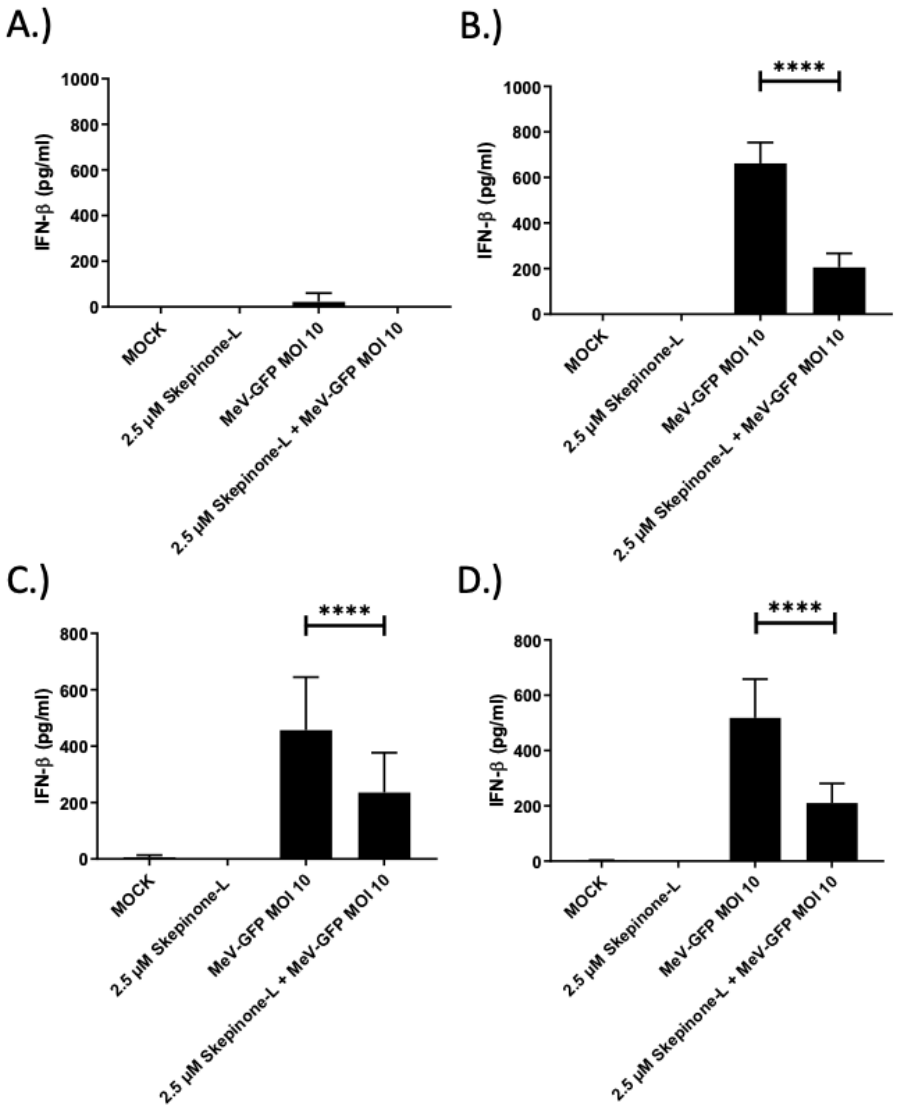

Figure 35: IFN-β release of HCT-15 cells after treatment with Skepinone-L and/or infection with MeV-GFP.

HCT-15 were treated with 2.5 µM Skepinone-L 24 hours post seeding or left untreated and then infected after 48 hours post seeding with MeV-GFP MOI 10 for 3 hours in Opti-MEM or left untreated. Supernatants of treated cells were collected at 24 **(A)**, 48 **(B)**, 72 **(C)** and 96 **(D)** hpi and IFN-β ELISA was performed according to manufacturer's protocol. Experiments were performed in triplicates. MOCK; untreated control.

HCT-15 cells did not release measurable IFN-β when left untreated or only treated with Skepinone-L. At 24 hpi, only the MeV-GFP infected cells showed IFN-β release of 22 pg/ml while in the combinational therapeutic approach (MeV-GFP + Skepinone-L) no IFN-β release was measured (**Figure 35A**). This observation was confirmed when looking at the results of the IFN-β ELISA at 48 - 96 hpi (**Figure 35B-D**). At 48 hpi, HCT-15 cells infected with MeV-GFP

released 662 pg/ml IFN-β which also marked the peak of IFN-β release, whereas IFN-β release slightly decreased again later in the experiment (72 and 96 hpi). Compared to the 48 hpi MeV-GFP IFN-β release (662 pg/ml) the IFN-β release of co-treated HCT-15 was reduced significantly to less than a third (205 pg/ml). At 72 hpi and 96 hpi a similar effect could be observed as co-treated HCT-15 cells released significantly less IFN-β in comparison to HCT-15 cells treated with MeV-GFP only (**Figure 35**).

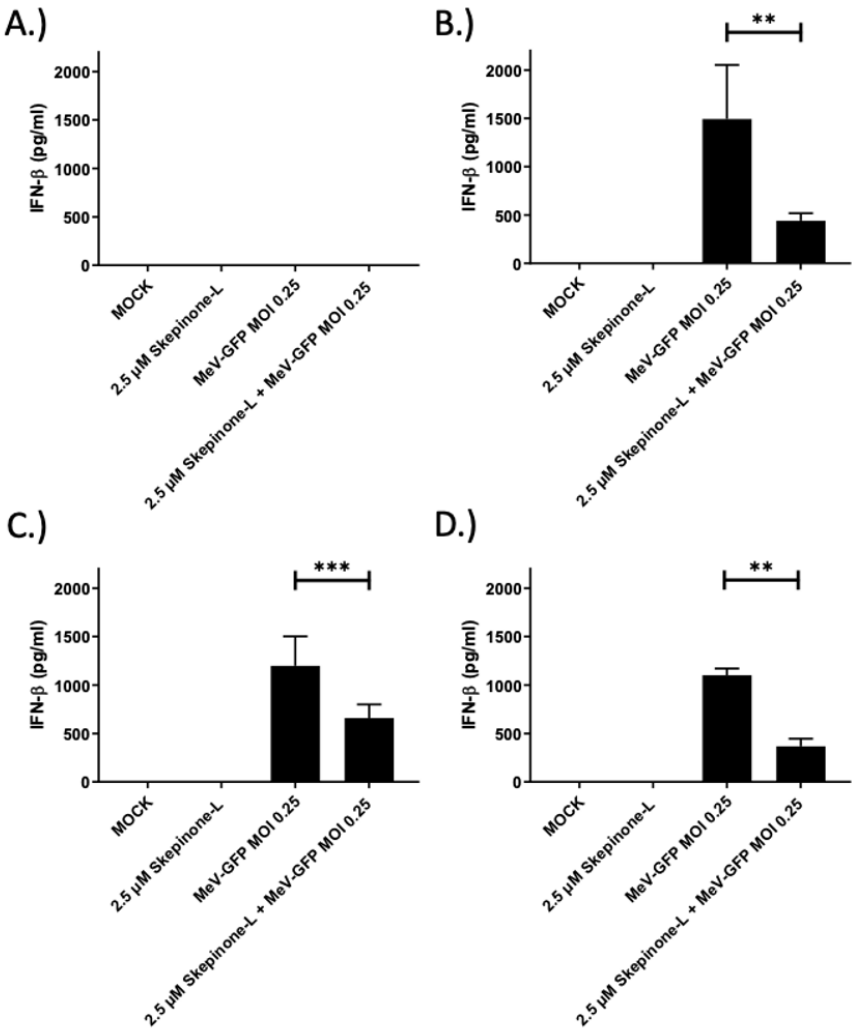

Figure 36: IFN-β release of HT-29 cells after treatment with Skepinone-L and/or infection with MeV-GFP.

HT-29 were treated with 2.5 µM Skepinone-L 24 hours post seeding or left untreated and then infected after 48 hours post seeding with MeV-GFP MOI 0.25 for 3 hours in Opti-MEM or left untreated. Supernatants of treated HT-29 cells were collected at 24 **(A)**, 48 **(B)**, 72 **(C)** and 96 **(D)** hpi and IFN-β

ELISA was performed according to manufacturer's protocol. Experiments were performed in triplicates. MOCK; untreated control.

HT-29 cells showed a similar response pattern as HCT-15 cells, but a generally higher IFN-β release. No IFN-β could be detected at 24 hpi regardless of the treatment suggesting that even when infected with MeV-GFP the IFN-β expression was not yet activated after 24 hpi (**Figure 36A**). At 48 hpi, IFN-β increased to a maximum of 1492 pg/ml when HT-29 were only infected with MeV-GFP. A co-treatment with Skepinone-L and MeV-GFP led to a reduction of IFN-β (440 pg/ml) (**Figure 36B**). The IFN-β release (72 hpi / 96 hpi) of co-treated HT-29 cells was significantly lower than the IFN-β release of HT-29 cells infected with MeV-GFP (**Figure 36C-D**).

In both colon tumor cell lines (HCT-15 and HT-29), a significant effect of Skepinone-L on the IFN-β release could be observed.

4 Discussion

In this thesis the resistance mechanism of tumor cell lines of the NCI-60 panel (HCT-15, HT-29, HCT-116, ACHN) and Hep3B against MeV-GFP were examined. Skepinone-L was used to inhibit p38α MAPK signaling to potentially reduce the antiviral response of tumor cells and therefore enhance the oncolytic effect of virotherapy.

4.1 Combinational treatment of tumor cell lines of the NCI-60 panel with MeV-GFP and Skepinone-L

Noll et al. classified the resistance of tumor cells against MeV-based virotherapeutics by determining the remaining cell mass at 96 hpi with an MOI 1 (Noll et al. 2013a). Though, Noll et al. used a different genetically modified measles vaccine virus (MeV-SCD), a limited comparison is valid, as the genetical structure is almost identical to MeV-GFP (1.2.4). Noll et al. could also discover differences in the IFN response of tumor cell lines of the NCI-60 panel when infected with MeV-SCD but could not identify a clear pattern of IFN response and tumor cell resistance.

In an attempt to overcome antiviral resistance of tumor cells to MeV-GFP, p38α MAPK signaling was inhibited via Skepinone-L to potentially affect the IFN-response of tumor cells.

Since one of the questions of the project was, whether inhibition of p38α MAPK signaling could enhance viral replication of MeV-GFP and thus oncolysis of tumor cells, several different tumor cell entities (colorectal, renal, liver) were examined. As a first step the oncolytic activity of MeV-GFP was tested via SRB assays, as an oncolytic benefit is the primary goal of this study and important for clinical development of anti-cancer drugs (Results 3.4).

In general, it could be demonstrated that all tested tumor cell lines showed cell mass reductions when treated with MeV-GFP monotherapy. As previous results from Noll et al. suggested, HCT-15 proved to be the most resistant cell line with a high concentration of virus (MOI 10) needed for an oncolytic effect. ACHN cells were treated with MeV-GFP MOI 1 and were resistant as well, while the

other tumor cell lines Hep3B, HCT-116 and HT-29 proved to be susceptible to monotherapy with MeV-GFP.

The colorectal tumor cell lines HCT-15, HT-29 and HCT-116 showed the most oncolytic benefits of the combinatorial therapy with Skepinone-L and MeV-GFP in comparison to the MeV-GFP monotherapy.

The oncolytic effect of the combinational treatment (MeV-GFP and Skepinone-L) varied in the three tested susceptible tumor cell lines (HT-29, HCT-116 and Hep3B). HT-29 cells showed a significant effect when co-treated with Skepinone-L and MeV-GFP while HCT-116 cells only showed significance at 72 hpi. Hep3B cells proved to be susceptible to MeV-GFP and only MOI 0.01 was needed to have a significant effect on the tumor cell mass. In Hep3B cells, no real benefit of the combinational therapy with Skepinone-L in oncolysis was demonstrated.

ACHN cells responded to MeV-GFP (MOI 1) infection, but no significant cell mass reduction could be detected when comparing Skepinone-L and combinational treatment.

A potential reason for this observation could be the different IFN response of tumor cell lines. These experiments focus on the modulation of the IFN expression in tumor cells, but how does IFN affect the expression of IFN-induced genes in these tumor cells? Noll et al. tested the IFN response of the above mentioned highly resistant tumor cell lines of the NCI-60 panel (ACHN, HCT-15, M14 and HOP-62). Phosphorylated Stat1, total Stat1 and IFIT-1 were used as markers for an active IFN response and therefore for an active antiviral state in these tumor cells. Interestingly, highly resistant tumor cells used in this project showed differences in Stat1 and IFIT1 expression as analyzed in immunoblots. While HCT-15 showed a strong expression of phosphorylated Stat1, total Stat1 and IFIT1 48 and 72 hpi, ACHN showed a very weak expression of phosphorylated Stat1 and, in comparison to HCT-15, weaker total Stat1 and IFIT1 expression (Noll et al. 2013a). This could be one of the explanations for the weaker response of Skepinone-L in ACHN cells in comparison to HCT-15 cells. Skepinone-L could be generally able to inhibit IFN

expression in this tumor cell lines, but if the signaling pathway of IFN-induced genes is blocked or limited, there would be subsequently no differences in antiviral activity and cell survival in tumor cells. Interestingly, Patel et al. used ruxolitinib to inhibit Jak/Stat signaling to overcome resistance of tumor cell lines against vesicular stomatitis virus (VSV), which are mainly caused by intact IFN response. A combinational treatment of ruxolitinib and VSV-IFN-β in NSCLC mice leading to a trend of increased survival rate of mice (Patel et al. 2019). It would be interesting to see, if an inhibition of Jak/Stat signaling could reduce IFN-mediated immune response in tumor cells infected with measles vaccine virus and lead to an increased oncolytic effect. Another interesting study was performed by Allagui et al. In these experiments human melanoma cells were infected with measles vaccine virus and it could be determined that all tested MV sensitive melanoma cell lines became resistant when pre-treating tumor cells with IFN-α and IFN-β (Allagui et al. 2017). A combinational treatment of melanoma cell lines with MV and above described Ruxolitinib could overcome resistant melanoma cell lines and the measles vaccine virus could replicate in these cells. These results are indicating that the IFN pathway is important for possible resistances of melanoma cells against MV (Allagui et al. 2017).

As this could be one of the explanations of the weaker Skepinone-L response in ACHN cells, it would be interesting to perform an IFN ELISA with ACHN cells treated with MeV-GFP and Skepinone-L to examine the effect of Skepinone-L on the IFN-β release. A sufficient IFN-β release of ACHN cells would implicate that the resistance phenomena of ACHN cells have other causes that needed to be investigated in future studies. In general, this would help to understand if the resistance mechanism is explainable in signaling pathways leading to the expression of IFN or in signaling pathways leading to the induction of IFN-induced genes.

Therefore, an interesting approach would be the comparison of the combinational effect of Skepinone-L and MeV-GFP in highly resistant cell lines with a presumably intact IFN response (Stat1 and IFIT1 detection via immunoblot) like HOP-24 and M14 (Noll et al. 2013a).

The IFN response of susceptible cell lines treated with MeV-SCD were not tested by Noll et al., unlike the six highly resistant cell lines. Therefore, a possible variation in IFN response of the susceptible tumor cell lines is not certain.

4.2 Skepinone-L and its potential in oncolytic virotherapy

Skepinone-L proved to be a very specific inhibitor of the p38α MAPK in prior experiments (Rudalska et al. 2014; Koeberle et al. 2011). The rationale was whether similar effects could be shown in MeV-GFP infected tumor cell lines. Although, it was expected that Skepinone-L would not be affected by an additional infection, evidence was needed to ensure that Skepinone-L functioned as expected in our set-up. This could be done by immunoblotting as differences in enzyme activation can be detected by different antibodies. A detection of p-HSP27 indicates an active HSP27 and therefore an active p38α MAPK pathway. Thinner p-HSP27 bands were detected in HCT-15, Hep3B, and HCT-116 tumor cells treated with Skepinone-L and MeV-GFP in comparison to tumor cells infected with MeV-GFP as monotherapy. This indicates an inhibitory effect of Skepinone-L on p38α MAPK signaling in these tumor cells. Unfortunately, in the cell line HT-29, treated with the same set-up, no activated p-HSP27 could be detected.

HSP27 bands indicate the amount of inactive HSP27 in treated or untreated cells and were not as easy to interpret and is not described as direct marker of p38α MAPK signaling in literature, as the amount of inactivated HSP27 does not necessarily function as a marker of a functioning p38α MAPK signaling. Besides other possible influences on HSP27 a higher expression of HSP27 could be caused by an external stimulus like a MeV-GFP infection and therefore a more active p38α pathway but this could also lead to a lack of detection of HSP27, as most HSP27 would be activated.

The enhancement of the IFN-type I and IFN-type 3 gene expression is well established with the activation of signaling cascades in response to RNA stimulation via TLRs and RLRs leading to a phosphorylation of IRF3 and IκBα. This results in binding of IRF and NF-κB to promoter elements of the IFN gene

and its regulation (Jiang et al. 2015). In moDCs, Jiang et al. demonstrated that activation of p38α MAPK triggered by RNA stimulation leads to increased expression of early IFN genes (IFN-λ1 and IFN-β), although the exact mechanism of p38α MAPK stimulation is unknown, whereas it has no effect on IRF7 and therefore on late IFN expression (IFN-α). Ludwig et al. observed the reduction of IFN-β expression upon inhibition of p38α MAPK after H5N1 and H7N7 infection in endothelial cells (Borgeling et al. 2014).

In this work, an IFN-β ELISA was used to provide information about a possible change in IFN release in tumor cells that were both infected with MeV-GFP and treated with Skepinone-L to inhibit p38α MAPK. Detected IFN-β in supernatants of tumor cells infected with MeV-GFP as monotherapy was high, indicating a functioning antiviral response of colorectal tumor cells (HT-29 and HCT-15). Co-treatment with Skepinone-L resulted in a significant reduction of IFN-β release supporting the above stated theory that p38α MAPK does play a role in antiviral responses against MeV-GFP in these cell lines. HCT-15 and HT-29 cells did not release measurable IFN-β when left untreated or only treated with Skepinone-L, which could be explained by the lack of external stimulation to active stress and immune response at all four time points (24, 48, 72, and 96 hpi), when supernatants were collected.

Examination of the effect of IFN-β on viral replication was the next logical step. Inserted GFP into the viral genome of measles vaccine virus could be used to examine viral replication in tumor cells. Noll et al. observed that the viral growth curve of the highly resistant cancer cell line HCT-15 infected with MeV-SCD peaked 48 hpi and then decreased (Noll et al. 2013a). HCT-15 cells infected with MeV-GFP also showed a decrease in viral particles in tumor cells 48 hpi (**Figure 33**). This results may be supported by the increased expression of IFIT1 in HCT-15 cells infected with MeV-SCD 48 and 72 hpi cited above, indicating an antiviral state of HCT-15 cells (Noll et al. 2013a). The decrease of viral replication in HCT-15 cells could therefore possibly be explained by an IFN-β induced antiviral state of HCT-15 cells. However, a reduced total amount of tumor cells (48 hpi) can also lead to a limited replication of virus, causing a

decreased detection of viral particles in the viral growth curves and therefore must be considered. A combinational treatment with Skepinone-L could stabilize the viral growth in HCT-15 cells at 72 and 96 hpi. In conclusion, the increased oncolytic effect of MeV-GFP in the combinational treatment with Skepinone-L in HCT-15 cells could be caused by the reduced IFN-β release of HCT-15 cells. It would be interesting to perform an additional immunoblot to examine if the detection of phosphorylated Stat1, total Stat1 and IFIT1 would differ in HCT-15 cells treated with MeV-GFP and Skepinone-L in comparison to both monotherapies. A similar pattern to a slightly lesser extent was observed in HT-29 cells: viral growth decreased drastically at 48 hpi in cell supernatants and moderately 72 hpi in cell lysate. Co-treatment with Skepinone-L and MeV-GFP stabilized viral replication or decreased it to a lesser extent than monotherapy at 96 hpi.

Although the in vitro efficacy and benefit of Skepinone-L and other p38 MAPK inhibitors have been demonstrated, Skepinone-L has not yet been tested in clinical studies.

In fact, there are currently no selective p38α MAPK inhibitors approved worldwide, but there are several drugs that are undergoing phase I and II clinical trials (Denny 2022). One example is ralimetinib (LY2228820), a selective p38α/p38β MAPK inhibitor which has been tested in phase I and II clinical studies (Campbell et al. 2014). In a phase Ib/II study including 118 women with platinum-sensitive epithelial ovarian cancer, ralimetinib was tested in combination with gemcitabine and carboplatin. In comparison to dual treatment with gemcitabine and carboplatin, triple therapy showed a modest improvement in progression-free survival, but median overall survival and overall response rate did not improve significantly. Importantly, the safety profile of the triple combination was comparable to that of the gemcitabine and carboplatin treatment combination (Vergote et al. 2020). In a phase I study including 18 patients with glioblastoma, the recommended dose of ralimetinib was tested in combination with radiotherapy and temozolomide (Biau et al. 2021). 15 patients received ralimetinib in combination with chemoradiotherapy with a maximum

tolerated dose of 100mg/12 hours (ralimetinib), the main dose limited toxicities were rash and hepatic cytolysis (Biau et al. 2021).

The p38 MAPK pathway plays a role in various inflammatory processes, and therefore a detailed examination of Skepinone-L safety and side effects in clinical studies would be the next logical step for its clinical use.

4.3 Can differences in oncolytic activity be explained by genetic differences in tumor cell lines?

Since the inhibitory effect triggered by Skepinone-L on the antiviral immune response via the p38 MAPK signaling pathway was observed exclusively in colorectal tumor cell lines (HCT-15, HT-29, HCT-116), it is of great importance to study the cell lines in more detail. HCT-15, HT-29 and HCT-116 are all classified as fast growing colorectal tumor cells with a doubling time of 20-24 hours (Ahmed et al. 2013). However, they differ in their epigenetic and genetic features, which were examined by Ahmed et al. in experiments including 24 colon cancer cell lines (Ahmed et al. 2013). Colorectal carcinoma is very heterogenous and classified in different genetic subtypes which can overlap. 85 % of colorectal carcinomas are mutated in the chromosomal instability pathway (CIN) which include mostly sporadic tumors (Nowak et al. 2002). 15 % of all colorectal carcinomas show microsatellite instabilities (MSI), which lead to a higher mutation rate caused by an insufficient DNA mismatch-repair system (Lothe 1997). HCT-15 cell lines proved to be CIN positive, while HT-29 and HCT-116 were CIN negative and all three tested tumor cell lines were from the CpG island methylator phenotype (CIMP) (Ahmed et al. 2013). HCT-15 (mutated *MSH6*) and HCT-116 (mutated *MLH1*) were MSI while HT-29 were MSS (microsatellite stable). HCT-15 and HCT-116 both have a mutation in the *KRAS* gene and have the *BRAF* wild type gene while HT-29 is mutated in *BRAF* (V600E) and has the *KRAS* wild type gene. *TP53* is mutated differently in HCT-15 (S241F) and HT-29 (R273H) but HCT-116 has the *TP53* wild type gene (Ahmed et al. 2013). Though there are many genetic differences between the HCT-15, HCT-116 and HT-29 tumor cell lines, no clear pattern has been identified, which could explain the differences in response of tumor cell lines to

measles vaccine virus infection. ACHN and Hep3B, the other cell lines used in this project had following genetical characteristics.

ACHN, one of the most cited renal carcinoma cell lines. ACHN did not show mutations in *BRAF*, *KRAS* and *TP53* in a study that tested 24 key oncogenic genes in tumor cells of the NCI-60 panel (Ikediobi et al. 2006). Hep3B is one of the most cited liver cell carcinomas, originally isolated from a primary liver carcinoma (Aden et al. 1979) and Bressac et al. describes a deleted *TP53* with a lack of *TP53* transcripts and protein expression (Bressac et al. 1990). An overview of genetically characteristics is provided by Qui et al. (Qiu et al. 2015).

Interestingly, the described tumor cell lines differed in expression of *TP53*, which seems to play an important role in CD46 expression of tumor cell lines and therefore is crucial for measles vaccine virus entry into tumor cells (Lok et al. 2018) (Dörig et al. 1993). *TP53* is a tumor suppressor gene, which is activated by numerous stress factors such as hypoxia and DNA damage and functions as a transcription factor that activates apoptosis, DNA repair, cell cycle arrest, cell senescence and other modulations of the cellular environment (Aubrey, Strasser, and Kelly 2016), *TP53* is mutated in over 50 % of human cancers and, if not mutated, is inactivated by oncoproteins such as MDM2 and MDM4, allowing tumor cells to escape apoptosis (Baugh et al. 2018). *TP53* is also crucial in regulating the antiviral response of cells and TP53 deficiency could be one of the reasons why some tumor cell lines are highly sensitive to viral infection (Lok et al. 2018).

Interestingly, Lok et al. could find a correlation between CD46 expression, the entry receptor for several viruses, and TP53 deficiency in myeloma cells. Lok et al. examined 37 multiple myeloma tumor cell lines and observed a correlation between infection and cell death and CD46 expression, but this was not applicable to all tumor cell lines tested (Lok et al. 2018). TP53 can directly and indirectly suppress CD46 expression in myeloma cells, which is why myeloma cells are highly sensitive to MV infection (MeV-GFP) (Lok et al. 2018). The mechanism behind these findings is the activation of the p53 pathway which directly inhibits CD46 expression and induces miR192 which also inhibits CD46

expression. The TP53 pathway is disrupted in *TP53*-mutated tumor cell lines, leading to a higher CD46 expression and therefore a higher sensitivity against oncolytic viruses like the measles vaccine virus (Lok et al. 2018). However, it is not granted that these results are transferable to other tumor cell lines.

It would be therefore interesting to examine this correlation in other tumor types and cell lines. Viral entry and replication to some extent could be demonstrated by fluorescence microscopy in infected tumor cells in this work (Results 4.5). Moreover, the existence of the CD46 receptor could be proven in all tumor cell lines of the NCI-60 panel including ACHN (Noll et al. 2013a) but could not be quantified. Although CD46, as the main entry receptor of measles vaccine virus (Dörig et al. 1993), could be detected in all highly resistant tumor cell lines by Noll et al, primary infection of tumor cell lines like HCT-15 and ACHN were rather low (MOI 1: HCT-15: 2.99 % and ACHN: 26.44 % when infected with MeV-SCD) (Noll et al. 2013a).

In this experiment two cell lines are described as *TP53* wildtype: ACHN (Ikediobi et al. 2006) and HCT-116 (Ahmed et al. 2013). Nevertheless, MeV-GFP had different oncolytic effects on both tumor cell lines, which is confirmed by the results of Noll et al. using MeV-SCD (Noll et al. 2013a), as ACHN is classified as a MeV resistant and HCT-116 as a susceptible tumor cell line. Interestingly, it could be shown that a *TP53* knock-out increased the CD46 expression in HCT-116 cells (Lok et al. 2018). Therefore, it would be interesting to see if this would result in an increased efficacy of MeV-GFP in HCT-116 cells in our setting, despite the already high susceptibility of this cell line. In ACHN cells the reduced primary infection shown above (Noll et al. 2013a), potentially caused by a low CD46 expression in ACHN cells, could be a reason for the resistance of ACHN cells against MeV-GFP. Therefore, a *TP53* knock-out also in ACHN cells and a following infection with MeV-GFP with/without Skepinone-L could give important answers to that question.

HT-29 is *TP53* mutated (R273H) and Hep3B *TP53* deficient (Ahmed et al. 2013; Bressac et al. 1990) and both are susceptible to MeV-GFP as well (Results 3.4) but varied in their response to treatment with Skepinone-L. The highly resistant

HCT-15 cell line is *TP53* mutated (S241F) and showed a low primary infection rate from monotherapy MeV-GFP (2.99 %) (Ahmed et al. 2013; Noll et al. 2013a). Further experiments of CD46 expression and the functioning of the TP53 pathway in HCT-15 cells would be interesting, because despite of the mutated *TP53*, the oncolytic effect of MeV-GFP was limited in HCT-15 cells indicating additional resistant mechanism of HCT-15 cells. Besides the viral titers obtained from monotherapy, MeV-GFP infection decreased from 48 to 96 hpi indicating a possible viral elimination of MeV-GFP in HCT-15 cells, which could be partly reversed with Skepinone-L treatment (Results 3.7).

4.4 Do other signaling pathways which induce IFN expression and IFN response affect the resistance of tumor cell lines against MeV-GFP?

Inhibition of MAPK signaling via Skepinone-L influences the antiviral response of colorectal tumor cell lines (HCT-15 and HT-29) by leading to a reduced IFN-β release in these cell lines. This presumably could have caused the increased oncolytic effect of the combinational therapy in these cell lines in comparison to monotherapy.

However, p38α MAPK signaling is not the only pathway catalyzing the antiviral response of tumor cells. Not all signaling cascades have been fully understood but most of the signaling cascades lead to binding of IRF 3 and IκBα binding of the promotor elements of the IFN gene (Jiang et al. 2015). The lack of cytotoxic effects of combinational treatment on ACHN and Hep3B cells suggests that antiviral resistance may be catalyzed by different pathways depending on the tumor entity.

Viral RNA stimulation leads via TLRs and RLRs (RIG-I and MDA5) to the activation of their respective downstream kinases including IKK, IKKε/TBK1 and to the phosphorylation of IRF 3 and IκBα. Especially the importance of RIG-1 and MDA5 in the antiviral defense of measles virus infected human cells could be proven (Ikegame et al. 2010). RIG-I can differentiate between endogenic and extrinsic RNA and detects 5'phosphorylated ssRNA (Hornung et al. 2006). RIG-I and MDA5, which detect long dsRNA, activate the mitochondrial protein MAVS (Osterlund et al. 2007). MAVS functions in two different ways: (1) MAVS

activates the IKK complex, which phosphorylates IκB enabling NF-κB to enter the nucleus and activate NF-κB-dependent transcription of the IFN genes (Seth et al. 2005); (2) MAVS also activates IKKε/TBK1, which phosphorylates IRF3 and IRF7, also acting as transcription factors for IFN genes (Seth et al. 2005).

Furthermore, the MyD88-IRF7 pathway is a possible option for increased IFN-β expression triggered by viral RNA stimuli (Kawai et al. 2004; Honda et al. 2004), as p38α MAPK does not initiate IFN-β expression via this pathway (Jiang et al. 2015).

In a different study eight sarcoma cell lines were infected with MeV-SCD, and three resistant cell lines (SRH, SCOS, CCS) showed upregulation of RIG-1 and strong IFIT1 mRNA expression, whereas predominantly susceptible cell lines did not show IFIT1 mRNA expression. The observed resistance could eventually be overcome by increasing the viral doses and/or addition of 5-FC but it indicates the important role of the innate immune response restricting the oncolytic effect of MeV-SCD. Interestingly, IFIT-1 knockdown did not lead to increased oncolytic effect of MeV-SCD in SCOS and CCS cells, indicating that there must be also other resistance mechanisms against MeV-SCD (Berchtold et al. 2013).

In conclusion, the inhibition of p38α MAPK signaling leads to a reduced IFN-β release in some tumor cells (HCT-15 and HT-29), but other pathways may also provide antiviral response against OVs which should be investigated in further studies.

4.5 Perspectives

The studies aimed to create a further understanding of potential resistance mechanisms in tumor cell lines against oncolytic measles vaccine virus (MeV-GFP).

Although it was possible to show an improved oncolytic effect of Skepinone-L and MeV-GFP in HCT-15 cells, results varied in different tumor cell lines and tumor entities. Still, the alteration of IFN-β with Skepinone-L in MeV-GFP infected HCT-15 and HT-29 is promising and affirms the results of Jiang et al.,

that p38α MAPK signaling is important in the regulation of IFN-β in some cells. Beyond this examined effect of p38α MAPK signaling there seem to be other factors involved in creating an antiviral state in tumor cells, which can result in resistances against oncolytic viruses like MeV-GFP. Other important factors that could limit the efficacy of the oncolytic virus could be the limited entry of the virus in tumor cells or the IFN-β-triggered signaling cascade, which causes an antiviral state in cells, as discussed above (Lok et al. 2018). As expected, the very heterogenous tumor cells react differently to external factors such as viral infections, which is why different tumor cell lines and entities must be examined individually.

Although measles vaccine virus has been effectively used as an oncolytic agent in various in vitro experiments and clinical studies, it remains important to investigate the mechanism behind the oncolytic effect, in order to develop potential combinational treatment options that make the virus safer and more effective. Besides clinical trials, basic research is underway to investigate the infection of measles vaccine virus in ex vivo organoid models. Recently, MeV-GFP and MeV-SCD have been tested in breast cancer derived stable organoid cell cultures (Carter et al. 2022) providing an excellent ex vivo method to test virotherapeutics in a patient-individual setting in the future (Kloker, Yurttas, and Lauer 2018).

Skepinone-L is a potent p38α MAPK inhibitor and proved to be effective as monotherapy and in combinational treatment with MeV-GFP. Here, Skepinone-L led to a significant reduction of IFN-β in the two tested tumor cell lines. Although Hep3B and ACHN did not show the desired oncolytic benefit of the combinational treatment, it would be interesting to examine if Skepinone-L would reduce IFN-β in these cells as well and moreover in other tumor cell lines of the NCI-60 panel. With this information a more accurate statement about the effectiveness of the IFN-β reduction via inhibition of p38α MAPK signaling could be made. Even though Skepinone-L is not yet used in clinical studies, its promising in vitro studies show great potential, therefore investigating its safety and in vivo effectivity would be the next logical step.

5 Summary

Oncolytic virotherapy is a biological approach to fight tumor cells and supposedly might be of help for more and more cancer patients in the future.

For the clinical setting of virotherapy, it is of great interest to get knowledge on the application possibilities of each and every virotherapeutic compound. Accordingly, it is important to understand (i) the phenomena of antiviral resistances and oncolytic futility as well as (ii) the mechanisms which enable the permissivity and oncolytic success of each and every virotherapeutic compound. For this purpose, a well-characterized oncolytic measles vaccine virus (MeV) that has been demonstrated to be oncolytically effective in most but not all cell lines of the NCI-60 tumor cell panel (Noll et al. 2013b) was investigated in more detail.

In previous studies an intact type I IFN response had been identified as a main factor for resistances of tumor cell lines against oncolytic measles viruses (Allagui et al. 2017). Further studies have shown that the p38α MAPK pathway is activated by type I IFNs and that this pathway is also involved in regulating type I IFN-dependent antiviral responses (Jiang et al. 2015).

In this context, we formulated the hypothesis that p38α MAPK inhibitors might have an impact on measles vaccine virus-based virotherapy:

- Blocking of the p38α MAPK signaling pathway might (i) inhibit the type I IFN response in tumor cells, thus leading to (ii) increased replication of MeV-GFP in those "IFN-depleted" tumor cells, which ultimately (iii) could enhance also the immunotherapeutic antitumoral effect of MeV-GFP.

To investigate this hypothesis, the highly effective p38α MAPK inhibitor Skepinone-L was studied in four tumor cell lines picked from the NCI-60 tumor cell panel:

- HCT-15 (of colorectal carcinoma (CRC) origin) and ACHN (of renal cancer origin), both of which had been demonstrated to be highly resistant to MeV-based oncolysis (Noll et al. 2013b);

- HCT-116 and HT-29 (of either CRC origin), both of which had been demonstrated to be highly permissive to MeV-based oncolysis (Noll et al. 2013b);
- Hep3B (of hepatocellular carcinoma origin), which is not part of the NCI-60 tumor cell panel and which was demonstrated in this work to be partially resistant / semi-permissive to MeV-based oncolysis.

Tumor cells were incubated with defined concentrations of Skepinone-L and 24 hours later infected with MeV-GFP and after 3 hours post-treated with Skepinone-L . Oncolytic effects were determined by the Sulforhodamine B (SRB) cell viability assay as well as by xCELLigence® Real-Time Cell Analysis. As a result, MeV-GFP-mediated oncolysis enhanced by Skepinone-L was detected only in the three CRC cell lines (HCT-15, HT-29, HCT-116), but not in the renal (ACHN) nor in the hepatocellular carcinoma cell line (Hep3B). Interestingly, a decrease of IFN-β release could be detected in HCT-15 and HT-29 cells treated with Skepinone-L/MeV-GFP indicating an effect of Skepinone-L on MeV-GFP-triggered humoral immune response via p38α MAPK signaling. Data for the other three tumor cell lines (HCT-116, ACHN, Hep3B) regarding the IFN release were not obtained within the scope of this thesis work.

In conclusion, resistance phenomena against oncolytic virotherapeutics are complex, multifactorial and vary between tumor cell lines. The experiments performed here show that the p38α MAPK signaling pathway is modulating the IFN-release of two CRC cell lines (HCT-15 and HT-29) which might explain the impact on the oncolytic efficacy of MeV-GFP. The lack of oncolytic benefits of other tested tumor cell lines (like ACHN) are indicating that there might be other signaling pathways leading to the induction of IFN-β, which need to be considered and addressed in further studies.

Although numerous virotherapeutic compounds are currently being tested in preclinical and clinical studies, it remains important to understand the phenomena of resistance caused by the tumor`s own immune response to potentially find combinational treatment options that increase the efficacy of virotherapeutics being in clinical use.

6 Zusammenfassung

Die onkolytische Virotherapie ist ein biologischer Ansatz zur Bekämpfung von Tumorzellen und bietet ein besonderes Potential für die Krebstherapie der Zukunft. Für die klinische Anwendung der Virotherapie ist es von großem Interesse, Kenntnisse über die Anwendungsmöglichkeiten jedes einzelnen virotherapeutischen Wirkstoffs zu erhalten. Deshalb ist es wichtig, (i) die Phänomene der antiviralen Resistenzen und die onkolytische Unwirksamkeit, sowie (ii) die Mechanismen, die die Permissivität und den onkolytischen Erfolg jedes einzelnen Virotherapeutikas ermöglichen, zu verstehen. Zu diesem Zweck wurde das gut charakterisierte Masern-Impfvirus (MeV), das nachweislich in den meisten, aber nicht allen Zelllinien des NCI-60 Tumorzellpanels onkolytisch wirksam ist, detaillierter untersucht.

In vorherigen Studien wurde eine intakte IFN Typ I Antwort als ein Hauptfaktor für die Entwicklung von Resistenzen der Tumorzellen gegenüber onkolytischer Masern-Impfviren festgestellt (Allagui et al. 2017). Weitere Studien haben gezeigt, dass der p38α MAPK Signalweg eine Rolle bei der IFN Typ I Expression spielt und damit für die Regulation der IFN Typ I vermittelten antiviralen Immunantwort von Bedeutung ist (Jiang et al. 2015).

In diesem Kontext haben wir die Hypothese formuliert, dass p38α MAPK Inhibitoren Auswirkungen auf eine Masern-Impfviren basierende Virotherapie haben könnten.

- Die Blockierung des p38α MAPK Signalwegs könnte (i) die Typ-I-IFN Antwort in Tumorzellen hemmen. Dies würde zu einer (ii) erhöhten Replikation von MeV-GFP in diesen „IFN-depletierten“ Tumorzellen führen, was letztlich (iii) auch die antitumorale Wirkung von MeV-GFP verstärken könnte.

Um diese Hypothese zu untersuchen, wurde der hocheffektive p38α MAPK Inhibitor Skepinone-L in vier Tumorzelllinien aus dem NCI-60 Panel untersucht.

- HCT-15 (Herkunft: kolorektales Karzinom) und ACHN (Herkunft: renales Karzinom), die sich beide als sehr resistent gegenüber MeV-basierender Onkolyse herausgestellt haben (Noll et al. 2013b).
- HCT-116 und HT-29 (Herkunft: beide kolorektales Karzinom), die sich beide als sehr empfindlich gegenüber MeV-basierender Onkolyse herausgestellt haben (Noll et al. 2013b).
- Hep3B (Herkunft: hepatozelluläres Karzinom), welches nicht zum NCI-60 Tumorzellpanel gehört und sich in der Arbeit als partiell-resistent/semi-permissiv gegenüber MeV-basierender Onkolyse herausgestellt hat.

Die Tumorzellen wurden mit zuvor definierten Skepinone-L Konzentrationen inkubiert und 24 Stunden später mit MeV-GFP infiziert und nach weiteren 3 Stunden mit Skepinone-L nachbehandelt. Onkolytische Effekte wurden mit Sulforhodamine B (SRB) Zytotoxizitäts-Assays und xCELLigence® Echtzeit-Analyse ermittelt. Es konnte gezeigt werden, dass Skepinone-L nur in den drei kolorektalen Karzinom Zelllinien (HCT-15, HT-29, HCT-116) die MeV-GFP-vermittelte Onkolyse verstärken konnte, aber nicht in den renalen (ACHN) und hepatozellulären (Hep3B) Tumorzelllinien. Interessanterweise wurde eine Abnahme der IFN-β Freisetzung in HCT-15 und HT-29 Zellen festgestellt, die mit Skepinone-L/MeV-GFP behandelt wurden. Dies weist auf einen Effekt von Skepinone-L auf die von MeV-GFP getriggerte humorale Immunantwort via des p38α MAPK Signalwegs hin. Daten zu den anderen drei Tumorzelllinien (HCT-116, ACHN, Hep3B) bezüglich der IFN-Freisetzung wurden im Rahmen dieser Arbeit nicht erhoben.

Zusammenfassend lässt sich sagen, dass Resistenzphänomene gegenüber onkolytischer Virotherapeutika komplex und multifaktoriell sind und stark zwischen den unterschiedlichen Tumorzelllinien variieren können. Die durchgeführten Experimente zeigen, dass der p38α MAPK Signalweg die IFN-β Freisetzung in den beiden kolorektalen Karzinom Zelllinien (HCT-15 und HT-29) moduliert. Dies könnte die Auswirkungen auf die onkolytische Wirksamkeit von MeV-GFP auf die beiden Tumorzelllinien erklären. Die fehlenden onkolytischen Vorteile der anderen getesteten Tumorzelllinien (wie ACHN) weisen auf weitere

wichtige Signalwege hin, die ebenfalls zu einer Induktion von IFN-β führen. Diese sollten in weiteren Studien berücksichtigt und untersucht werden.

Obwohl derzeit zahlreiche Virotherapeutika in präklinischen und klinischen Studien getestet werden, ist es wichtig, die durch die tumoreigene Immunantwort hervorgerufenen Resistenzphänomene zu verstehen, um potentielle Kombinationstherapien zu entwickeln, die die Wirksamkeit von Virotherapeutika für den klinischen Einsatz verbessern.

7 Appendix

7.1 List of Tables

7.2 List of Figures

8 References

Aden, D. P., A. Fogel, S. Plotkin, I. Damjanov, and B. B. Knowles. 1979. 'Controlled synthesis of HBsAg in a differentiated human liver carcinoma-derived cell line', *Nature*, 282: 615-6.

Ahmed, D., P. W. Eide, I. A. Eilertsen, S. A. Danielsen, M. Eknaes, M. Hektoen, G. E. Lind, and R. A. Lothe. 2013. 'Epigenetic and genetic features of 24 colon cancer cell lines', *Oncogenesis*, 2: e71.

Ajina, A., and J. Maher. 2017. 'Prospects for combined use of oncolytic viruses and CAR T-cells', *J Immunother Cancer*, 5: 90.

Allagui, F., C. Achard, C. Panterne, C. Combredet, N. Labarriere, B. Dreno, A. B. Elgaaied, D. Pouliquen, F. Tangy, J. F. Fonteneau, M. Gregoire, and N. Boisgerault. 2017. 'Modulation of the Type I Interferon Response Defines the Sensitivity of Human Melanoma Cells to Oncolytic Measles Virus', *Curr Gene Ther*, 16: 419-28.

Anderson, B. D., T. Nakamura, S. J. Russell, and K. W. Peng. 2004. 'High CD46 receptor density determines preferential killing of tumor cells by oncolytic measles virus', *Cancer Res*, 64: 4919-26.

Andtbacka, R. H., H. L. Kaufman, F. Collichio, T. Amatruda, N. Senzer, J. Chesney, K. A. Delman, L. E. Spitler, I. Puzanov, S. S. Agarwala, M. Milhem, L. Cranmer, B. Curti, K. Lewis, M. Ross, T. Guthrie, G. P. Linette, G. A. Daniels, K. Harrington, M. R. Middleton, W. H. Miller, Jr., J. S. Zager, Y. Ye, B. Yao, A. Li, S. Doleman, A. VanderWalde, J. Gansert, and R. S. Coffin. 2015. 'Talimogene Laherparepvec Improves Durable Response Rate in Patients With Advanced Melanoma', *J Clin Oncol*, 33: 2780-8.

Aref, Sarah, Katharine Bailey, and Adele Fielding. 2016. 'Measles to the Rescue: A Review of Oncolytic Measles Virus', *Viruses*, 8: 294.

Aubrey, B. J., A. Strasser, and G. L. Kelly. 2016. 'Tumor-Suppressor Functions of the TP53 Pathway', *Cold Spring Harb Perspect Med*, 6.

Baldo, A., E. Galanis, F. Tangy, and P. Herman. 2016. 'Biosafety considerations for attenuated measles virus vectors used in virotherapy and vaccination', *Hum Vaccin Immunother*, 12: 1102-16.

Baugh, E. H., H. Ke, A. J. Levine, R. A. Bonneau, and C. S. Chan. 2018. 'Why are there hotspot mutations in the TP53 gene in human cancers?', *Cell Death Differ*, 25: 154-60.

Berchtold, S., J. Lampe, T. Weiland, I. Smirnow, S. Schleicher, R. Handgretinger, H. G. Kopp, J. Reiser, F. Stubenrauch, N. Mayer, N. P. Malek, M. Bitzer, and U. M. Lauer. 2013. 'Innate immune defense defines susceptibility of sarcoma cells to measles vaccine virus-based oncolysis', *J Virol*, 87: 3484-501.

Biau, J., E. Thivat, E. Chautard, D. Stefan, M. Boone, B. Chauffert, C. Bourgne, D. Richard, I. Molnar, S. Levesque, R. Bellini, F. Kwiatkowski, L. Karayan-Tapon, P. Verrelle, C. Godfraind, and X. Durando. 2021. 'Phase 1 trial of ralimetinib (LY2228820) with radiotherapy plus concomitant temozolomide in the treatment of newly diagnosed glioblastoma', *Radiother Oncol*, 154: 227-34.

Bluming, A. Z., and J. L. Ziegler. 1971. 'Regression of Burkitt's lymphoma in association with measles infection', *Lancet*, 2: 105-6.

Bonaventura, P., T. Shekarian, V. Alcazer, J. Valladeau-Guilemond, S. Valsesia-Wittmann, S. Amigorena, C. Caux, and S. Depil. 2019. 'Cold Tumors: A Therapeutic Challenge for Immunotherapy', *Front Immunol*, 10: 168.

Borgeling, Y., M. Schmolke, D. Viemann, C. Nordhoff, J. Roth, and S. Ludwig. 2014. 'Inhibition of p38 mitogen-activated protein kinase impairs influenza virus-induced primary and secondary host gene responses and protects mice from lethal H5N1 infection', *J Biol Chem*, 289: 13-27.

Borst, O., B. Walker, P. Munzer, A. Russo, E. Schmid, C. Faggio, B. Bigalke, S. Laufer, M. Gawaz, and F. Lang. 2013. 'Skepinone-L, a novel potent and highly selective inhibitor of p38 MAP kinase, effectively impairs platelet activation and thrombus formation', *Cell Physiol Biochem*, 31: 914-24.

Bressac, B., K. M. Galvin, T. J. Liang, K. J. Isselbacher, J. R. Wands, and M. Ozturk. 1990. 'Abnormal structure and expression of p53 gene in human hepatocellular carcinoma', *Proc Natl Acad Sci U S A*, 87: 1973-7.

Buckland, R., and T. F. Wild. 1997. 'Is CD46 the cellular receptor for measles virus?', *Virus research*, 48: 1-9.

Buettner, R., M. Huang, T. Gritsko, J. Karras, S. Enkemann, T. Mesa, S. Nam, H. Yu, and R. Jove. 2007. 'Activated signal transducers and activators of transcription 3 signaling induces CD46 expression and protects human cancer cells from complement-dependent cytotoxicity', *Mol Cancer Res*, 5: 823-32.

Busch, E., K. D. Kubon, J. K. M. Mayer, G. Pidelaserra-Marti, J. Albert, B. Hoyler, J. P. W. Heidbuechel, K. B. Stephenson, B. D. Lichty, W. Osen, S. B. Eichmuller, D. Jager, G. Ungerechts, and C. E. Engeland. 2020. 'Measles Vaccines Designed for Enhanced CD8(+) T Cell Activation', *Viruses*, 12.

Campbell, R. M., B. D. Anderson, N. A. Brooks, H. B. Brooks, E. M. Chan, A. De Dios, R. Gilmour, J. R. Graff, E. Jambrina, M. Mader, D. McCann, S. Na, S. H. Parsons, S. E. Pratt, C. Shih, L. F. Stancato, J. J. Starling, C. Tate, J. A. Velasco, Y. Wang, and X. S. Ye. 2014. 'Characterization of LY2228820 dimesylate, a potent and selective inhibitor of p38 MAPK with antitumor activity', *Mol Cancer Ther*, 13: 364-74.

Carter, M. E., A. D. Hartkopf, A. Wagner, L. L. Volmer, S. Y. Brucker, S. Berchtold, U. M. Lauer, and A. Koch. 2022. 'A Three-Dimensional Organoid Model of Primary Breast Cancer to Investigate the Effects of Oncolytic Virotherapy', *Front Mol Biosci*, 9: 826302.

Cheng, F., L. Twardowski, S. Fehr, C. Aner, E. Schaeffeler, T. Joos, T. Knorpp, B. Dorweiler, S. Laufer, M. Schwab, and M. Torzewski. 2017. 'Selective p38alpha MAP kinase/MAPK14 inhibition in enzymatically modified LDL-stimulated human monocytes: implications for atherosclerosis', *FASEB J*, 31: 674-86.

Chesney, J. A., A. Ribas, G. V. Long, J. M. Kirkwood, R. Dummer, I. Puzanov, C. Hoeller, T. F. Gajewski, R. Gutzmer, P. Rutkowski, L. Demidov, P. Arenberger, S. J. Shin, P. F. Ferrucci, A. Haydon, J. Hyngstrom, J. V. van Thienen, S. Haferkamp, J. M. Guilera, B. L. Rapoport, A.

VanderWalde, S. J. Diede, J. R. Anderson, S. Treichel, E. L. Chan, S. Bhatta, J. Gansert, F. S. Hodi, and H. Gogas. 2022. 'Randomized, Double-Blind, Placebo-Controlled, Global Phase III Trial of Talimogene Laherparepvec Combined With Pembrolizumab for Advanced Melanoma', *J Clin Oncol*: JCO2200343.

Cutts, F. T., and F. Dabis. 1994. '[Measles control in developing countries]', *Sante*, 4: 163-71.

Darnell, J. E., Jr., I. M. Kerr, and G. R. Stark. 1994. 'Jak-STAT pathways and transcriptional activation in response to IFNs and other extracellular signaling proteins', *Science*, 264: 1415-21.

de Vries, R. D., A. W. Mesman, T. B. Geijtenbeek, W. P. Duprex, and R. L. de Swart. 2012. 'The pathogenesis of measles', *Curr Opin Virol*, 2: 248-55.

Denny, W. A. 2022. 'Inhibitors and Activators of the p38 Mitogen-Activated MAP Kinase (MAPK) Family as Drugs to Treat Cancer and Inflammation', *Curr Cancer Drug Targets*, 22: 209-20.

Dingli, D., K. W. Peng, M. E. Harvey, P. R. Greipp, M. K. O'Connor, R. Cattaneo, J. C. Morris, and S. J. Russell. 2004. 'Image-guided radiovirotherapy for multiple myeloma using a recombinant measles virus expressing the thyroidal sodium iodide symporter', *Blood*, 103: 1641-6.

Dock, G. 1904. 'The influence of complicating diseases upon leukemia', *The American Journal of the Medical Sciences*.

Dörig, R. E., A. Marcil, A. Chopra, and C. D. Richardson. 1993. 'The human CD46 molecule is a receptor for measles virus (Edmonston strain)', *Cell*, 75: 295-305.

Elvington, M., M. K. Liszewski, and J. P. Atkinson. 2020. 'CD46 and Oncologic Interactions: Friendly Fire against Cancer', *Antibodies (Basel)*, 9.

Galanis, Evanthia, Pamela J. Atherton, Matthew J. Maurer, Keith L. Knutson, Sean C. Dowdy, William A. Cliby, Paul Haluska, Jr., Harry J. Long, Ann Oberg, Ileana Aderca, Matthew S. Block, Jamie Bakkum-Gamez, Mark J. Federspiel, Stephen J. Russell, Kimberly R. Kalli, Gary Keeney, Kah Whye Peng, and Lynn C. Hartmann. 2015. 'Oncolytic measles virus expressing the sodium iodide symporter to treat drug-resistant ovarian cancer', *Cancer Research*, 75: 22-30.

Galanis, Evanthia, Lynn C. Hartmann, William A. Cliby, Harry J. Long, Prema P. Peethambaram, Brigitte A. Barrette, Judith S. Kaur, Paul J. Haluska, Jr., Ileana Aderca, Paula J. Zollman, Jeff A. Sloan, Gary Keeney, Pamela J. Atherton, Karl C. Podratz, Sean C. Dowdy, C. Robert Stanhope, Timothy O. Wilson, Mark J. Federspiel, Kah-Whye Peng, and Stephen J. Russell. 2010. 'Phase I trial of intraperitoneal administration of an oncolytic measles virus strain engineered to express carcinoembryonic antigen for recurrent ovarian cancer', *Cancer Research*, 70: 875-82.

Geller, A., and J. Yan. 2019. 'The Role of Membrane Bound Complement Regulatory Proteins in Tumor Development and Cancer Immunotherapy', *Front Immunol*, 10: 1074.

Gordiienko, I. M., L. M. Shlapatska, L. M. Kovalevska, and S. P. Sidorenko. 2016. 'Differential expression of CD150/SLAMF1 in normal and malignant B cells on the different stages of maturation', *Exp Oncol*, 38: 101-7.

Greig, S. L. 2016. 'Talimogene Laherparepvec: First Global Approval', *Drugs*, 76: 147-54.
Griffin, Diane E. 2018. 'Measles Vaccine', *Viral immunology*, 31: 86-95.
Guenthoer, P., K. Fuchs, G. Reischl, L. Quintanilla-Martinez, I. Gonzalez-Menendez, S. Laufer, B. J. Pichler, and M. Kneilling. 2019. 'Evaluation of the therapeutic potential of the selective p38 MAPK inhibitor Skepinone-L and the dual p38/JNK 3 inhibitor LN 950 in experimental K/BxN serum transfer arthritis', *Inflammopharmacology*, 27: 1217-27.
Guo, Z. S., Z. Liu, S. Kowalsky, M. Feist, P. Kalinski, B. Lu, W. J. Storkus, and D. L. Bartlett. 2017. 'Oncolytic Immunotherapy: Conceptual Evolution, Current Strategies, and Future Perspectives', *Front Immunol*, 8: 555.
Hasegawa, K., L. Pham, M. K. O'Connor, M. J. Federspiel, S. J. Russell, and K. W. Peng. 2006. 'Dual therapy of ovarian cancer using measles viruses expressing carcinoembryonic antigen and sodium iodide symporter', *Clin Cancer Res*, 12: 1868-75.
Hazini, A., M. Pryshliak, V. Bruckner, K. Klingel, M. Sauter, S. Pinkert, J. Kurreck, and H. Fechner. 2018. 'Heparan Sulfate Binding Coxsackievirus B3 Strain PD: A Novel Avirulent Oncolytic Agent Against Human Colorectal Carcinoma', *Hum Gene Ther*, 29: 1301-14.
Heinzerling, Lucie, Valerie Künzi, Patrick A. Oberholzer, Thomas Kündig, Hussein Naim, and Reinhard Dummer. 2005. 'Oncolytic measles virus in cutaneous T-cell lymphomas mounts antitumor immune responses in vivo and targets interferon-resistant tumor cells', *Blood*, 106: 2287-94.
Hilleman, M. R., E. B. Buynak, R. E. Weibel, J. Stokes, Jr., J. E. Whitman, Jr., and M. B. Leagus. 1968. 'Development and evaluation of the Moraten measles virus vaccine', *JAMA*, 206: 587-90.
Honda, K., H. Yanai, T. Mizutani, H. Negishi, N. Shimada, N. Suzuki, Y. Ohba, A. Takaoka, W. C. Yeh, and T. Taniguchi. 2004. 'Role of a transductional-transcriptional processor complex involving MyD88 and IRF-7 in Toll-like receptor signaling', *Proc Natl Acad Sci U S A*, 101: 15416-21.
Hornung, V., J. Ellegast, S. Kim, K. Brzozka, A. Jung, H. Kato, H. Poeck, S. Akira, K. K. Conzelmann, M. Schlee, S. Endres, and G. Hartmann. 2006. '5'-Triphosphate RNA is the ligand for RIG-I', *Science*, 314: 994-7.
Hoster, Herman A., Robert P. Zanes, and Emmerich von Haam. 1949. 'The Association of „viral“ Hepatitis and Hodgkin's Disease', *Cancer Research*, 9: 473.
Hutzler, S., S. Erbar, R. A. Jabulowsky, J. R. H. Hanauer, J. H. Schnotz, T. Beissert, B. S. Bodmer, R. Eberle, K. Boller, T. Klamp, U. Sahin, and M. D. Muhlebach. 2017. 'Antigen-specific oncolytic MV-based tumor vaccines through presentation of selected tumor-associated antigens on infected cells or virus-like particles', *Sci Rep*, 7: 16892.
Hwang, J. K., J. Hong, and C. O. Yun. 2020. 'Oncolytic Viruses and Immune Checkpoint Inhibitors: Preclinical Developments to Clinical Trials', *Int J Mol Sci*, 21.
Ikediobi, O. N., H. Davies, G. Bignell, S. Edkins, C. Stevens, S. O'Meara, T. Santarius, T. Avis, S. Barthorpe, L. Brackenbury, G. Buck, A. Butler, J. Clements, J. Cole, E. Dicks, S. Forbes, K. Gray, K. Halliday, R. Harrison,

K. Hills, J. Hinton, C. Hunter, A. Jenkinson, D. Jones, V. Kosmidou, R. Lugg, A. Menzies, T. Mironenko, A. Parker, J. Perry, K. Raine, D. Richardson, R. Shepherd, A. Small, R. Smith, H. Solomon, P. Stephens, J. Teague, C. Tofts, J. Varian, T. Webb, S. West, S. Widaa, A. Yates, W. Reinhold, J. N. Weinstein, M. R. Stratton, P. A. Futreal, and R. Wooster. 2006. 'Mutation analysis of 24 known cancer genes in the NCI-60 cell line set', *Mol Cancer Ther*, 5: 2606-12.

Ikegame, S., M. Takeda, S. Ohno, Y. Nakatsu, Y. Nakanishi, and Y. Yanagi. 2010. 'Both RIG-I and MDA5 RNA helicases contribute to the induction of alpha/beta interferon in measles virus-infected human cells', *J Virol*, 84: 372-9.

Jiang, M., P. Osterlund, R. Fagerlund, D. N. Rios, A. Hoffmann, M. M. Poranen, D. H. Bamford, and I. Julkunen. 2015. 'MAP kinase p38alpha regulates type III interferon (IFN-lambda1) gene expression in human monocyte-derived dendritic cells in response to RNA stimulation', *J Leukoc Biol*, 97: 307-20.

Johnstone, R. W., B. E. Loveland, and I. F. McKenzie. 1993. 'Identification and quantification of complement regulator CD46 on normal human tissues', *Immunology*, 79: 341-7.

Jung, K. H., I. K. Choi, H. S. Lee, H. H. Yan, M. K. Son, H. M. Ahn, J. Hong, C. O. Yun, and S. S. Hong. 2017. 'Oncolytic adenovirus expressing relaxin (YDC002) enhances therapeutic efficacy of gemcitabine against pancreatic cancer', *Cancer Lett*, 396: 155-66.

Kärber, G. 1931. 'Beitrag zur kollektiven Behandlung pharmakologischer Reihenversuche', *Naunyn-Schmiedebergs Archiv für experimentelle Pathologie und Pharmakologie*, 162: 480-83.

Kawai, T., S. Sato, K. J. Ishii, C. Coban, H. Hemmi, M. Yamamoto, K. Terai, M. Matsuda, J. Inoue, S. Uematsu, O. Takeuchi, and S. Akira. 2004. 'Interferon-alpha induction through Toll-like receptors involves a direct interaction of IRF7 with MyD88 and TRAF6', *Nat Immunol*, 5: 1061-8.

Kelly, E., and S. J. Russell. 2007. 'History of oncolytic viruses: genesis to genetic engineering', *Mol Ther*, 15: 651-9.

Kirn, D., R. L. Martuza, and J. Zwiebel. 2001. 'Replication-selective virotherapy for cancer: Biological principles, risk management and future directions', *Nat Med*, 7: 781-7.

Kloker, L. D., C. Yurttas, and U. M. Lauer. 2018. 'Three-dimensional tumor cell cultures employed in virotherapy research', *Oncolytic Virother*, 7: 79-93.

Koeberle, S. C., J. Romir, S. Fischer, A. Koeberle, V. Schattel, W. Albrecht, C. Grutter, O. Werz, D. Rauh, T. Stehle, and S. A. Laufer. 2011. 'Skepinone-L is a selective p38 mitogen-activated protein kinase inhibitor', *Nat Chem Biol*, 8: 141-3.

Kohlhapp, F. J., A. Zloza, and H. L. Kaufman. 2015. 'Talimogene laherparepvec (T-VEC) as cancer immunotherapy', *Drugs Today (Barc)*, 51: 549-58.

Kratzer, R. F., S. Espenlaub, A. Hoffmeister, M. W. Kron, and F. Kreppel. 2017. 'Covalent decoration of adenovirus vector capsids with the carbohydrate epitope alphaGal does not improve vector immunogenicity, but allows to study the in vivo fate of adenovirus immunocomplexes', *PLoS One*, 12: e0176852.

Laemmli, U. K. 1970. 'Cleavage of Structural Proteins during the Assembly of the Head of Bacteriophage T4', *Nature*, 227: 680-85.

Lampe, J., S. Bossow, T. Weiland, I. Smirnow, R. Lehmann, W. Neubert, M. Bitzer, and U. M. Lauer. 2013. 'An armed oncolytic measles vaccine virus eliminates human hepatoma cells independently of apoptosis', *Gene Ther*, 20: 1033-41.

Leber, M. F., B. Hoyler, S. Prien, S. Neault, C. E. Engeland, J. M. Forster, S. Bossow, C. Springfeld, C. von Kalle, D. Jager, J. C. Bell, and G. Ungerechts. 2020. 'Sequencing of serially passaged measles virus affirms its genomic stability and reveals a nonrandom distribution of consensus mutations', *J Gen Virol*, 101: 399-409.

Leber, M. F., S. Neault, E. Jirovec, R. Barkley, A. Said, J. C. Bell, and G. Ungerechts. 2020. 'Engineering and combining oncolytic measles virus for cancer therapy', *Cytokine Growth Factor Rev*, 56: 39-48.

Li, Y., H. Deng, D. Zheng, and H. Li. 2004. 'Role of p38 mitogen-activated protein kinase in mediating monocyte chemoattractant protein-1 in human umbilical vein endothelial cells', *Chin Med Sci J*, 19: 71.

Lok, A., G. Descamps, B. Tessoulin, D. Chiron, M. Eveillard, C. Godon, Y. Le Bris, A. Vabret, C. Bellanger, L. Maillet, S. Barille-Nion, M. Gregoire, J. F. Fonteneau, S. Le Gouill, P. Moreau, F. Tangy, M. Amiot, A. Moreau-Aubry, and C. Pellat-Deceunynck. 2018. 'p53 regulates CD46 expression and measles virus infection in myeloma cells', *Blood Adv*, 2: 3492-505.

Long, G., R. Dummer, D. Johnson, O. Michielin, S. Martin-Algarra, S. Treichel, E. Chan, S. Diede, and A. Ribas. 2020. 'Long-Term Analysis of Masterkey-265 Phase 1b Trial of Talimogene Laherparepvec (T-Vec) Plus Pembrolizumab in Patients with Unresectable Stage Iiib-Ivm1c Melanoma', *Journal for Immunotherapy of Cancer*, 8: A261-A61.

Lothe, R. A. 1997. 'Microsatellite instability in human solid tumors', *Mol Med Today*, 3: 61-8.

Mach, N., J. Gao, L. Schaffarczyk, S. Janz, E. Ehrke-Schulz, T. Dittmar, A. Ehrhardt, and W. Zhang. 2020. 'Spectrum-Wide Exploration of Human Adenoviruses for Breast Cancer Therapy', *Cancers (Basel)*, 12.

Marelli, G., A. Howells, N. R. Lemoine, and Y. Wang. 2018. 'Oncolytic Viral Therapy and the Immune System: A Double-Edged Sword Against Cancer', *Front Immunol*, 9: 866.

Martuza, RL, A Malick, JM Markert, KL Ruffner, and DM Coen. 1991. 'Experimental therapy of human glioma by means of a genetically engineered virus mutant', *Science*, 252: 854-56.

Moore, A. E. 1951. 'Inhibition of growth of five transplantable mouse tumors by the virus of Russian Far East encephalitis', *Cancer*, 4: 375-82.

Naniche, D., G. Varior-Krishnan, F. Cervoni, T. F. Wild, B. Rossi, C. Rabourdin-Combe, and D. Gerlier. 1993. 'Human membrane cofactor protein (CD46) acts as a cellular receptor for measles virus', *J Virol*, 67: 6025-32.

Nettelbeck, D. M., M. F. Leber, J. Altomonte, A. Angelova, J. Beil, S. Berchtold, M. Delic, J. Eberle, A. Ehrhardt, C. E. Engeland, H. Fechner, K. Geletneky, K. Goepfert, P. S. Holm, S. Kochanek, F. Kreppel, L. Krutzke, F. Kuhnel, K. S. Lang, A. Marchini, M. Moehler, M. D. Muhlebach, U. Naumann, R. Nawroth, J. Nuesch, J. Rommelaere, U. M. Lauer, and G.

Ungerechts. 2021. 'Virotherapy in Germany-Recent Activities in Virus Engineering, Preclinical Development, and Clinical Studies', *Viruses*, 13.
Noll, M., S. Berchtold, J. Lampe, N. P. Malek, M. Bitzer, and U. M. Lauer. 2013a. 'Primary resistance phenomena to oncolytic measles vaccine viruses', *Int J Oncol*, 43: 103-12.
Noll, Markus, Susanne Berchtold, Johanna Lampe, Nisar P. Malek, Michael Bitzer, and Ulrich M. Lauer. 2013b. 'Primary resistance phenomena to oncolytic measles vaccine viruses', *International journal of oncology*, 43: 103-12.
Nowak, M. A., N. L. Komarova, A. Sengupta, P. V. Jallepalli, M. Shih Ie, B. Vogelstein, and C. Lengauer. 2002. 'The role of chromosomal instability in tumor initiation', *Proc Natl Acad Sci U S A*, 99: 16226-31.
Noyce, Ryan S., Daniel G. Bondre, Michael N. Ha, Liang-Tzung Lin, Gary Sisson, Ming-Sound Tsao, and Christopher D. Richardson. 2011. 'Tumor cell marker PVRL4 (nectin 4) is an epithelial cell receptor for measles virus', *PLoS pathogens*, 7: e1002240-e40.
Ono, K., and J. Han. 2000. 'The p38 signal transduction pathway: activation and function', *Cell Signal*, 12: 1-13.
Osterlund, P. I., T. E. Pietila, V. Veckman, S. V. Kotenko, and I. Julkunen. 2007. 'IFN regulatory factor family members differentially regulate the expression of type III IFN (IFN-lambda) genes', *J Immunol*, 179: 3434-42.
Parato, K. A., D. Senger, P. A. Forsyth, and J. C. Bell. 2005. 'Recent progress in the battle between oncolytic viruses and tumours', *Nat Rev Cancer*, 5: 965-76.
Park, A. K., Y. Fong, S. I. Kim, J. Yang, J. P. Murad, J. Lu, B. Jeang, W. C. Chang, N. G. Chen, S. H. Thomas, S. J. Forman, and S. J. Priceman. 2020. 'Effective combination immunotherapy using oncolytic viruses to deliver CAR targets to solid tumors', *Sci Transl Med*, 12.
Patel, M. R., A. Dash, B. A. Jacobson, Y. Ji, D. Baumann, K. Ismail, and R. A. Kratzke. 2019. 'JAK/STAT inhibition with ruxolitinib enhances oncolytic virotherapy in non-small cell lung cancer models', *Cancer Gene Ther*, 26: 411-18.
Peng, K. W., S. Facteau, T. Wegman, D. O'Kane, and S. J. Russell. 2002. 'Non-invasive in vivo monitoring of trackable viruses expressing soluble marker peptides', *Nat Med*, 8: 527-31.
Peng, Zhaohui. 2005. 'Current Status of Gendicine in China: Recombinant Human Ad-p53 Agent for Treatment of Cancers', *Human Gene Therapy*, 16: 1016-27.
Platanias, L. C. 2003. 'The p38 mitogen-activated protein kinase pathway and its role in interferon signaling', *Pharmacol Ther*, 98: 129-42.
———. 2005. 'Mechanisms of type-I- and type-II-interferon-mediated signalling', *Nat Rev Immunol*, 5: 375-86.
Qiu, G. H., X. Xie, F. Xu, X. Shi, Y. Wang, and L. Deng. 2015. 'Distinctive pharmacological differences between liver cancer cell lines HepG2 and Hep3B', *Cytotechnology*, 67: 1-12.
Rehman, H., A. W. Silk, M. P. Kane, and H. L. Kaufman. 2016. 'Into the clinic: Talimogene laherparepvec (T-VEC), a first-in-class intratumoral oncolytic viral therapy', *J Immunother Cancer*, 4: 53.

Rudalska, R., D. Dauch, T. Longerich, K. McJunkin, T. Wuestefeld, T. W. Kang, A. Hohmeyer, M. Pesic, J. Leibold, A. von Thun, P. Schirmacher, J. Zuber, K. H. Weiss, S. Powers, N. P. Malek, M. Eilers, B. Sipos, S. W. Lowe, R. Geffers, S. Laufer, and L. Zender. 2014. 'In vivo RNAi screening identifies a mechanism of sorafenib resistance in liver cancer', *Nat Med*, 20: 1138-46.

Russell, S. J., and K. W. Peng. 2007. 'Viruses as anticancer drugs', *Trends Pharmacol Sci*, 28: 326-33.

Russell, S. J., K. W. Peng, and J. C. Bell. 2012. 'Oncolytic virotherapy', *Nat Biotechnol*, 30: 658-70.

Sanford, K. K., W. R. Earle, and G. D. Likely. 1948. 'The growth in vitro of single isolated tissue cells', *J Natl Cancer Inst*, 9: 229-46.

Schattner, A. 1984. 'Therapeutic role of measles vaccine in Hodgkin's disease', *Lancet*, 1: 171.

Scheubeck, G., S. Berchtold, I. Smirnow, A. Schenk, J. Beil, and U. M. Lauer. 2019. 'Starvation-Induced Differential Virotherapy Using an Oncolytic Measles Vaccine Virus', *Viruses*, 11.

Seth, R. B., L. Sun, C. K. Ea, and Z. J. Chen. 2005. 'Identification and characterization of MAVS, a mitochondrial antiviral signaling protein that activates NF-kappaB and IRF 3', *Cell*, 122: 669-82.

Shoemaker, R. H. 2006. 'The NCI60 human tumour cell line anticancer drug screen', *Nat Rev Cancer*, 6: 813-23.

Silvennoinen, O., J. N. Ihle, J. Schlessinger, and D. E. Levy. 1993. 'Interferon-induced nuclear signalling by Jak protein tyrosine kinases', *Nature*, 366: 583-5.

Skehan, P., R. Storeng, D. Scudiero, A. Monks, J. McMahon, D. Vistica, J. T. Warren, H. Bokesch, S. Kenney, and M. R. Boyd. 1990. 'New colorimetric cytotoxicity assay for anticancer-drug screening', *J Natl Cancer Inst*, 82: 1107-12.

SPEARMAN, C. 1908. 'THE METHOD OF ‘RIGHT AND WRONG CASES’ (‘CONSTANT STIMULI’) WITHOUT GAUSS'S FORMULAE', *British Journal of Psychology, 1904-1920*, 2: 227-42.

Sugawara, K., M. Iwai, H. Ito, M. Tanaka, Y. Seto, and T. Todo. 2021. 'Oncolytic herpes virus G47Delta works synergistically with CTLA-4 inhibition via dynamic intratumoral immune modulation', *Mol Ther Oncolytics*, 22: 129-42.

Tatsuo, Hironobu, Nobuyuki Ono, Kotaro Tanaka, and Yusuke Yanagi. 2000. 'SLAM (CDw150) is a cellular receptor for measles virus', *Nature*, 406: 893-97.

Todo, T., H. Ito, Y. Ino, H. Ohtsu, Y. Ota, J. Shibahara, and M. Tanaka. 2022. 'Intratumoral oncolytic herpes virus G47Δ for residual or recurrent glioblastoma: a phase 2 trial', *Nat Med*, 28: 1630-39.

Vergote, I., F. Heitz, P. Buderath, M. Powell, J. Sehouli, C. M. Lee, A. Hamilton, J. Fiorica, K. N. Moore, M. Teneriello, L. Golden, W. Zhang, C. Pitou, R. Bell, R. Campbell, D. L. Farrington, K. Bell-McGuinn, and R. M. Wenham. 2020. 'A randomized, double-blind, placebo-controlled phase 1b/2 study of ralimetinib, a p38 MAPK inhibitor, plus gemcitabine and

carboplatin versus gemcitabine and carboplatin for women with recurrent platinum-sensitive ovarian cancer', *Gynecol Oncol*, 156: 23-31.

Wu, Y., L. Li, L. Frank, J. Wagner, P. Andreozzi, B. Hammer, M. D'Alicarnasso, M. Pelliccia, W. Liu, S. Chakrabortty, S. Krol, J. Simon, K. Landfester, S. L. Kuan, F. Stellacci, K. Mullen, F. Kreppel, and T. Weil. 2019. 'Patchy Amphiphilic Dendrimers Bind Adenovirus and Control Its Host Interactions and in Vivo Distribution', *ACS Nano*, 13: 8749-59.

Xia, Z. J., J. H. Chang, L. Zhang, W. Q. Jiang, Z. Z. Guan, J. W. Liu, Y. Zhang, X. H. Hu, G. H. Wu, H. Q. Wang, Z. C. Chen, J. C. Chen, Q. H. Zhou, J. W. Lu, Q. X. Fan, J. J. Huang, and X. Zheng. 2004. '[Phase III randomized clinical trial of intratumoral injection of E1B gene-deleted adenovirus (H101) combined with cisplatin-based chemotherapy in treating squamous cell cancer of head and neck or esophagus]', *Ai Zheng*, 23: 1666-70.

Yamamoto, H., A. F. Fara, P. Dasgupta, and C. Kemper. 2013. 'CD46: the 'multitasker' of complement proteins', *Int J Biochem Cell Biol*, 45: 2808-20.

Zarezadeh Mehrabadi, Ali, Fatemeh Roozbahani, Reza Ranjbar, Mahdieh Farzanehpour, Alireza Shahriary, Ruhollah Dorostkar, and Hadi Esmaeili Gouvarchin Ghaleh. 2022. 'Overview of the pre-clinical and clinical studies about the use of CAR-T cell therapy of cancer combined with oncolytic viruses', *World Journal of Surgical Oncology*, 20: 16.

Zhang, B., and P. Cheng. 2020. 'Improving antitumor efficacy via combinatorial regimens of oncolytic virotherapy', *Mol Cancer*, 19: 158.

Zhang, W., J. Fu, J. Liu, H. Wang, M. Schiwon, S. Janz, L. Schaffarczyk, L. von der Goltz, E. Ehrke-Schulz, J. Dorner, M. Solanki, P. Boehme, T. Bergmann, A. Lieber, C. Lauber, A. Dahl, A. Petzold, Y. Zhang, A. F. Stewart, and A. Ehrhardt. 2017. 'An Engineered Virus Library as a Resource for the Spectrum-wide Exploration of Virus and Vector Diversity', *Cell Rep*, 19: 1698-709.

Zhang, W., K. Mese, S. Schellhorn, N. Bahlmann, N. Mach, O. Bunz, A. Dhingra, E. Hage, M. E. Lafon, H. Wodrich, A. Heim, and A. Ehrhardt. 2020. 'High-Throughput Cloning and Characterization of Emerging Adenovirus Types 70, 73, 74, and 75', *Int J Mol Sci*, 21.

9 Erklärung des Eigenanteils

Die Arbeit wurde in der Inneren Medizin VIII des medizinischen Universitätsklinikums Tübingen unter Betreuung von Herrn Prof. Dr. med. Ulrich M. Lauer durchgeführt.

Die Konzeption der Studie erfolgte in Zusammenarbeit mit Herrn Prof. Dr. med. Ulrich M. Lauer und Frau Dr. med. Susanne Berchtold (Laborleitung).

Sämtliche Versuche, mit Ausnahme der Experimente zur Testung der Viruskonzentration (MeV-GFP) der Zelllinien ACHN und HCT-15, die von Andrea Schenk (MTA) durchgeführt wurden, wurden nach Einarbeitung durch Frau Irina Smirnow (MTA) von mir eigenständig durchgeführt.

Die Datenanalyse und statistische Auswertung erfolgten durch mich.

Ich versichere das Manuskript selbständig unter Anleitung und Korrektur durch Frau Dr. med. Susanne Berchtold, Frau Dr. rer. nat. Julia Beil (wiss. Mitarbeiterin) und Prof. Dr. med. Ulrich M. Lauer verfasst zu haben und keine weiteren als die von mir angegebenen Quellen verwendet zu haben.

Tübingen, den 01.12.2023

Joschka Gottesleben

10 Danksagung

Ich möchte mich ganz herzlich bei allen bedanken, die mich bei der Erstellung dieser Arbeit unterstützt haben.

Mein erster Dank gilt meinem Doktorvater Prof. Dr. med. Ulrich M. Lauer für die rundum perfekte Betreuung dieser Arbeit und die Unterstützung der Bewerbung für das IZKF Promotionskolleg, sowie die konstruktive Arbeitsweise und das Feedback während meiner Arbeit im Labor und während der Verfassung der Dissertationsschrift.

Ein großes Dankeschön gilt Dr. med. Susanne Berchtold, die mich als meine direkte Betreuerin in meinem praktischen Semester immer unterstützt hat und Dr. rer. nat. Julia Beil, die zusammen alle meine Fragen im Verlauf der Arbeit beantworten konnten und mein Manuskript Korrektur gelesen haben.

Außerdem möchte ich mich bei Irina Smirnow und Andrea Schenk bedanken, die mich in die Arbeitsweisen des Labors eingearbeitet haben und immer offen für meine Fragen waren.

Ich möchte beim IZKF Promotionskolleg für die finanzielle und ideelle Förderung bedanken. Das ausgiebige Programm und die enge Begleitung der Arbeit haben mir im Verlauf meiner Arbeit sehr geholfen und haben mir noch einen tieferen Einblick in der Welt der medizinischen Forschung gegeben.

Einen großen Dank gilt der kompletten AG Lauer und der AG Venturelli, die im Labor eine produktive und herzliche Arbeitsatmosphäre geschaffen haben, die für mich eine bestmögliche Umgebung für die Erstellung dieser Arbeit ermöglichten. Das hat dafür gesorgt, dass man zur jederzeit gerne ins Labor gekommen ist und man sich dort immer willkommen fühlt.

Ich bedanke mich außerdem für die Unterstützung meiner Familie und Freunden.